Politecnico di Torino

U.PORTO
FEUP FACULDADE DE ENGENHARIA
UNIVERSIDADE DO PORTO

Politecnico di Torino

Master of Science in Energy Engineering – Renewable Energy Systems

A.a. 2025/2026

Techno-Economic Optimization of Wave Energy Converter Technologies for Site-Specific Installations

Supervisors:

Prof. Giuseppe Giorgi
Dr. Gianmaria Giannini
Prof. Paulo Jorge Rosa Santos

Author:

Marco Bolla

Abstract

The transition towards a decarbonised energy system has reinforced the strategic importance of resilient, low-carbon generation. Within this context, ocean energy, and in particular Wave Energy Converters (WECs), represent a promising technology for coastal nations. This thesis investigates two WEC concepts: a tightly moored point absorber (CorPower) and a submerged point absorber (CETO 6) across multiple maritime locations characterised by diverse sea states. Their performance is assessed through numerical simulations based on a linear potential flow model to describe wave–structure interactions, combined with hydrodynamic analysis and subsequent modelling, optimisation, and performance evaluation in MATLAB. The resulting configurations are then extended to additional sites in order to explore scalability and adaptability under different wave climates. Two distinct scaling methodologies are compared: the widely adopted Froude scaling approach and a Physical scaling method. The technical analysis is complemented by an economic assessment based on key performance indicators, including Annual Energy Production (AEP) and Levelised Cost of Energy (LCOE), with the aim of identifying the most suitable technology for each sea condition. The results indicate, for example, that the CorPower device deployed in the North Sea off Scotland, when co-located with an offshore wind farm, achieves an LCOE 39% lower than the same technology operating as a standalone system. The study also highlights the limitations of Froude scaling when applied to complex techno-economic evaluations. Overall, this work provides an integrated techno-economic assessment of wave energy and its potential contribution to future energy systems.

Contents

1 Introduction **10**

1.1 Context and motivation 10

1.2 Objectives of the Thesis 15

1.3 Thesis structure 15

2 State of the Art **17**

2.1 Wave Energy Converter Technology 17

2.1.1 Operation 17

2.1.2 Costs and technical assessment 19

2.1.3 Classification of WECs 20

2.2 WECs considered in the portfolio 22

2.2.1 CorPower 22

2.2.2 CETO 6 24

2.3 Selected areas and metocean conditions 25

2.3.1 Figueira da Foz 25

2.3.2 North Sea, Scotland region 27

2.3.3 Albany, West Australia 28

2.3.4 North Sea, Germany region 29

3 Methodological Framework **31**

3.1 Tools and Software used 31

3.1.1 Copernicus 31

3.1.2 NEMOH 31

3.1.3 MATLAB 32

3.2 Workflow 32

3.3 Evaluation metrics 34

3.3.1 CAPEX 34

3.3.2 OPEX 34

3.3.3 LCOE 34

3.4 Wave dataset 35

4 Hydrodynamic Modelling and Numerical Simulations **40**

4.1 Metrics used in the WECs design 40
4.1.1 Power matrix 40
4.1.2 Annual Energy Production 40
4.1.3 Average Power 41
4.1.4 Capacity Factor 41
4.2 WECs design 41
4.2.1 CorPower 41
4.2.2 CETO 6 53

5 Scaling Methods and WEC Simulations 59
5.1 Scaling procedures 59
5.1.1 Procedure and scaling workflow 59
5.1.2 Specimen choice 60
5.2 Pressure-based structural analysis 61
5.2.1 Hydrodynamic load definition 61
5.2.2 Stress evaluation and thickness sizing 62
5.3 Sensitivity Analysis of Device Radius and Site Location 66
5.3.1 Froude scaling 66
5.3.2 Physical model 69
5.4 Cost formation 74
5.4.1 CAPEX 74
5.4.2 OPEX 74
5.5 Economic calculations 75
5.5.1 KPI, Key Performance Indicator 75
5.5.2 LCOE 75
5.5.3 Particular cases 76

6 Results and Discussion 78
6.1 KPI 78
6.1.1 Physical Scaling Method 79
6.1.2 Froude scaling 84
6.2 LCOE 91
6.2.1 Physical Scaling Method 91
6.2.2 Froude Scaling Method 99

7 Conclusions 108

Bibliography 111

List of Figures

1.1 Share of Renewable Energy Sources (RES) in electricity production in the EU-27 over time. 10
1.2 Global temperature increase over the last 50 years 11
1.3 Global CO_2 emissions from 1900 to 2024 11
1.4 Annual and cumulative wave energy capacity in Europe 13
1.5 Wave and tidal stream project that received a revenue support for full- scale deployments 14
1.6 LCOE in 2020 versus LCOE projected in 2050 with conservative and optimistic scenario 14

2.1 Schematic representation of a WEC system and its main subsystems. 17
2.2 Classification of WECs according to their energy capture principle . . 20
2.3 Comprehensive classification of WECs based on multiple criteria . . . 21
2.4 CorPower internal structure 23
2.5 Operating modes of the CorPower device 23
2.6 Schematic representation of the CETO 6 25
2.7 Designated areas for offshore energy in Portugal 27
2.8 Geographic overview of the study area in Scotland 28
2.9 Geographic overview of the study area in Australia 29
2.10 Geographic overview of the study area in Germany 30

3.1 Sea state occurrence matrix of selected area in Germany 36
3.2 Sea state occurrence matrix of selected area in Scotland 36
3.3 Sea state occurrence matrix of the selected area in Portugal 36
3.4 Sea state occurrence matrix of selected area in Australia 37
3.5 Energy density matrix of the selected area in Germany 38
3.6 Energy density matrix of the selected area in Scotland 38
3.7 Energy density matrix of the selected area in Portugal 38
3.8 Energy density matrix of the selected area in Australia 39

4.1 Power matrix of CorPower for the base case in Portugal 43
4.2 AEP analysis of CorPower for the base case in Portugal 44
4.3 Power matrix of CorPower for the optimised case in Portugal 48

4.4 AEP analysis of CorPower for the optimised case in Portugal 48
4.5 Heave motion 53
4.6 Power matrix of CETO 6 for the base case in Australia 56
4.7 AEP analysis of CETO 6 for the base case in Australia 56
4.8 Power matrix of CETO 6 for the optimised case in Australia 57
4.9 AEP analysis of CETO 6 for the optimised case in Australia 57

5.1 Geometric archetypes used for the scaling analysis 60
5.2 Structure of the Fusion360 design files used for WEC modelling . . . 70
5.3 Organization of NEMOH simulation output files 71
5.4 MATLAB scripts used for CorPower and CETO 6 simulations 72
5.5 Scaling scripts 73

6.1 Relationship between cost and AEP for the Winch of CorPower and CETO 6 in Portugal using PSM 79
6.2 Relationship between cost and AEP for the Vertical Cylinder of CorPower and CETO 6 in Portugal using PSM 80
6.3 Relationship between KPI and AEP for Winch component in Portugal for CorPower and CETO 6 using PSM 81
6.4 Relationship between KPI and AEP for the Vertical Cylinder component in Portugal for CorPower and CETO 6 using PSM 82
6.5 Normalized growth of AEP and component costs as a function of increasing radius in Portugal for CorPower and CETO 6 using PSM . 83
6.6 Relationship between cost and AEP for the Winch of CorPower and CETO 6 in Portugal using FSM 85
6.7 Relationship between cost and AEP for the Vertical Cylinder of CorPower and CETO 6 in Portugal using FSM 86
6.8 Relationship between KPI and AEP for Winch component in Portugal for CorPower and CETO 6 using FSM 88
6.9 Relationship between KPI and AEP for Vertical Cylinder component in Portugal for CorPower and CETO 6 using FSM 89
6.10 Normalized growth of AEP and component costs as a function of increasing radius in Portugal for CorPower and CETO 6 using FSM . 90
6.11 Thickness breakdown for the hull for CorPower and CETO 6 in Portugal using PSM 92
6.12 CAPEX breakdown evolution with thickness for CorPower and CETO 6 in Portugal using PSM 93
6.13 LCOE variation with radius for CorPower and CETO 6 in Germany using PSM 95

6.14 LCOE variation with radius for CorPower and CETO 6 in Scotland using PSM 96
6.15 LCOE variation with radius for CorPower and CETO 6 in Portugal using PSM 97
6.16 LCOE variation with radius for CorPower and CETO 6 in Australia using PSM 98
6.17 LCOE relation with Wave Energy Potential 99
6.18 Thickness breakdown for the hull for CorPower and CETO 6 in Portugal using FSM 100
6.19 LCOE variation with radius for CorPower and CETO 6 in Germany using FSM 101
6.20 LCOE variation with radius for CorPower and CETO 6 in Scotland using FSM 102
6.21 LCOE variation with radius for CorPower and CETO 6 in Portugal using FSM 103
6.22 LCOE variation with radius for CorPower and CETO 6 in Australia using FSM 104

List of Tables

2.1 Breakdown of CAPEX components for a WEC 19
2.2 Percentage contribution of each component to the total WEC cost . . 19
2.3 Geographical coordinates of the selected study area in Portugal . . . 26
2.4 Geographical coordinates of the selected study area in Scotland . . . 28
2.5 Geographical coordinates of the selected study area in Australia . . . 29
2.6 Geographical coordinates of the selected study area in Germany . . . 30

4.1 Comparison base and optimised case 52
4.2 Comparison base and optimised case 58

6.1 LCOE values for a single WEC installation across different locations [€/MWh] 105
6.2 Optimal device radius for different locations [m] 105
6.3 LCOE values for WEC farms across different locations [€/MWh] . . 107
6.4 LCOE values for co-located WEC and OWF [€/MWh] 107

Chapter 1

Introduction

1.1 Context and motivation

Renewable energy has been a key element in the transition toward a more sustainable world for several years. It plays a fundamental role for multiple reasons, primarily because it enables energy production without the emissions of CO_2, NOx, and SOx that are typically associated with conventional fossil fuel-based energy generation.

As shown in Figure 1.1, the share of Renewable Energy Sources (RES) in electricity production has steadily increased over the years.

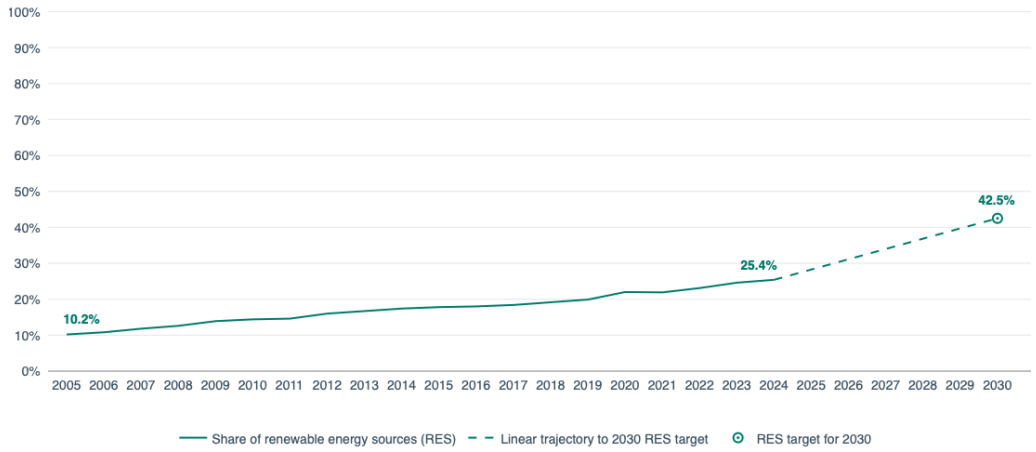

Figure 1.1: Share of Renewable Energy Sources (RES) in electricity production in the EU-27 over time[1]

Developing and increasing the share of RES in the production of energy, and in particular the implementation of different RES technologies, is fundamental for different reasons:

- Energy security: A diversified energy portfolio that includes multiple energy sources significantly enhances the energy security of a country or region. According to the International Energy Agency (IEA), *"Energy security is not just about having uninterrupted access to energy, but also about securing energy supplies at an affordable price."* [2]

- Energy independence: Closely related to energy security, energy independence refers to reducing reliance on countries with abundant fossil fuel and natural gas resources. Increasing the share of RES substantially decreases this external dependence and strengthens national autonomy.
- Environmental aspects: An examination of Figures 1.2 and 1.3 highlights that the significant increase in CO_2 emissions and other greenhouse gases (GHGs) over the past century is widely recognized as one of the main drivers of global warming. The energy sector plays a central role in this trend, accounting for approximately 35% of total greenhouse gas emissions.

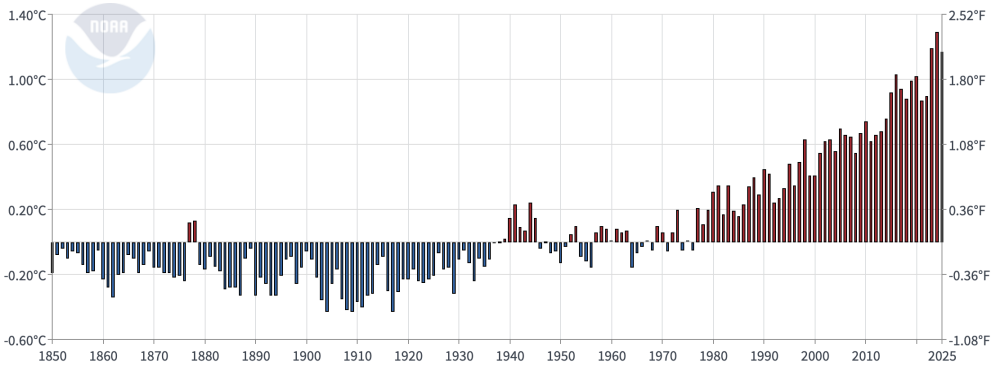

Figure 1.2: Global temperature increase over the last 50 years.[3]

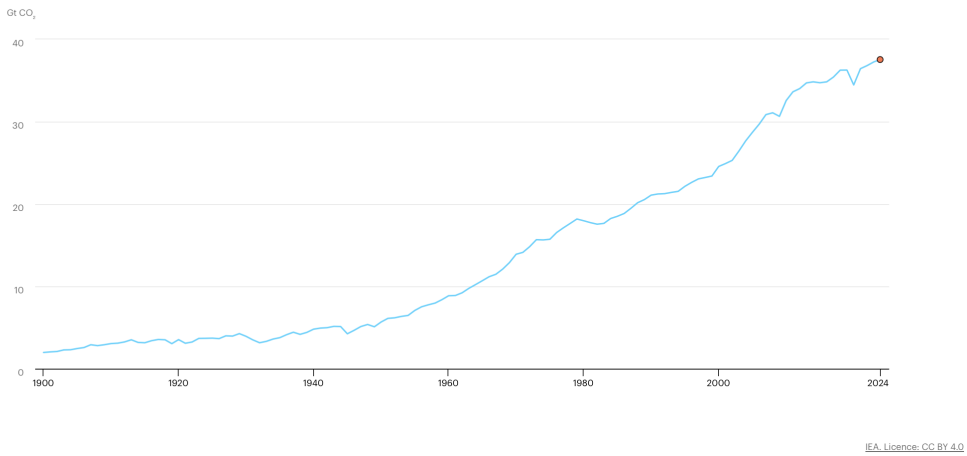

Figure 1.3: Global CO_2 emissions from 1900 to 2024][4]

To address these challenges, investment in renewable energy sources is essential. Among them, wave energy can play a significant role. Wave energy refers to the exploitation of ocean waves for electricity generation. Ocean wave energy originates from wind energy transferred to the sea through air–sea interactions. As wind blows over the ocean surface, part of its energy is transferred to the water, generating waves. This energy is stored partly as potential energy, associated with the displacement of water from the mean sea level, and partly as kinetic energy,

related to the motion of water particles. Renewable energy resources in the ocean originate from eight distinct sources, each with different physical mechanisms and requiring specific conversion technologies. These sources include waves, tides, ocean currents, ocean thermal energy conversion, salinity gradients, marine biomass, offshore geothermal energy, and offshore wind. With the exception of tidal barrages and offshore wind, most ocean energy technologies are not yet fully commercial and are still undergoing research and development or are at the pre-commercial prototype and demonstration stage. Tidal energy, including both tidal range and tidal stream technologies, is the most mature among ocean energy technologies, with a Technology Readiness Level (TRL) of 9 for tidal range systems and 8 for tidal stream systems. Wave Energy Converters are generally less mature technologies, typically at a Technology Readiness Level (TRL) of 6–7, although some devices have reached TRL 8, with only a limited number of full-scale systems deployed at sea. One of the most notable examples is the CorPower C4 device, developed within the HiWave-5 project. The device was initially launched from the port of Viana do Castelo, Portugal, and subsequently towed to the Aguçadoura test site located approximately 4 km offshore[5].

Several governments have introduced initiatives to promote and accelerate the development and deployment of ocean energy technologies. However, information on their environmental and social impacts remains limited, mainly due to the lack of operational experience. Despite this, potential adverse environmental effects are expected to be relatively low. Similarly, both current and future costs of most ocean energy technologies are difficult to estimate accurately, as limited fabrication and deployment experience is available to validate cost assumptions[6].

Ocean energy is a relatively recent technology that has experienced substantial growth, with cumulative installed capacity increasing from 1 MW to almost 14 MW over the past fifteen years, as is possible to see in Figure 1.4.

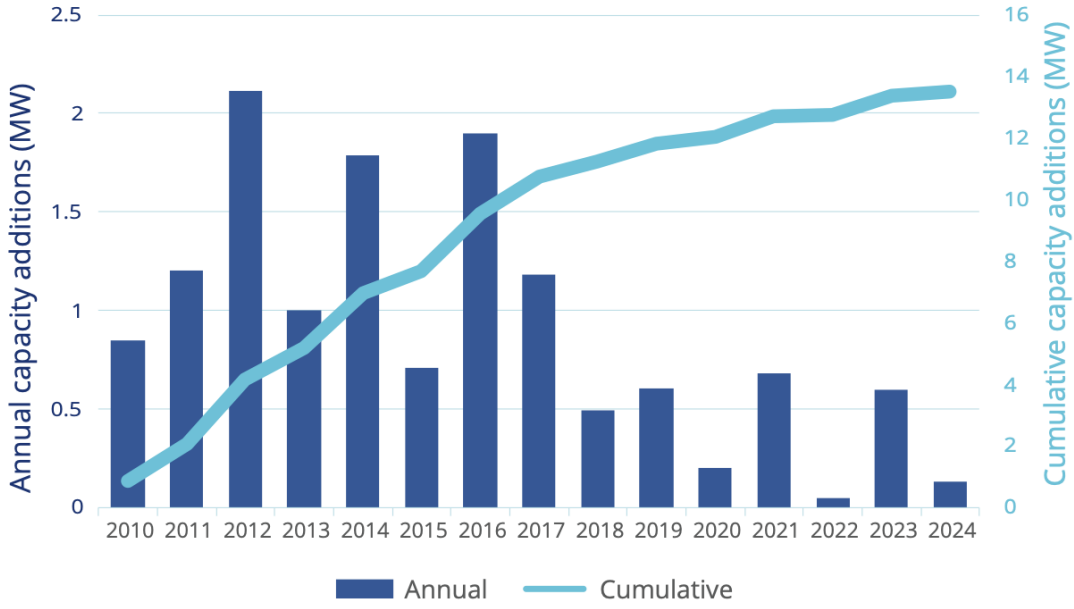

Figure 1.4: Annual and cumulative wave energy capacity in Europe [7]

The targets include approximately 26 MW of installed capacity for Wave Energy Converters by 2030 and 180 MW for tidal energy. To achieve these objectives, a significant number of new projects, many of which have already secured funding, are expected to be deployed across Europe in the coming years. As shown in Figure 1.4, the majority of these projects concern tidal stream technologies and are primarily located in the North Sea, particularly around the United Kingdom.

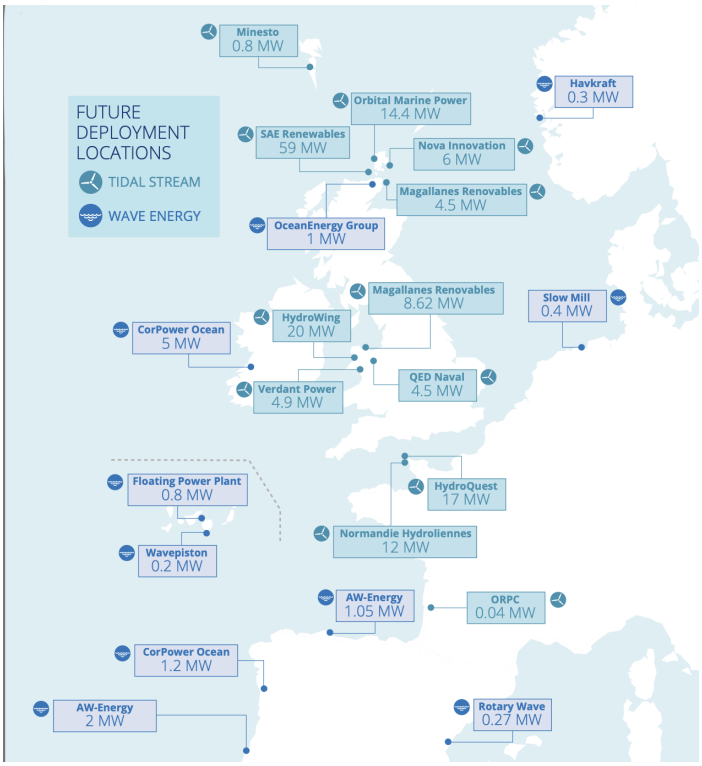

Figure 1.5: Wave and tidal stream project that received a revenue support for full-scale deployments [7]

The cost of ocean energy remains relatively high, which explains its limited deployment to date. However, Figure 1.6, shows projections which indicate that costs are expected to decrease over the next decade, driven by the installation of a larger number of projects and continued increases in Technology Readiness Level (TRL).

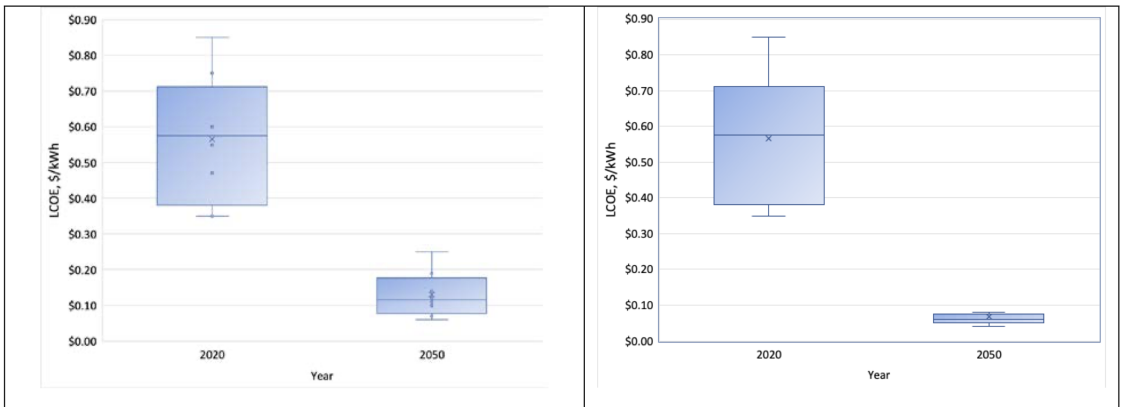

Figure 1.6: LCOE in 2020 versus LCOE projected in 2050 with conservative and optimistic scenario[8]

From Figure 1.6 it is possible to appreciate that the LCOE is expected to decrease significantly in both the conservative and optimistic scenarios, driven by increases in TRL and capacity factor. The range remains quite wide due to the substantial cost differences among the various devices and the strong dependence on location.

Ocean energy is still far from playing a central role in a country's energy production due to its high costs and relatively low TRL. However, significant progress has been made in recent years, and if this trend continues, it is expected to play an important role in the energy mix of countries with access to energetic seas or oceans. This would enhance national energy security, increase the share of renewable energy generation, and reduce dependence on other countries and fossil fuel sources.

1.2 Objectives of the Thesis

The transition towards site-specific optimization of Wave Energy Converters (WECs) requires an integrated approach that combines both technical performance and economic feasibility. In this context, this thesis aims to develop a comprehensive framework capable of supporting decision making in the design and deployment of WEC technologies across different locations.

This thesis has two primary objectives:

- The first objective is the development of a techno-economic optimization approach that complements traditional technological optimization. This framework enables the identification of the optimal trade-off between energy performance and cost, enhancing the efficiency of each WEC while explicitly accounting for the economic implications of design and configuration choices.
- The second objective is the definition of a standardized economic metric that allows for a consistent comparison of different WEC technologies across multiple locations. This enables the identification of the most suitable WEC for a given site, considering both performance and economic viability.

Together, these objectives aim to establish a generalized and scalable procedure through which, by varying site conditions and device parameters, the optimal WEC-location pairing can be efficiently determined.

1.3 Thesis structure

This thesis is organised into six chapters, each addressing a specific aspect of the techno-economic assessment of Wave Energy Converters (WECs).

Chapter 1 introduces the context and motivation of the study, highlighting the current challenges of ocean energy technologies and defining the main objectives of the thesis.

Chapter 2 presents the state of the art of WEC technologies, including their op-

erating principles, classification, and cost structure. The WECs considered in this work are described together with the selected deployment sites and their metocean characteristics.

Chapter 3 describes the methodological framework adopted in the study. It includes the definition of the main performance indicators, such as AEP and Levelised Cost of Energy (LCOE), as well as the processing of wave climate data and the assumptions used for the analysis.

Chapter 4 focuses on the hydrodynamic modelling and numerical simulations. The dynamic response of the devices is evaluated and an optimisation of the Power Take-Off (PTO) parameters is performed in order to maximise energy production under different sea states.

Chapter 5 introduces the scaling procedures and the techno-economic modelling of the WEC components. A structural scaling approach is adopted to relate device size to cost and performance, allowing the evaluation of different design configurations. The analysis also incorporates economic calculations, including CAPEX, OPEX and LCOE, and considers the effect of WEC farms and economies of scale, which are modelled through scaling laws to account for cost reductions at larger deployment sizes.

Chapter 6 presents and discusses the results of the scaling and techno-economic analysis. Key performance indicators (KPI) are evaluated to assess the trade-off between cost and energy production for different components and device sizes. The results obtained with the Physical Scaling Method are compared with those derived from the Froude Scaling Method, highlighting differences in trends and the ability to identify optimal design configurations. Finally, the main outcomes of the study are summarised and discussed.

Chapter 2

State of the Art

2.1 Wave Energy Converter Technology

Wave Energy Converters are devices designed to harness energy from ocean waves and convert it into a usable form of energy, typically electricity. The first patent related to wave energy conversion technology was registered in the 18th century, specifically in 1799 in France by Pierre-Henri-Joseph Girard. However, significant development of this technology, both from academic and industrial perspectives, began in the 1970s following the oil crisis, and gained further momentum since the 2000s with the aim of increasing the share of Renewable Energy Sources (RES)[9].

2.1.1 Operation

Despite differences in operating principles, most WECs share a common overall structure and comprise the same primary subsystems, as illustrated in Figure 2.1.

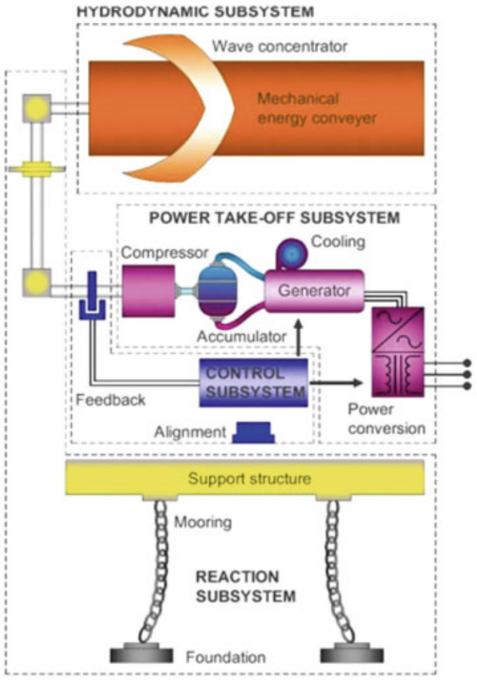

Figure 2.1: Schematic representation of a WEC system and its main subsystems [10]

The main subsystems found in all WECs include:

- **Hydrodynamic subsystem** – This is the primary wave-absorption system that extracts energy from the waves. Its configuration depends on the specific technology, such as oscillating body, oscillating water column, or overtopping devices. It is mechanically linked to both the reaction and PTO subsystems, to which it transfers forces and motions.
- **Power take-off (PTO) subsystem** – This subsystem converts the energy captured by the hydrodynamic subsystem into electricity. PTO technologies vary and may include hydraulic systems, direct-drive mechanical systems, linear generators, air turbines, and low-head water turbines.
- **Reaction subsystem** – This subsystem holds the WEC in position relative to the seabed (e.g., via a mooring system) and provides the reaction point needed by the PTO and/or mechanical support for the hydrodynamic subsystem(s), such as a fixed reference or structural support.
- **Control and instrumentation subsystem** – This is the "intelligent" component of the WEC, responsible for system control and monitoring. It includes processors for automation and electromechanical tasks, sensors and data acquisition systems, communication and data transfer equipment, and the human–machine interface.

WECs must have the following characteristics in order to demonstrate long-term economic viability:

- **Survivability:** The WEC must be equipped with a reliable mooring system and, ideally, a passive safety mechanism capable of reducing extreme loads.
- **Reliability and maintainability:** The most critical components of the WEC should be easily accessible for inspection and servicing.
- **Overall power performance:** The WEC must employ an efficient wave-energy absorption technology and an effective PTO system.
- **Scalability:** For economic viability, a full-scale WEC must reach the multi-MW range.
- **Environmental benefit:** As sustainable energy technologies, WECs are expected to deliver clear environmental advantages while maintaining a minimal ecological footprint [10]

2.1.2 Costs and technical assessment

The costs associated with a WEC throughout its project lifetime are typically divided into distinct categories: pre-operational costs (PC), capital expenditures (CAPEX), operational expenditures (OPEX), and end of life decommissioning costs (DC). Tables 2.1 and 2.2 summarise these cost components and highlight the dominant role of CAPEX within the overall cost structure of a WEC project. The main CAPEX contributions include the device structure and prime mover, the PTO system, the foundations or mooring systems, and the grid connection infrastructure.

Table 2.1: Breakdown of CAPEX components for a WEC[11]

Category	**Value [unity]**
Development costs	250 [€/kW]
Wave Energy Converter (Structure and Prime Mover)	1340 [€/kW]
Balance of Plant	1600 [€/kW]
Installation and Commissioning	590 [€/kW]
Decommissioning	420 [€/kW]
WEC and installation	2.5 - 6 [M€/MW]
Mooring system	0.265 [€/day]
Mooring Installation	50,000 [€/day]
Cable installation	2.07 [€/m]
Electrical substation	≈ 1.2 [M€] million

Table 2.2: Percentage contribution of each component to the total WEC cost[11]

Category	**Percentage of total cost (%)**
Structure	38.2%
Foundation and mooring	19.1%
Installation	10.2%
PTO component	24.2%
Grid connection	8.3%

GUO et al. [11] review several studies that provide cost estimations for different WECs. In particular, certain costs, such as those associated with the installation of mooring systems, are expressed in euro per day, as they primarily depend on the duration of use of specialized vessels and skilled personnel required for the operations.

The main technical assessment ratios for a WEC are:

- **Capture width ratio (CWR):** The CWR quantifies the efficiency with

which a WEC absorbs the incident wave energy.

$$CWR = \frac{CW}{Device\ Width} = \frac{P_{\text{out}}}{W \cdot P_w}\,[\%] \tag{2.1}$$

- **WEC weight-to-installed-kW ratio:** This ratio is frequently employed as an indicator of the material intensity of a WEC relative to its rated power.
- **Capacity factor:** The capacity factor, defined as the ratio of average electrical power output to the device's installed capacity, characterises the utilisation efficiency of the PTO system.

2.1.3 Classification of WECs

There are several WEC typologies, based on different criteria, the main ones are:

- Location of the device in relation to the bathymetry and distance to the coast, distinguish between onshore, nearshore and offshore facilities
- Position of the device related to the sea level, distinguish between emerged, semi-submerged and submerged
- Size and orientation of the device
- Energy captures principle, as shown in Figure 2.2.

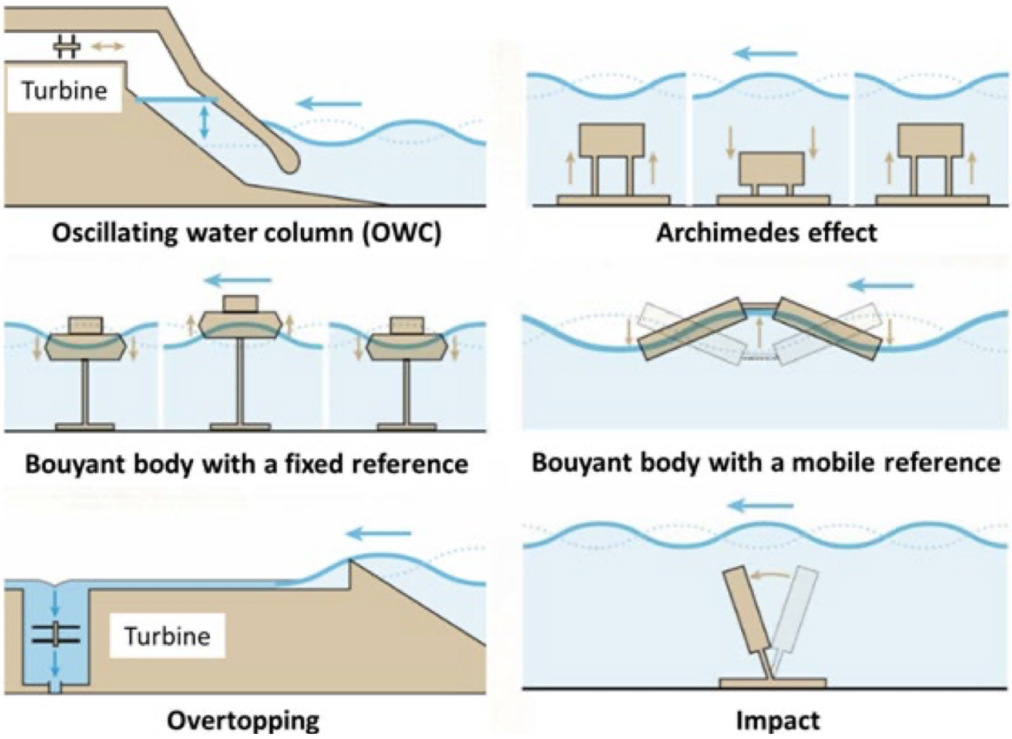

Figure 2.2: Classification of WECs according to their energy capture principle [12]

The energy capture principle distinguishes between several categories WECs. These include Oscillating Water Column (OWC) devices, which exploit the variation in water level within a chamber to drive an air turbine; systems based on the Archimedes effect, which utilise pressure changes induced by wave motion; buoyant body devices with fixed or mobile reference frames, which harness the relative motion between different parts of the system; overtopping devices, which capture energy from water flowing over the structure's freeboard; and impact devices, which are driven directly by wave action.

Another classification taking into account all the different criteria is the following:

- Attenuator
- Point absorber
- Oscillating Wave Surge Converter
- Oscillating Water Column
- Overtopping/Terminator
- Submerged Pressure Differential
- Bulge Wave
- Rotating mass

Figure 2.3 provides a visual overview of this classification.

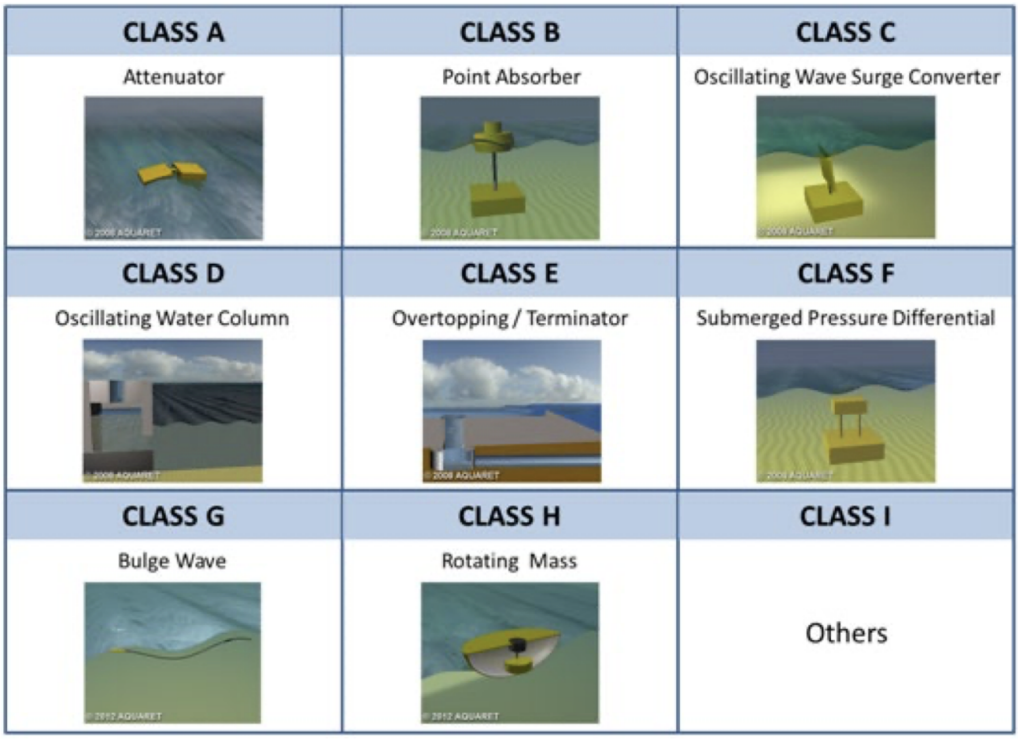

Figure 2.3: Comprehensive classification of WECs based on multiple criteria [12]

Among all these types the most studied are the Point Absorber WEC, like CorPower, PowerBuoy and CETO, followed by the attenuators and the oscillating water column.

2.2 WECs considered in the portfolio

2.2.1 CorPower

CorPower is one of the most developed point absorber WECs. Built by the CorPower Ocean company, they developed the first idea of wave energy converter in 2009 and in 2022 they started with the first commercial phase of the C4 WEC.

Operation:

WECs of this type employ a pre-tension system that pulls the buoy downward, while incoming waves drive it upward. The stored pressure provides a restoring force, enabling motion in both directions and resulting in energy production during both the upward and downward phases. This configuration allows for a lightweight system that remains largely transparent to incoming waves (detuned) unless active control is applied. The wave-induced motion is converted into rotational motion through a piston mechanism, while a cascade gearbox transforms the linear motion into rotation with high efficiency and durability. The generated rotational motion is then converted into electrical energy within the buoy. A key feature of this technology is the implementation of phase control, which enables the system to be tuned or detuned depending on sea conditions. During extreme conditions, the detuned configuration reduces the interaction with waves, allowing the device to behave in a survivability mode similar to that of wind turbines. Under normal operating conditions, the system is tuned to achieve optimal phase alignment with the incoming waves, enhancing motion and maximising energy capture. The WaveSpring technology introduces a negative spring effect that amplifies the buoy motion, leading to a significant increase in energy production for a given device size [13]. The buoy is anchored to the seabed through a mooring system that includes a tidal regulator. UMACK anchors are employed, offering advantages over traditional gravity anchors and monopiles in terms of holding capacity, cost efficiency, and reduced environmental impact. Installation is performed using a high-speed, low-noise vibro-driving method, which minimises disturbance to marine life

Technical characteristics:

- 9 m of diameter
- 18 meters tall

- 70 tonnes of weight
- 8505kW of rated power [14].
- Sea depth installation range between 40 and 100 m [15]

In particular, the rated power of the device is assumed to be 850 kW, based on the latest updates from CorPower Ocean. As reported, "electrical data collected during operation has informed further upgrades aimed at increasing the system's peak power capacity from the confirmed 600 kW towards 850 kW" [14].

The internal structure of the CorPower device, along with its tuning and detuning procedures, is shown in Figures 2.4 and 2.5.

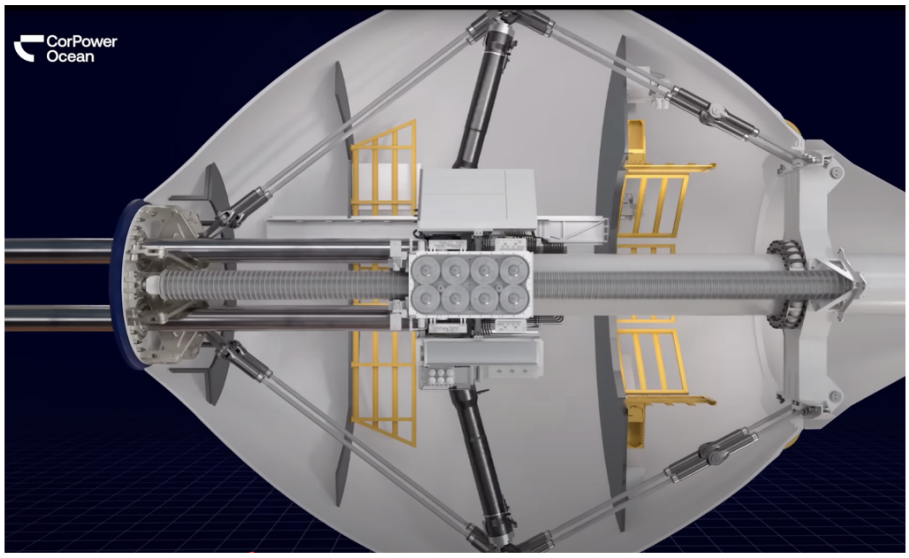

Figure 2.4: CorPower internal structure[15]

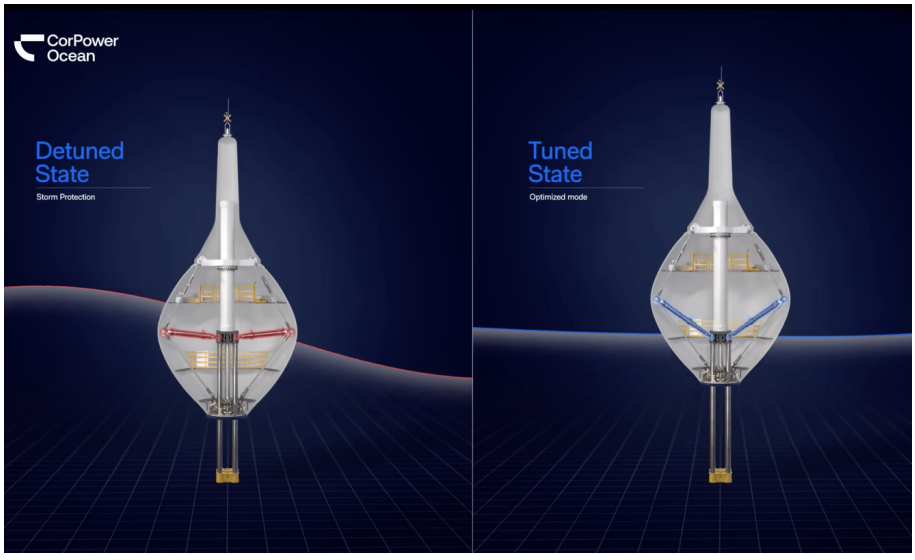

Figure 2.5: Operating modes of the CorPower device[15]

In CorPower's wave energy converter, the concepts of tuning and detuning refer to

distinct operational modes of the device's phase control system, based on sea state conditions. In normal operating conditions, the device operates in "tuned" mode, where the phase-control technology (WaveSpring) actively regulates the hydraulic PTO to bring the motion of the buoyant body into resonance with the incident waves. By modulating the hydraulic damping and stiffness, the system adjusts the phase relationship between the body motion and the wave excitation, effectively amplifying the oscillatory response and maximizing energy capture. In contrast, in extreme sea states (storm conditions), the system switches to "detuned" or survival mode, where the WaveSpring is deactivated or significantly reduced, allowing the PTO to yield and the body to become almost transparent to the incoming waves. This detuning drastically reduces the mechanical forces and stroke amplitudes, thereby protecting the structure and the power take-off system; tests on the C4 device have shown that, even in waves with significant heights up to 11 m and individual waves reaching about 18.5 m, the device's motion remains on the order of a few decimetres, confirming the effectiveness of detuning for survivability.

2.2.2 CETO 6

CETO 6 is a point-absorber WEC and a fully submerged device. A submerged buoy, located a few meters below the ocean surface, follows the orbital motion of the waves and drives a hydraulic PTO system that converts this motion into electricity [16]. Figure 2.6 shows the configuration of the CETO 6 device

Operation:

CETO 6 represents an evolution of the earlier CETO 5 technology, featuring an increase in rated power output, buoy diameter, and an enhanced ability to capture energy from the wave's orbital motion at depth. Unlike the CETO 5 system, where hydraulic power was transmitted to onshore facilities for electricity generation, in CETO 6 the electrical conversion is performed directly on the buoy, improving system efficiency and reducing transmission losses [17]. The CETO 6 WEC tracks and captures the circular motion of waves below the sea surface, converting the resulting heave and surge motions into pressurized hydraulic flow. As the unit moves with the forces of each wave, belts located at the bottom of the buoy drive a unique drum system that powers an integrated hydraulic motor–generator set, producing electricity directly within the submerged structure. The generated electricity is then exported via underwater cables to the grid. In storm conditions, the CETO 6 unit can dive below the most turbulent wave zone, settling at a depth of around 20m to minimize exposure to extreme surface forces. For station-keeping, CETO 6 employs a multi-tether mooring system that combines durability, flexibility, and precise positioning, allowing the device to remain aligned with the wave field while maintaining

structural integrity [18].

Technical characteristics:

- Buoyant actuator diameter: 20 m
- 4 m of height
- 376 tonnes of weight [19]
- 1 MW rated power
- Sea depth installation range between 35 and 60 m

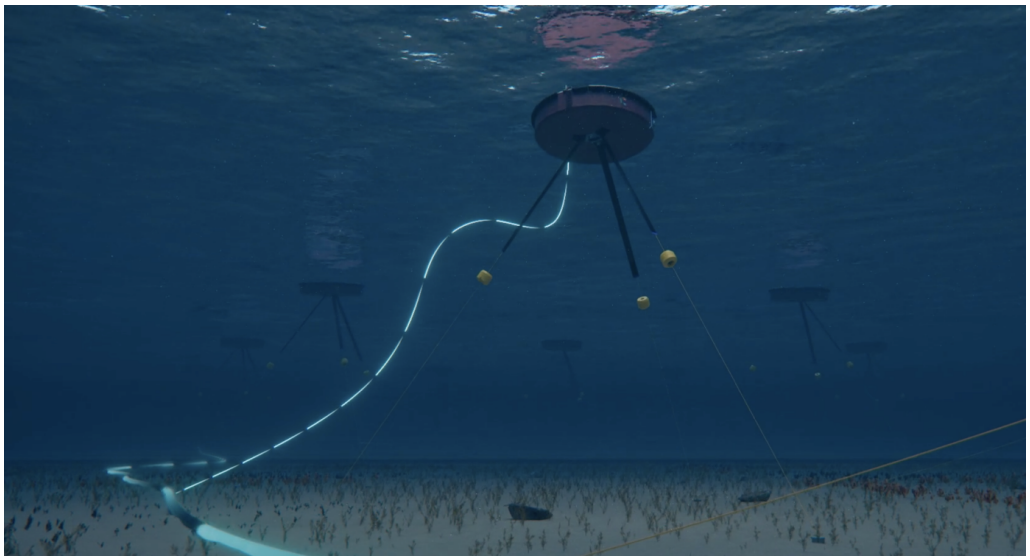

Figure 2.6: Schematic representation of the CETO 6[16]

2.3 Selected areas and metocean conditions

Different locations are considered in this study, with each device initially assigned to the site that best matches its characteristics and operating requirements. Sea state data for all locations are obtained from the Copernicus database [20]. The platform provides NetCDF files containing the relevant sea state parameters required for the analysis. These datasets have a spatial resolution of approximately 22 km (north–south) and 18 km (east–west). Due to this resolution, it was not possible to extract data exclusively for the specific area of interest; instead, the data correspond to the grid cell that includes the selected location.

2.3.1 Figueira da Foz

The location of Figueira da Foz is chosen to study the performance of the CorPower wave energy converter. CorPower Ocean already has a demonstration site for their project in Portugal, Agucadoura (Povòa de Varzim), but it which cannot be used

to study a farm of wave energy converters. To consider the installation of a wave farm of CorPower, other location in Portugal have to be analysed. The document: Approval of the offshore renewable energy allocation plan [21] presents the location which can welcome an offshore energy farm. In the document different areas were selected to host offshore wind and ocean energy farm: Viana do Castelo (0.8 GW), Leixoes (2.5 GW), Figueira da Foz (4,6 GW) and Sines (1,5 GW). The area chosen for the wave farm of CorPower is the one of Figueira da Foz, which is between the cities of Leiria and Aveiro, in front of the city Figueira da Foz as it is possible to see in Figure 2.7. The area of Figueira da Foz, is around 1325 km^2 and, as stated in the docuemnt, has the water depth needed by a point absorber WEC like the CorPower, to work, being between 75 – 100 m.

The geographical coordinates of the selected study area are reported in Table 2.3.

Table 2.3: Geographical coordinates of the selected study area in Portugal

Vertices	**Decimal Coordinates (DD)**	**Sexagesimal Coordinates (DMS)**
Vertix 1	40.4427° N, 9.6825° W	40°21′36.42″ N, 9°40′57.13″ W
Vertix 2	40.4427° N, 9.3859° W	40°26′33,60″ N, 9°23′09,32″ W
Vertix 3	39.9351° N, 9.3730° W	39°56′06,21″ N, 9°22′22,92″ W
Vertix 4	39.8664° N, 9.5875° W	39°51′59,20″ N, 9°35′14,93″ W
Vertix 5	40.3601° N, 9.6825° W	40°21′36,42″ N, 9°40′57,13″ W

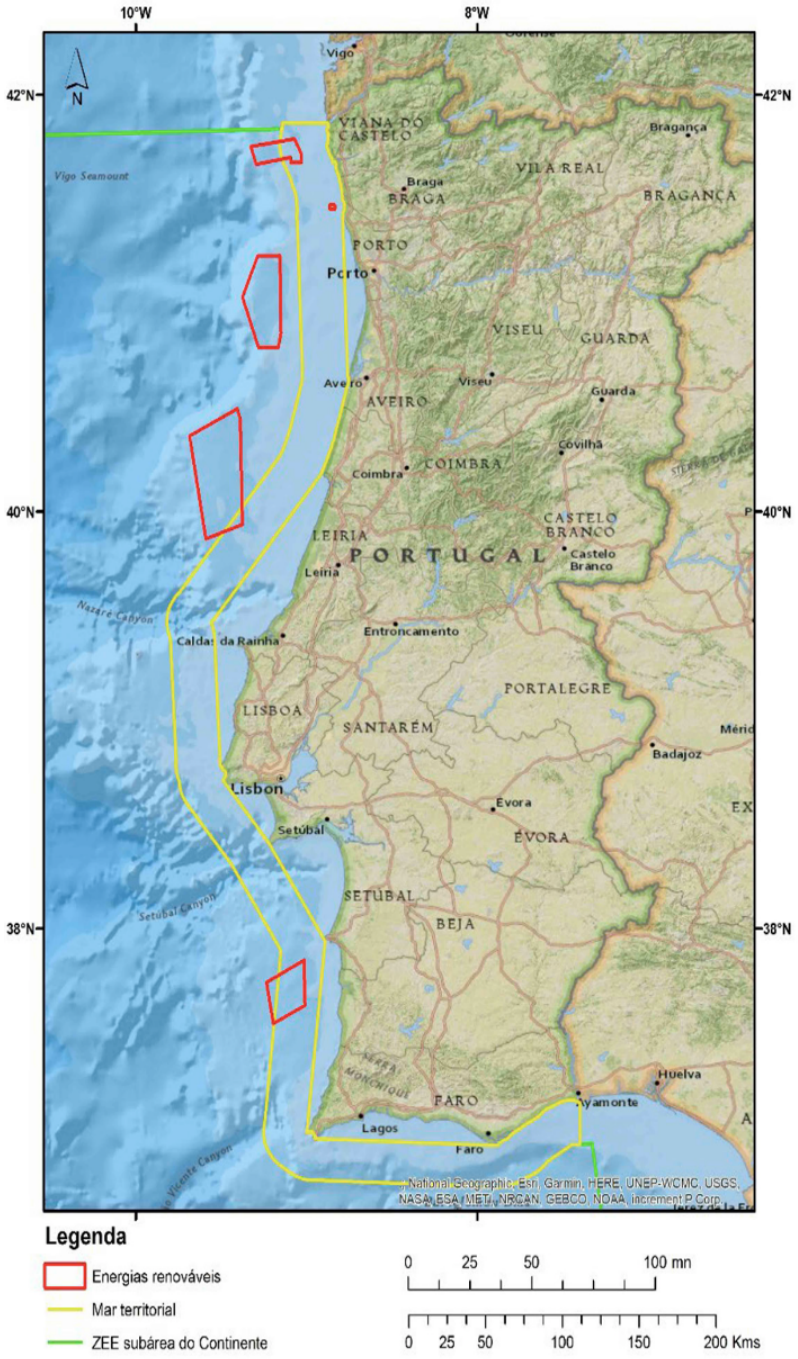

Figure 2.7: Designated areas for offshore energy in Portugal[21]

2.3.2 North Sea, Scotland region

The Scotland region of the North Sea, located off the northern coast of Scotland, as shown in Figure 2.8, has been selected to evaluate the performance of the CorPower and CETO 6 devices under a range of environmental conditions. This site was chosen due to its high wave energy potential, combined with severe sea states that are generally less destructive than those typically encountered along the Portuguese Atlantic coast. In addition, an existing offshore wind farm in the area has

been considered. This enables future analyses to assess the potential benefits of co-locating wave and wind energy systems, particularly in terms of shared electrical infrastructure and grid connection, thereby reducing installation and transmission costs. The site conditions are also well suited for the CorPower device, with a water depth ranging between 45 and 60 m.

The geographical coordinates of the selected study area are reported in Table 2.4.

Table 2.4: Geographical coordinates of the selected study area in Scotland

Vertices	Decimal Coordinates (DD)	Sexagesimal Coordinates (DMS)
North-West (NW)	56.2225° N, 2.3977° W	56°13′21″ N, 2°23′52″ W
North-East (NE)	56.2225° N, 2.3169° W	56°13′21″ N, 2°19′01″ W
South-East (SE)	56.1775° N, 2.3169° W	56°10′39″ N, 2°19′01″ W
South-West (SW)	56.1775° N, 2.3977° W	56°10′39″ N, 2°23′52″ W

Figure 2.8: Geographic overview of the study area in Scotland

2.3.3 Albany, West Australia

The location of Albany, in the south-west region of Australia is chosen as location for the study of the CETO 6 technology. This choice has been made considering the project Carnegie CETO 6 Technology, which a real project taken out by Carneige and ARENA. The project was founded by ARENA (Australian renewable energy agency) with a financing of 2.18 M$ out of the 5.3M$ of the total project cost [22]. The selected site is located in Albany, Western Australia. This choice offers the

advantage of relying on a location that has already been studied and implemented in a real-world project. The area definition is also inspired by the Carnegie approach, considering a 5 km^2 square at the south of Albany, as illustrated in Figure 2.9. This site is well suited to the operational requirements of the CETO 6 system, with water depths ranging between 40 and 80 meters.

The geographical coordinates of the selected study area are reported in Table 2.5.

Table 2.5: Geographical coordinates of the selected study area in Australia

Vertices	**Decimal Coordinates (DD)**	**Sexagesimal Coordinates (DMS)**
North-West (NW)	35.4054° S, 117.854° E	35°24′19″ S, 117°51′14″ E
North-East (NE)	35.4054° S, 117.909° E	35°24′19″ S, 117°54′32″ E
South-East (SE)	35.4514° S, 117.909° E	35°27′05″ S, 117°54′32″ E
South-West (SW)	35.4514° S, 117.854° E	35°27′05″ S, 117°51′14″ E

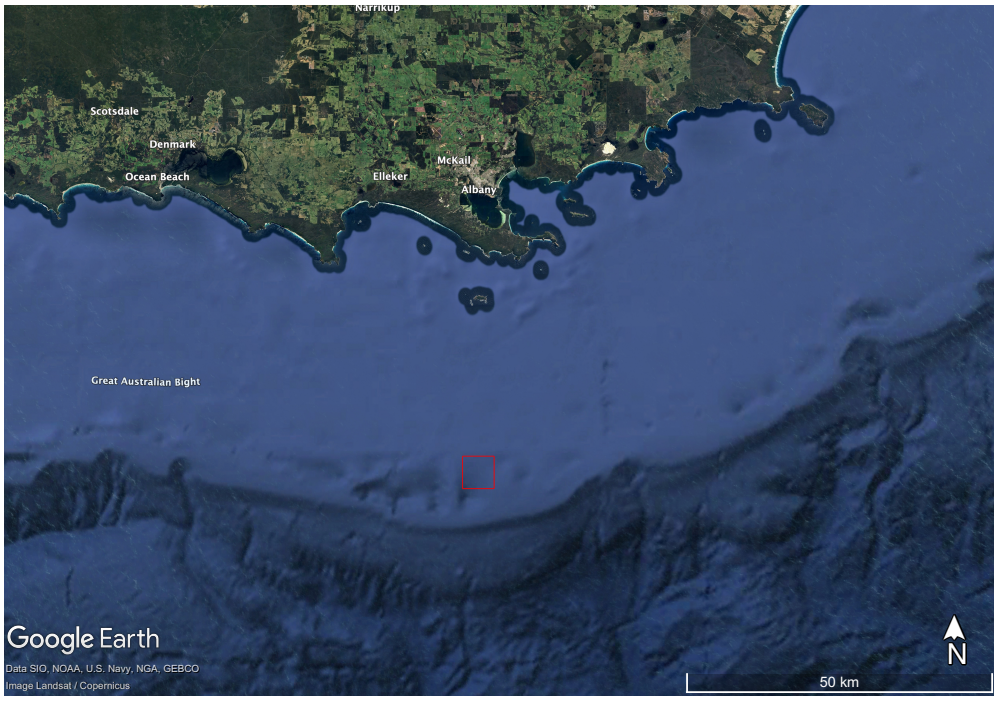

Figure 2.9: Geographic overview of the study area in Australia

Considering that this site was already chose by Carnegie and ARENA, it's possible to assess that the bathymetry and sea condition are favourable for the CETO 6 installation.

2.3.4 North Sea, Germany region

The North Sea, and in particular the GODE I & II wind farm area in the German sector, has been selected as a representative site to analyse WEC performance under

moderate wave energy conditions. Unlike other locations considered in this study, this site is characterised by a relatively lower wave energy potential, making it suitable for comparative analyses with more energetic environments. This allows the influence of wave energy availability on device performance to be systematically assessed. As shown in Figure 2.10, the selected area is located in the German sector of the North Sea, where several offshore wind farms are already installed. A square area of 25 km^2 centred around the GODE I & II wind farm has been considered for the analysis. The water depth at the site ranges from 35 to 55 m, making it suitable for the deployment of point absorber WECs.

The geographical coordinates of the selected study area are reported in Table 2.6.

Table 2.6: Geographical coordinates of the selected study area in Germany

Vertices	**Deciaml Coordinates (DD)**	**Sexagesimal Coordinates (DMS)**
North-West (NW)	54.0975° N, 6.9686° E	54°05′51″ N, 6°58′07″ E
North-East (NE)	54.0975° N, 7.0452° E	54°05′51″ N, 7°02′43″ E
South-East (SE)	54.0525° N, 7.0452° E	54°03′09″ N, 7°02′43″ E
South-West (SW)	54.0525° N, 6.9686° E	54°03′09″ N, 6°58′07″ E

Figure 2.10: Geographic overview of the study area in Germany

Chapter 3

Methodological Framework

3.1 Tools and Software used

The development of this research relied on multiple tools to characterise sea-state conditions, assess WEC converter performance, and process the data needed to compute performance metrics.

3.1.1 Copernicus

The Copernicus platform was used to obtain the sea-state data required to construct the sea-state occurrence matrix and the wave energy power density matrix, which are essential for evaluating WEC performance at a given site. The datasets were downloaded from the Copernicus Marine Data Store [20], part of the European Union's Earth observation programme. In this study, the Global Ocean Waves Reanalysis dataset (WAVERYS) was adopted. Based on the MFWAM third-generation wave model, it provides wave parameters such as significant wave height and mean wave period on a regular 1/5° grid with a 3-hour temporal resolution. Due to the spatial resolution of approximately 22 km (north–south) and 18 km (east–west), it was not possible to extract data exclusively for the exact area of interest. Therefore, the data used correspond to the grid cell containing the selected location, as discussed in Chapter 2.

3.1.2 NEMOH

NEMOH is an open-source boundary element method (BEM) code used for the computation of first-order wave loads on offshore structures. Developed at Ecole Centrale de Nantes, it is widely applied in marine hydrodynamics to evaluate the dynamic response of floating systems and the performance of wave energy converters (WECs). The numerical approach is based on linear potential flow theory, assuming an incompressible, inviscid, and irrotational fluid. The wetted surface of the structure is discretised into panels, and the boundary integral equations are solved to obtain the velocity potential. The geometry, created in Fusion360, is converted

into the format required by NEMOH. From this solution, NEMOH computes radiation and diffraction effects, providing key hydrodynamic coefficients such as added mass, radiation damping, and wave excitation forces. These frequency-dependent parameters are used to define the equations of motion and to evaluate the Response Amplitude Operator (RAO). Additional post-processing is performed in MATLAB or Python to analyse the dynamic response and overall performance of the device under different wave conditions [23].

3.1.3 MATLAB

MATLAB is used as the main computational tool for the simulations, analysis, and optimisation carried out in this study. In particular, it is employed to investigate the behaviour of the two WEC types in the frequency domain. The entire analysis workflow is developed within this environment, starting from the initial design phase, through the optimisation and scaling procedures, and culminating in the evaluation and interpretation of the results. MATLAB is also used to generate all plots and figures, providing a clear visual representation of the obtained results.

3.2 Workflow

All the tools described in the previous section are used in sequence to analyze the performance of a Wave Energy Converter. Due to different formats and data file between the tools some conversions are required leading to the full work path that now will be explained.

1. The geometry of the WEC is designed using Fusion 360, and the final model is exported as a stereolithography (.stl) file. The geometry considered is a simplified representation of the real structure.

2. The .stl file of the WEC geometry, already meshed using the dedicated meshing tool in Fusion 360, is then converted into a mesh (.msh) file using GMSH, a software that allows the creation and modification of meshes starting from a CAD geometry.

3. Since NEMOH requires a mesh in its specific format (.dat) to perform the hydrodynamic analysis, a MATLAB script is used to convert the .msh file into a .dat file. The script also rescales the geometry dimensions from millimeters, used in the CAD model, to meters, which are required for the hydrodynamic simulations.

4. Once the scaled .dat file is obtained, NEMOH is executed through Python to compute the required hydrodynamic coefficients.

5. After the NEMOH output files are generated, the results are imported into MATLAB, where the main analysis of the wave energy converters is carried out.

6. For each simulation, the average absorbed power is computed and stored, allowing the construction of the power matrix of the WEC.

7. Using the power matrix together with the sea state occurrence matrix of the selected location, the AEP can be calculated. This value can also be compared with the Annual Energy Potential estimated in Chapter 2.

8. Once the AEP of the WEC at the reference location is obtained, an optimization procedure is performed. This process focuses on the PTO parameters of the WEC in order to determine the optimal configuration for both devices in the default location.

9. Subsequently, scaling and economic analyses are carried out to identify the optimal geometric parameters of each WEC for the other locations considered in the study. In particular, a comparison between two methods is performed. On one hand, the AEP of the two devices at different locations is estimated by scaling the power matrix, as commonly done in the literature, using the Froude scaling. On the other hand, a direct approach is adopted obtaining the AEP by running the code used for the standard case across all combinations of radius and location. This enables a direct comparison between the two methodologies.

10. A structural and sensitivity analysis is then performed to determine the minimum structural thickness required to withstand the applied loads, as well as to evaluate how this thickness varies with changes in the device radius. In the case of Froude scaling, the loads are derived by scaling those of the reference (standard) configuration. Conversely, when physical scaling is adopted, the loads are directly obtained from the NEMOH results corresponding to each specific case.

11. The costs are estimated considering the structural thickness, the device radius, the resulting mass and the AEP consideing the two methods. This allow the calculation of the Levelised Cost of Energy (LCOE) and other relevant economic indicators, related to other components of the WEC.

12. Finally, the most suitable device configuration is identified for each location.

3.3 Evaluation metrics

After evaluating the performance of the different WECs and computing the power matrix, together with the AEP, an economic analysis is conducted to assess whether the use of a specific type of WEC is financially viable and profitable for the given sea location. To examine the project from an economic perspective, standard economic indicators are considered.

3.3.1 CAPEX

Capital Expenditure (CapEx) represents the total upfront cost that a company must invest to initiate a project. For WEC obtaining these data is challenging because the technology is still relatively new, and companies typically do not disclose their full economic information. This cost is not only composed by the device cost but also all the costs concerning the moorings, the grud connection and the installation costs.

3.3.2 OPEX

Operational Expenditure (OpEx) includes all those costs related to the operational and maintenance, not only of the WEC itself but also of all the the operations related to the maintenance of all that equipment which allow the WEC to work in a proper way, like the moorings, the cables for the transmission of the produced energy.

3.3.3 LCOE

The LCOE is a fundamental economic parameter which takes into account all the costs associated to the construction and maintenance, dividing them for the energy produced by a plant during its whole lifetime. The LCOE takes into account the interest rate, which depends on the market and also on the incentives and programme that different countries, where the location of the WEC is set, must incentivise investment in renewable energy technology and in particular in wave energy technology, which are still a novel technology, with some difficult aspects but a very high potential. It is a very important parameter because it allows the comparison between different technologies.

The LCOE is calculated as follow:

$$\mathrm{LCOE} = \frac{\mathrm{PV}_{\mathrm{cost}}}{\mathrm{PV}_{\mathrm{energy}}} \tag{3.1}$$

where *PV (Present Value)* represents the value of future cash flows discounted to year zero using a discount rate r, accounting for the time value of money.

The discount rate r is optimistically considered equal to 0.05 (5%) [24].

For a project lifetime of n years:

$$\mathrm{PV}_{\mathrm{cost}} = CAPEX_0 + \sum_{t=1}^{n} \frac{OPEX_t}{(1+r)^t} + \frac{DECOM}{(1+r)^n} \tag{3.2}$$

$$\mathrm{PV}_{\mathrm{energy}} = \sum_{t=1}^{n} \frac{E_t}{(1+r)^t} \tag{3.3}$$

In this model:

- $CAPEX_0$ is the upfront investment at year 0,
- $OPEX_t = f_{\mathrm{opex}} \cdot CAPEX_0$ is the annual operational expenditure,
- $DECOM$ is the decommissioning cost at the end of life,
- $E_t = AEP_{\mathrm{net}}$ is the annual net energy production, including availability effects.

The final LCOE is typically expressed in €/MWh.

3.4 Wave dataset

As mentioned in the previous paragraph, the Copernicus database is used to retrieve sea-state data, which are then used to characterise the wave climate, one of the most critical factors in the analysis. The key parameters for describing the sea state are the significant wave height (H_s) and the characteristic time period, which can be expressed either as the zero up-crossing period or the peak period (T_z). By considering these two parameters, it is possible to construct a sea state occurrence matrix, which indicates the probability of specific combinations of significant wave height and time period occurring.

The sea state occurrence matrices for the selected locations are shown in Figures 3.1–3.4.

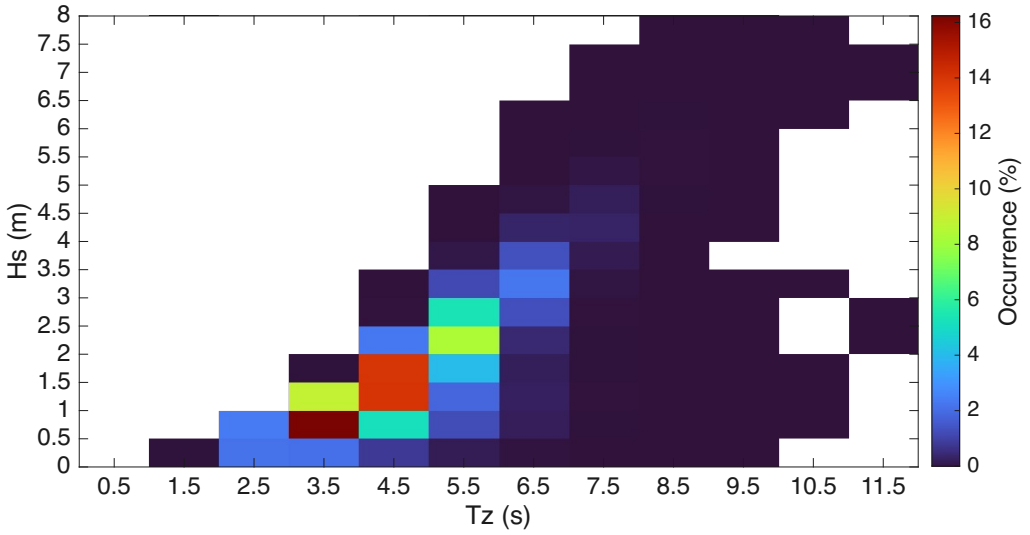

Figure 3.1: Sea state occurrence matrix of selected area in Germany

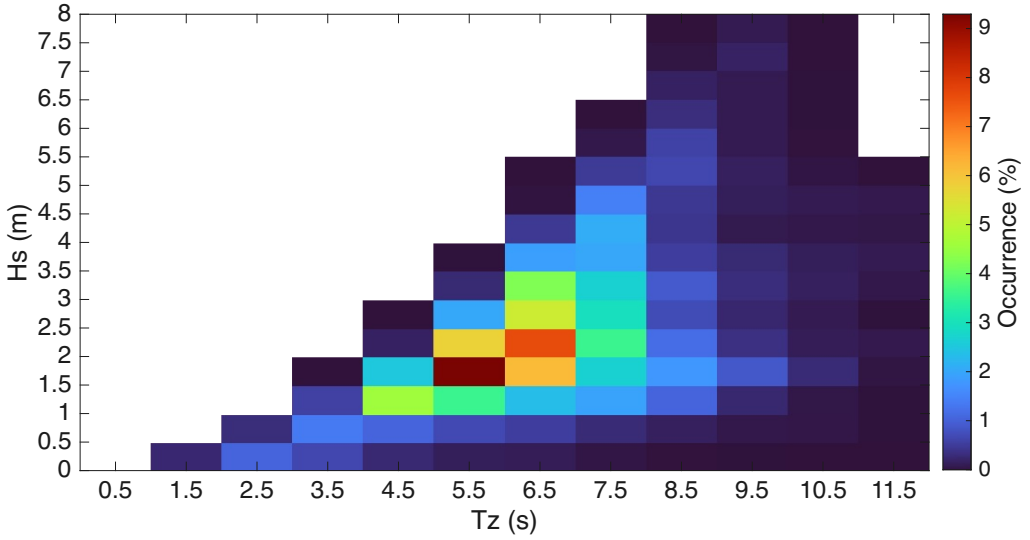

Figure 3.2: Sea state occurrence matrix of selected area in Scotland

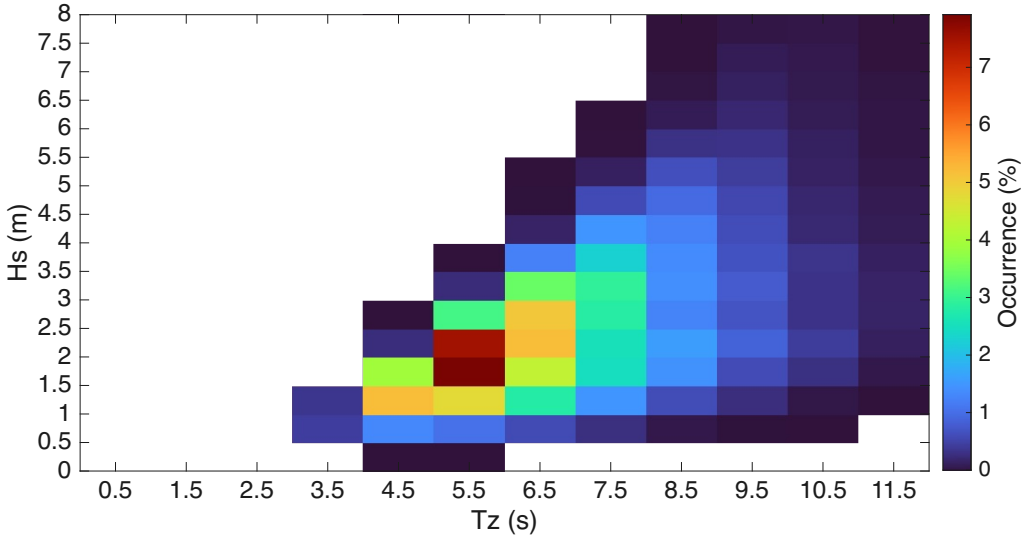

Figure 3.3: Sea state occurrence matrix of the selected area in Portugal

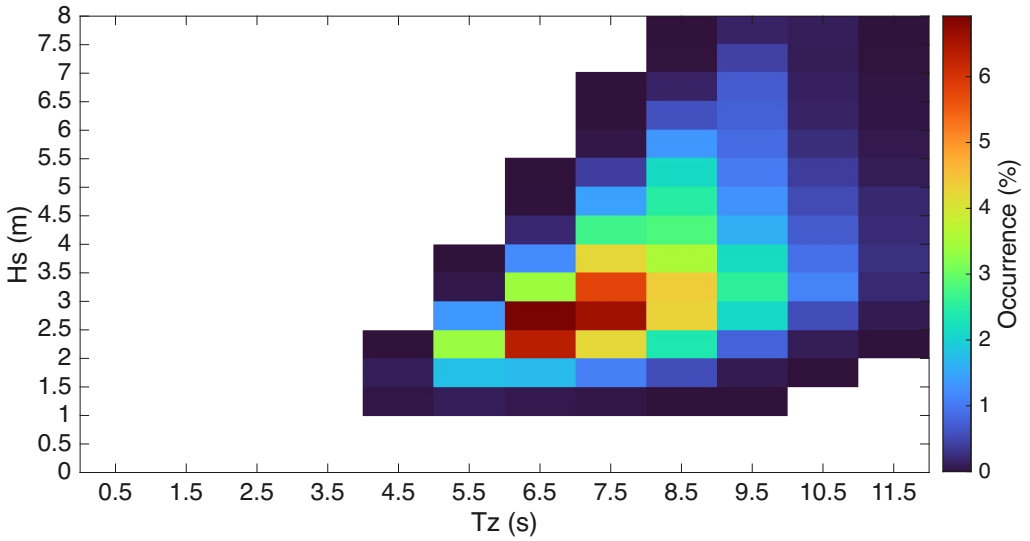

Figure 3.4: Sea state occurrence matrix of selected area in Australia

The sea state occurrence for the wave farm location in Figueira da Foz, Portugal, and for the GODE I & II wind farms in the North Sea are presented here as examples. The different cells in the matrix change color according to their corresponding percentage values. From the images, it is also possible to observe the contrast between the Atlantic Ocean at the Portuguese site, which exhibits a wider range of wave conditions, and the North Sea site, which, due to its more stable sea conditions, shows higher percentages for a smaller combination of wave heights and periods, resulting in a narrower spectrum. Once the occurrence matrix is calculated, the energy density matrix for different locations can be derived, providing a detailed assessment of the site's energy potential. This matrix is obtained by multiplying the occurrence matrix with the power density matrix, yielding the energy density in MWh per month or per year. The power density matrix itself is determined through theoretical calculations.

In particular then, the summation of the value of all the cell of the Energy Density matrix gives the Average wave energy potential.

The energy density matrices for the selected locations are shown in Figures 3.5–3.8.

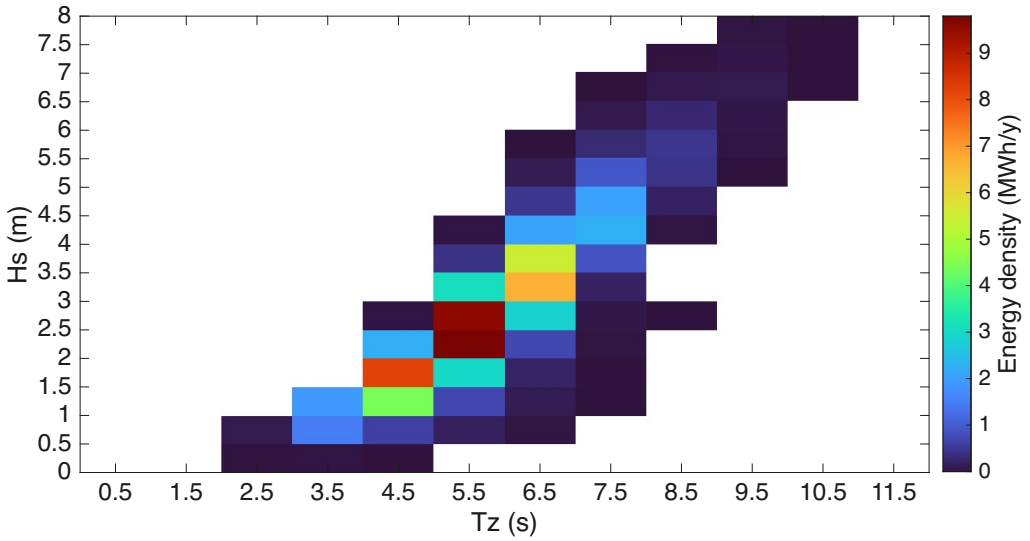

Figure 3.5: Energy density matrix of the selected area in Germany

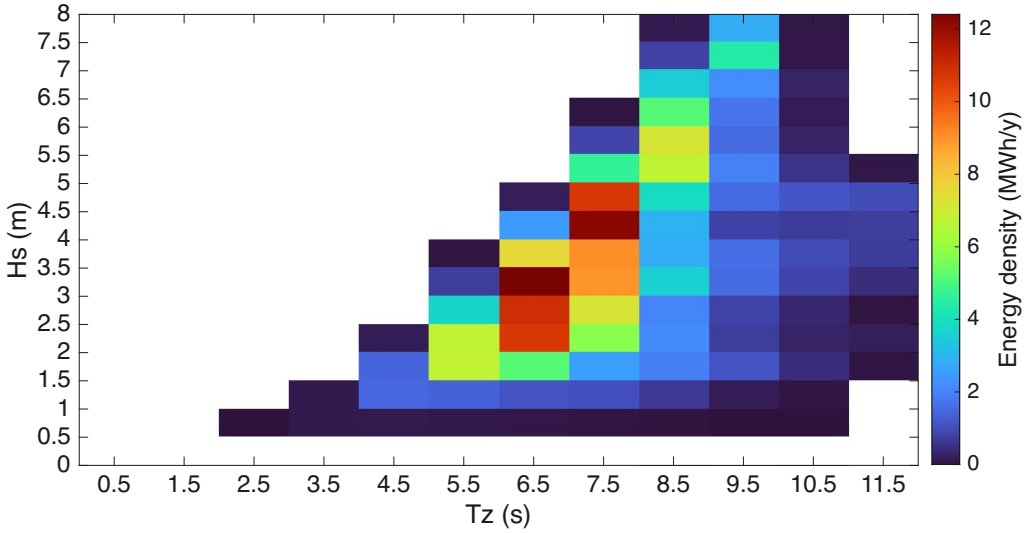

Figure 3.6: Energy density matrix of the selected area in Scotland

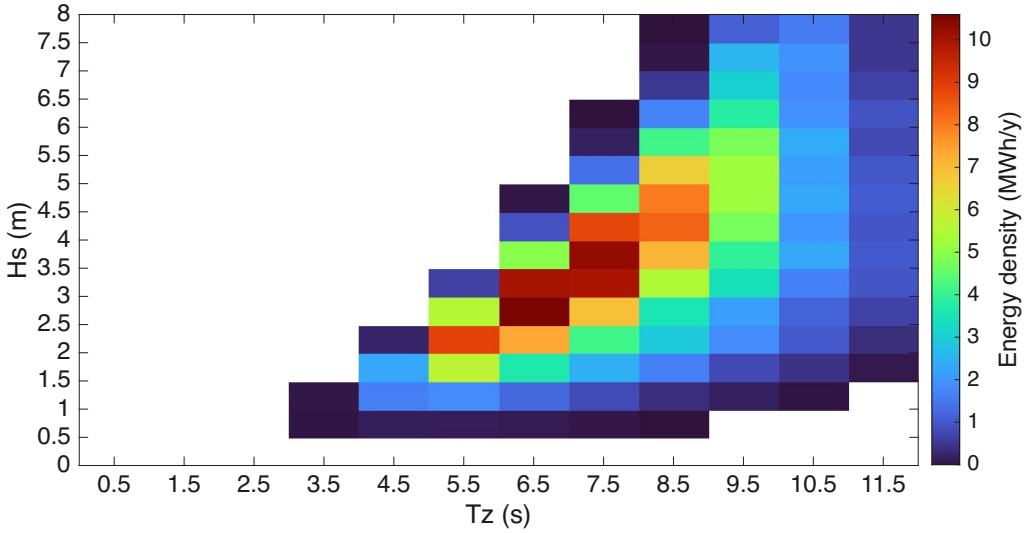

Figure 3.7: Energy density matrix of the selected area in Portugal

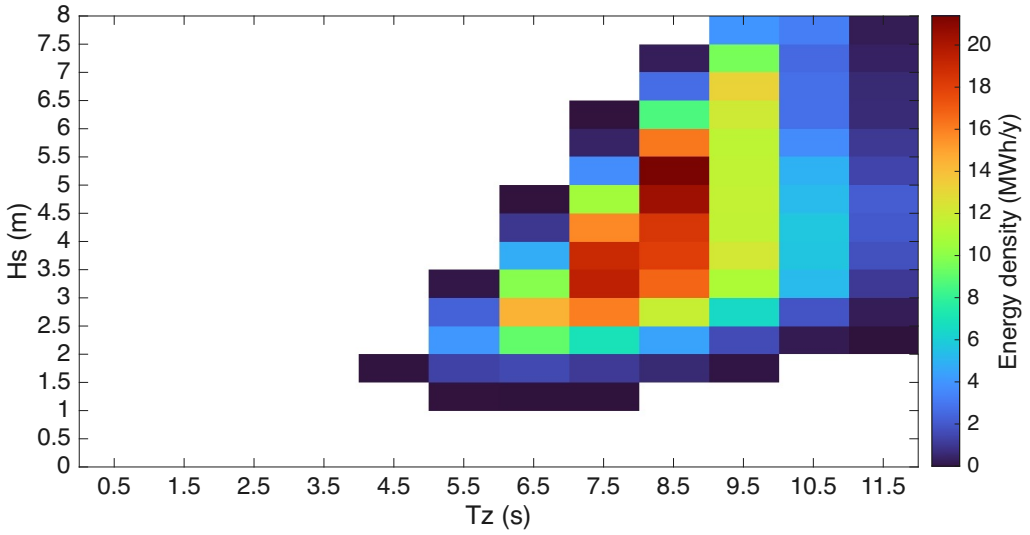

Figure 3.8: Energy density matrix of the selected area in Australia

As written before, the summation of the value of all the cell of the Energy Density matrix gives the Average wave energy potential. In this case, proceeding with that calculation the following values are obtained for different location, which represent Annual energy Potential

- Figueira Da Foz, Portugal: 255.26 MWh/m/y
- MORAY East offshore wind farm, North Sea, Scotland: 231.92 MWh/m/y
- Albany, Australia: 472.36 MWh/m/y
- GODE I and IIoffshore wind farm, North Sea, Germany: 74.097 MWh/m/y

These results represent the potential wave energy of each location, without yet considering the technology.

Chapter 4

Hydrodynamic Modelling and Numerical Simulations

4.1 Metrics used in the WECs design

The main metrics used in the design of a WEC include the Power Matrix, the AEP in the selected location, considering so the sea state of the location, the Capacity Factor (CF) and the Average Power.

4.1.1 Power matrix

The Power Matrix is a tabulated representation of the average power absorbed by a wave energy converter over a set of discrete sea states, defined by combinations of significant wave height and characteristic wave period. Each entry of the matrix corresponds to the mean power output obtained when the WEC is excited by a standard wave spectrum (e.g., JONSWAP) associated with that sea state, under a specified control strategy. The power matrix thus characterises the device performance across the wave climate and is a fundamental input for estimating the AEP.

4.1.2 Annual Energy Production

The AEP is one the most important parameters about the production analysis of a Wave Energy Converter. The parameter is calculated, exploiting the Energy Density matrix obtained multiplying the Occurrence Sea State matrix of the considered location and Power matrix of the wave energy converter itself, multiplying so the average power for a certain sea state with the number of hours in a year having that particular sea state condition. The AEP is then computed as the summation of every bin of the Energy density matrix.

$$AEP = \sum_{i,j} P(H_{s,i}, T_{p,j}) \times \text{hours}(H_{s,i}, T_{p,j})[\frac{Wh}{year}] \tag{4.1}$$

where:

- $H_{s,i}$ is the significant wave height
- $T_{p,j}$ is the peak period

4.1.3 Average Power

The average Power is then calculated dividing the Annual Energy Production with the hours in a year.

$$P_{avg} = \frac{AEP}{8760}[W] \tag{4.2}$$

where:

- AEP is the Annual Energy Production [Wh/year]
- 8760 is the number of hours in a year [h/year]

4.1.4 Capacity Factor

The capacity factor (also called load factor) is the ratio between the average produced power and the installed power on the WEC. It describes the utility rate of the PTO system and is very interesting as it gives an idea of what the WEC delivers (average produced power) and what it costs (driven by installed power). However, this value is also wave condition dependant (location).

4.2 WECs design

4.2.1 CorPower

The CorPower wave energy converter is analysed in the frequency domain using linear hydrodynamic coefficients obtained from NEMOH. Added mass, radiation damping, excitation force and hydrostatic stiffness are extracted and post-processed to ensure physical consistency, in particular enforcing non-negative radiation damping and robust interpolation over the frequency range of interest. The system response is evaluated through the linear Response Amplitude Operator, which is combined with a JONSWAP spectrum to represent irregular sea states. Annual Energy Production is then computed by integrating the absorbed power over the full wave climate using occurrence matrices.

The PTO system is modelled as a linear combination of damping and stiffness, allowing both dissipative and reactive control. Absorbed power is computed from

the viscous damping contribution, while the reactive stiffness modifies the phase relationship between excitation force and velocity, enabling improved energy capture near resonance. Compared to an idealised PTO model, this formulation explicitly accounts for physical limitations of the conversion system.

Base Case

In the base case, the only features implemented to obtain realistic results are the constraints imposed on the PTO in terms of maximum stroke, velocity, force, and rated electrical power. Peak responses are estimated from spectral RMS values using a conservative peak factor, ensuring that extreme motions and loads are not underestimated. Rather than discarding sea states that violate these limits, a derating strategy is adopted. Specifically, when one or more constraints are exceeded, the absorbed power is not abruptly cut off; instead, it is progressively reduced so that it remains within the allowable rated power of the PTO. In this way, the system output is smoothly limited, mimicking the behaviour of a real PTO operating in saturation, where performance is capped but the device continues to produce power under constrained conditions.

In the frequency-domain model, mechanical constraints are enforced through an explicit power derating strategy rather than by discarding non-compliant sea states. For each sea state, the heave response is computed in terms of root-mean-square (RMS) displacement and velocity from the response amplitude operator and the wave spectrum. Representative peak values are then estimated using a peak factor α_{pk}, such that $x_{\mathrm{pk}} = \alpha_{\mathrm{pk}} x_{\mathrm{rms}}$ and $v_{\mathrm{pk}} = \alpha_{\mathrm{pk}} v_{\mathrm{rms}}$. The corresponding peak PTO force is estimated as $F_{\mathrm{pk}} \approx K_{\mathrm{pto}} x_{\mathrm{pk}} + B_{\mathrm{pto}} v_{\mathrm{pk}}$.

The response is compared against predefined mechanical limits on stroke, velocity, and force, namely $X_{\max}$, $V_{\max}$, and $F_{\max}$. When any of these limits is exceeded, a derating factor $d \in (0, 1]$ is applied to the absorbed power, defined as

$$d = \min \left[\left(\frac{X_{\max}}{x_{\mathrm{pk}}} \right)^2, \left(\frac{V_{\max}}{v_{\mathrm{pk}}} \right)^2, \left(\frac{F_{\max}}{F_{\mathrm{pk}}} \right)^2 \right]. \tag{4.3}$$

where:

- X_{max}, V_{max}, F_{max} are the mechanical limits on stroke, velocity, and PTO force, respectively
- $x_{pk} = \alpha_{pk}\, x_{rms}$ is the estimated peak displacement
- $v_{pk} = \alpha_{pk}\, v_{rms}$ is the estimated peak velocity

- $F_{pk} \approx K_{pto}\, x_{pk} + B_{pto}\, v_{pk}$ is the estimated peak PTO force
- α_{pk} is the peak factor used to estimate extreme values from RMS quantities

The mean absorbed power for the sea state is then scaled as $\bar{P}_{\text{eff}} = d\,\bar{P}$. Sea states for which $d < 1$ are counted as derated bins (reported as `fail_bins`), indicating operating conditions where the unconstrained response would exceed mechanical limits and active limitation is required. This approach allows the optimization to retain all sea states in the annual energy calculation while explicitly accounting for realistic operational constraints. A derating factor equal to 0.75 is assumed.

A baseline PTO configuration is defined with moderate damping and limited reactive action, representing a conservative and robust design. This case exhibits relatively low absorbed power per sea state and limited engagement of the PTO constraints, resulting in a stable but sub-optimal Annual Energy Production.

The rated power is set equal to 850kW, following the data found in literature [25].

The power matrix and the energy density, from which is possible to obtain the AEP, for the base case, are displayed in Figure 4.1 and 4.2.

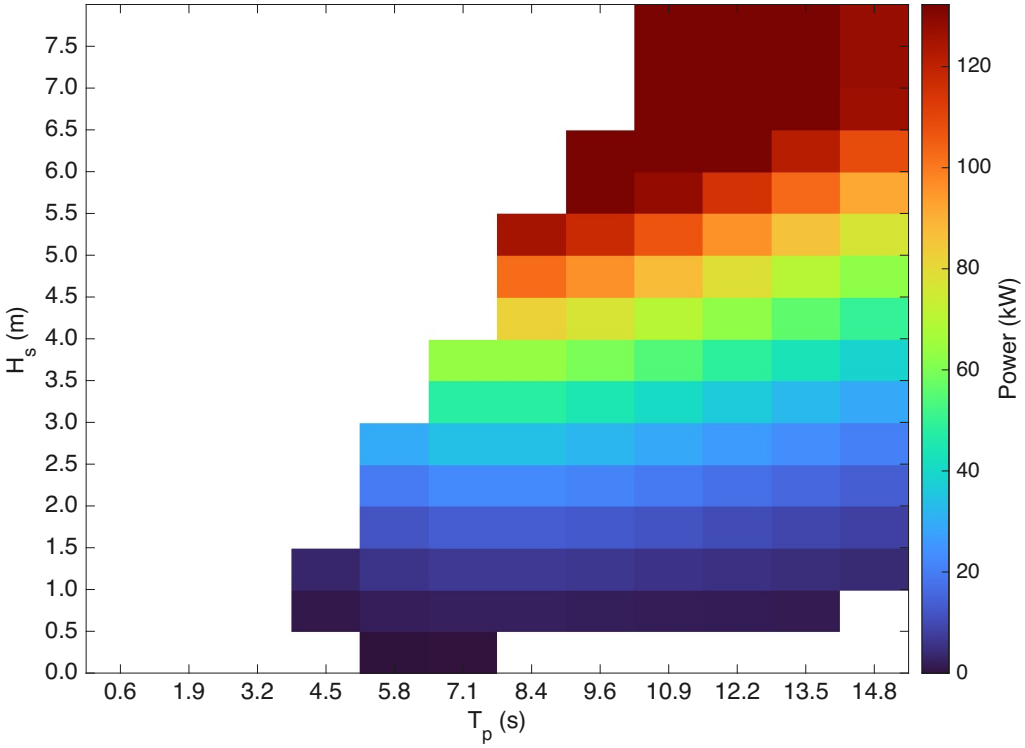

Figure 4.1: Power matrix of CorPower for the base case in Portugal

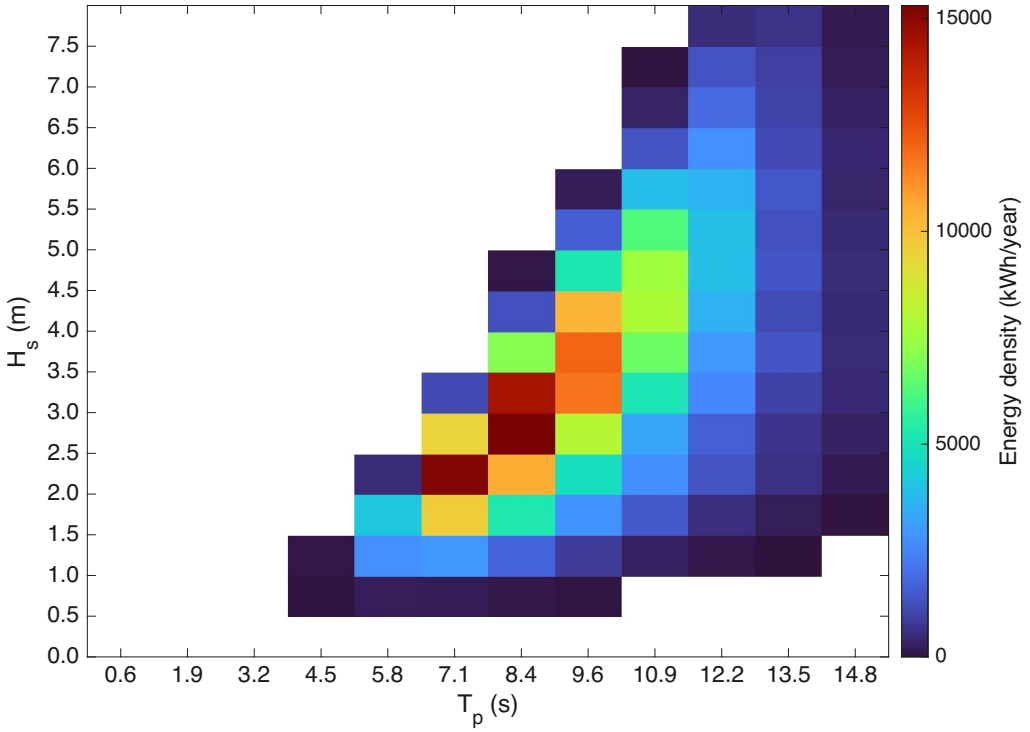

Figure 4.2: AEP analysis of CorPower for the base case in Portugal

Optimised Case

The optimised PTO configuration is obtained through a grid-based search over damping and stiffness parameters, with the objective of maximising Annual Energy Production under the imposed constraints. The optimal solution features higher damping and significant reactive stiffness, leading to increased response in energetic sea states. As a consequence, the PTO operates closer to its physical limits and constraint activation becomes more frequent. However, thanks to the derating strategy, system responses remain bounded and the rated power is not exceeded.

The PTO optimization is carried out in the frequency domain by maximizing the annual absorbed energy $\mathrm{AEP}(K_{\mathrm{pto}}, B_{\mathrm{pto}})$ over a regular grid of PTO stiffness K_{pto} and damping B_{pto}.

The device heave dynamics are modeled through the complex mechanical impedance

$$Z(\omega) = -\omega^2(M_{\mathrm{body}} + A(\omega)) + i\omega(B(\omega) + B_{\mathrm{pto}} + B_{\mathrm{moor}}) + (C_{\mathrm{hs}} + K_{\mathrm{moor}} + K_{\mathrm{pto}}), \quad (4.4)$$

where:

- M_{body} is the rigid body mass [kg]
- $A(\omega)$ is the frequency-dependent added mass [kg]
- $B(\omega)$ is the frequency-dependent radiation damping [N·s/m]

- B_{pto} is the PTO damping coefficient [N·s/m]
- B_{moor} is the mooring damping coefficient [N·s/m]
- C_{hs} is the hydrostatic restoring stiffness [N/m]
- K_{moor} is the mooring stiffness [N/m]
- K_{pto} is the PTO stiffness [N/m]
- ω is the angular wave frequency [rad/s]

and the heave RAO is

$$\mathrm{RAO}(\omega) = \frac{F_{\mathrm{exc}}(\omega)}{Z(\omega)}. \tag{4.5}$$

where:

- $F_{exc}(\omega)$ is the complex wave excitation force in heave [N]
- $Z(\omega)$ is the mechanical impedance of the system [N·s/m]

For each sea state (H_s, T_p) from the site scatter diagram, a JONSWAP spectrum $S_\eta(\omega; H_s, T_p)$ is generated. The displacement and velocity spectra are

$$S_x(\omega) = |\mathrm{RAO}(\omega)|^2 S_\eta(\omega), \quad S_v(\omega) = \omega^2 S_x(\omega), \tag{4.6}$$

where:

- $S_x(\omega)$ is the displacement spectral density [m^2/(rad/s)]
- $S_v(\omega)$ is the velocity spectral density [$\mathrm{m}^2/\mathrm{s}^2$/(rad/s)]
- $RAO(\omega)$ is the Response Amplitude Operator in heave [m/m]
- $S_\eta(\omega;\, H_s, T_p)$ is the JONSWAP wave energy spectrum [m^2/(rad/s)]

from which variances $m_{0x} = \int S_x(\omega)\, d\omega$ and $m_{0v} = \int S_v(\omega)\, d\omega$ are obtained by numerical integration. Peak values are estimated as $x_{\mathrm{pk}} = \alpha_{\mathrm{pk}}\sqrt{m_{0x}}$, $v_{\mathrm{pk}} = \alpha_{\mathrm{pk}}\sqrt{m_{0v}}$, and an analogous force spectrum is used to derive F_{pk}.

In the just described formula the different members indicate:

- $m_{0x} = \int S_x(\omega)\, d\omega$ is the variance of the displacement response [m^2]
- $m_{0v} = \int S_v(\omega)\, d\omega$ is the variance of the velocity response [$\mathrm{m}^2/\mathrm{s}^2$]
- $x_{pk} = \alpha_{pk}\sqrt{m_{0x}}$ is the estimated peak displacement [m]
- $v_{pk} = \alpha_{pk}\sqrt{m_{0v}}$ is the estimated peak velocity [m/s]

- F_{pk} is the estimated peak PTO force, derived analogously from the force spectrum [N]
- α_{pk} is the peak factor used to convert RMS values into representative extreme values [-]

The mean mechanical power absorbed by the PTO in a given sea state is

$$P_{\text{abs}} = \int \frac{1}{2} B_{\text{pto}}\, \omega^2 |\text{RAO}(\omega)|^2 S_\eta(\omega)\, d\omega, \tag{4.7}$$

where:

- B_{pto} is the PTO linear damping coefficient [N·s/m]
- $RAO(\omega)$ is the heave Response Amplitude Operator [m/m]
- $S_\eta(\omega)$ is the incident wave energy spectrum [m^2/(rad/s)]
- ω is the angular wave frequency [rad/s]

and the corresponding electrical active power is $P_{\text{el}} = \eta_{\text{pto}} P_{\text{abs}}$, where η_{PTO} is the electrical efficiency of the PTO. A reactive power metric is obtained from the PTO stiffness as

$$Q_{\text{el}} = \eta_{\text{pto}} \int \frac{1}{2} |K_{\text{pto}}|\, \omega\, |\text{RAO}(\omega)|^2 S_\eta(\omega)\, d\omega, \tag{4.8}$$

where:

where:

- η_{pto} is the PTO efficiency [-]
- K_{pto} is the PTO stiffness coefficient [N/m]
- $RAO(\omega)$ is the heave Response Amplitude Operator [m/m]
- $S_\eta(\omega)$ is the incident wave energy spectrum [m^2/(rad/s)]
- $S = \sqrt{P_{el}^2 + Q_{el}^2}$ is the apparent power [W]

leading to the apparent power $S = \sqrt{P_{\text{el}}^2 + Q_{\text{el}}^2}$.

Mechanical limits on stroke, velocity and force,

$$x_{\text{pk}} \le X_{\max}, \quad v_{\text{pk}} \le V_{\max}, \quad F_{\text{pk}} \le F_{\max}, \tag{4.9}$$

where:

- x_{pk} is the estimated peak displacement [m]

- v_{pk} is the estimated peak velocity [m/s]
- F_{pk} is the estimated peak PTO force [N]
- X_{max}, V_{max}, F_{max} are the prescribed mechanical limits on stroke, velocity and force, respectively

are imposed through a continuous derating factor $0 \leq d \leq 1$ applied to P_{el} and Q_{el}. Electrical constraints are enforced by capping real power at P_{rated} and, in the penalized case, capping apparent power at $S_{\text{rated}} = \kappa_S P_{\text{rated}}$, again via derating when $P_{\text{el}} > P_{\text{rated}}$ or $S > S_{\text{rated}}$.

For each $(K_{\text{pto}}, B_{\text{pto}})$ on the grid, the derated mean powers over all sea states form a power matrix $P(H_s, T_p)$. The corresponding annual energy is

$$\text{AEP}(K_{\text{pto}}, B_{\text{pto}}) = \sum_{i,j} P(H_{s,i}, T_{p,j}) \, \text{Occ}_{ij} \, h_{\text{year}}, \tag{4.10}$$

where:

- $P(H_{s,i}, T_{p,j})$ is the derated mean absorbed power for sea state (i, j) [W]
- Occ_{ij} is the annual occurrence probability of sea state (i, j) [-]
- h_{year} is the number of hours per year [h/year]
- K_{pto}, B_{pto} are the PTO stiffness [N/m] and damping [N·s/m] coefficients

The optimised case is defined by

$$(K^*_{\text{pto}}, B^*_{\text{pto}}) = \arg \max_{(K_{\text{pto}}, B_{\text{pto}})} \text{AEP}(K_{\text{pto}}, B_{\text{pto}}) \tag{4.11}$$

where:

- K^*_{pto}, B^*_{pto} are the optimal PTO stiffness [N/m] and damping [N·s/m]
- $AEP(K_{pto}, B_{pto})$ is the annual energy production as a function of the PTO parameters [Wh/year]
- The optimization is subject to all mechanical constraints on stroke, velocity, force, and electrical power

under all mechanical and electrical constraints, and its output includes the optimal AEP, power matrix, capacity factor, peak absorbed power and key RAO-based response indicators.

It is noted that the optimised PTO configuration operates close to the imposed mechanical limits in a significant portion of the sea states, as indicated by the number

of derated bins (34 out of 97). Therefore, the achieved increase in annual energy production is obtained through an actively constrained operation, where mechanical limits are frequently reached and enforced via power derating. The obtained power matrix and energy density matrix, for the optimised case, are displayed in Figure 4.3 and 4.4.

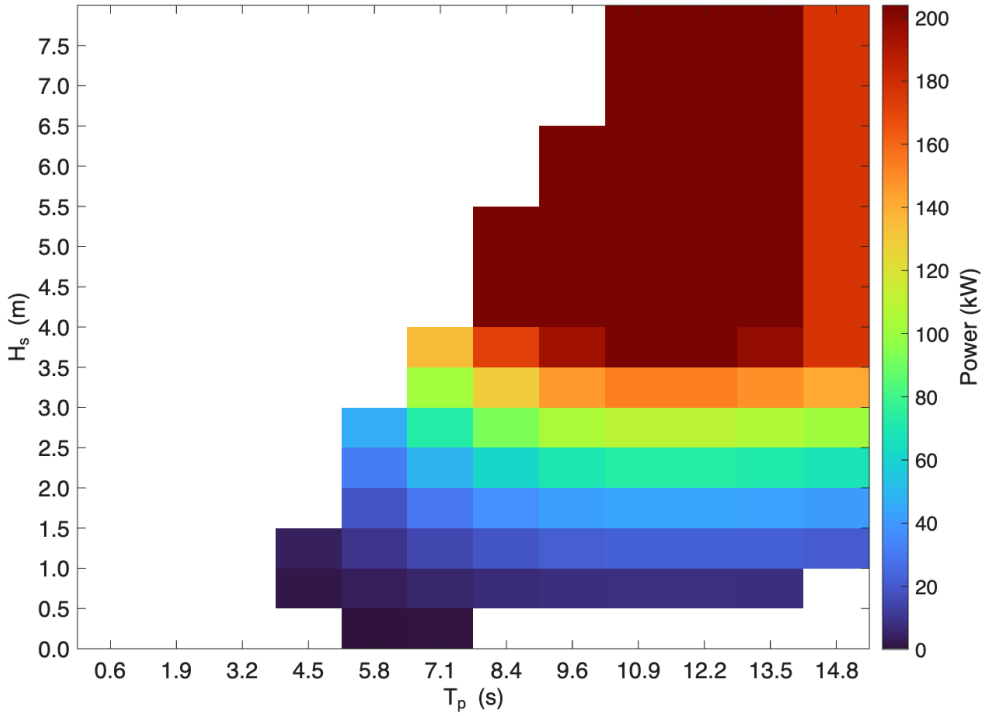

Figure 4.3: Power matrix of CorPower for the optimised case in Portugal

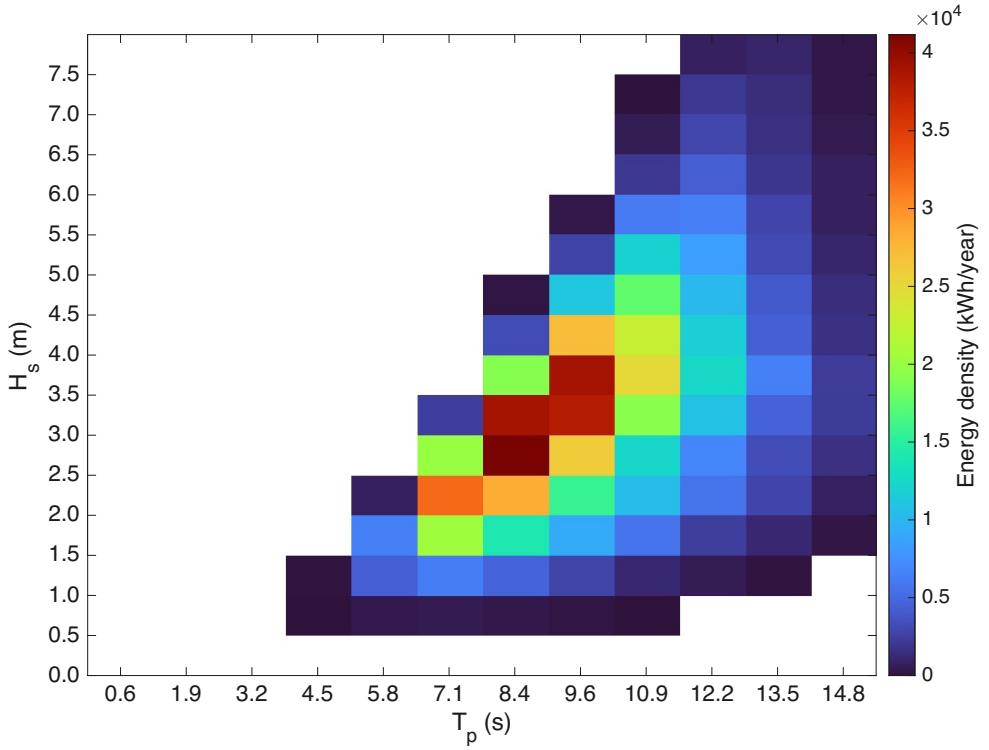

Figure 4.4: AEP analysis of CorPower for the optimised case in Portugal

The comparison between the baseline and optimised configurations highlights the importance of including PTO constraints in the optimisation process. While unconstrained models tend to overestimate achievable energy capture by allowing unrealistically large motions and forces, the constrained and derated model provides a more accurate representation of deployable performance. The observed reduction in Annual Energy Production compared to idealised results is therefore physically meaningful and expected. At the same time, the optimised PTO still achieves a substantial gain over the baseline case, demonstrating the effectiveness of reactive control when properly limited.

The optimization results reported above show that the highest annual energy production (AEP) is obtained for a PTO configuration with a strongly negative stiffness and relatively high damping, which corresponds to an "aggressive" reactive control strategy with pronounced bidirectional power flow in the PTO. This behaviour is consistent with classical unconstrained optimal control formulations for wave energy converters, where the PTO force is allowed to both absorb and supply power in order to maximize the time-integral of absorbed energy. In physical terms, the PTO occasionally operates in motoring mode, injecting energy into the mechanical system so as to shape the oscillation and recover a larger amount of energy later in the cycle, leading to an overall increase in net absorbed power.

However, this ideal behaviour presupposes an actuator with essentially unbounded force, stroke and power ratings, which is not compatible with realistic PTO technologies. As highlighted in recent reviews and performance studies, bidirectional operation and high peak-to-average power ratios significantly increase the required rating of converters, electrical machines and auxiliary storage, with a direct impact on capital cost, component sizing and reliability. For this reason, modern WEC control formulations increasingly incorporate explicit constraints or penalties on PTO force, torque and instantaneous power, in order to balance energy maximization with limitations imposed by hardware and structural design.

In this work, the introduction of a penalty on the apparent power S of the PTO, enforced via a rated value $S_{\text{rated}} = \kappa_S P_{\text{rated}}$, follows exactly this "power-to-load" philosophy. The penalty term discourages solutions that require apparent power levels substantially beyond a prescribed multiple of the nominal rating, thereby embedding the economic and technological costs of oversizing the PTO into the control objective itself. The sensitivity analysis over different values of κ_S shows that, for the parameter ranges considered here, the optimal settings that maximize AEP can be achieved without significant saturation of the apparent power constraint ($\text{sat}_S = 0$), indicating that the selected rating is sufficient to support the reactive control strategy while remaining consistent with plausible PTO design limits. This

confirms that the proposed control and penalty structure are not only theoretically sound but also aligned with current trends in practical optimal control design for wave energy converters [26].

Moorings

When $B_{\text{moor}} = 0$, the mooring system in heave is modeled as:

- purely elastic (only K_{moor}),
- lossless (no energy dissipation).

Introducing a nonzero B_{moor} adds a dissipative component to the mooring force:

$$F_{\text{moor}} = -K_{\text{moor}}x - B_{\text{moor}}\dot{x} \tag{4.12}$$

where:

- K_{moor} is the mooring stiffness [N/m]
- B_{moor} is the mooring damping coefficient [N·s/m]
- x is the heave displacement [m]
- $\dot{x}$ is the heave velocity [m/s]

In the frequency domain, this term appears in the dynamic impedance as:

$$Z(\omega) = -(M + A)\omega^2 + i\omega(B_{\text{rad}} + B_{\text{pto}} + B_{\text{moor}}) + (C_{\text{hs}} + K_{\text{pto}} + K_{\text{moor}}) \tag{4.13}$$

where:

- M is the rigid body mass [kg]
- A is the added mass [kg]
- B_{rad} is the radiation damping coefficient [N·s/m]
- B_{pto} is the PTO damping coefficient [N·s/m]
- B_{moor} is the mooring damping coefficient [N·s/m]
- C_{hs} is the hydrostatic restoring stiffness [N/m]
- K_{pto} is the PTO stiffness [N/m]
- K_{moor} is the mooring stiffness [N/m]
- ω is the angular wave frequency [rad/s]

Increasing B_{moor} raises the total damping, which consequently decreases the RAO (Response Amplitude Operator), velocity, and hence the power output.

In the adopted model, the average power extracted under irregular conditions is strongly dependent on the velocity response. When B_{tot} increases, the RAO decreases—particularly in energy-rich sea states—leading to a reduction in annual energy production (AEP).

This behavior matches the observed results:

- Moderate reduction in the BASE case: approximately -3.87%.
- Stronger reduction in the BEST case: approximately -8.42%.

The larger decrease in the BEST configuration can be explained by its more aggressive control strategy (reactive tuning combined with high PTO damping). This configuration amplifies the response around the energetic frequency band; thus, adding external damping directly undermines that amplification, leading to a stronger reduction in AEP.

It is important to distinguish between two types of tuning effects:

A) Tuning as Frequency Shifting (Natural Frequency)

Given that $K_{\text{moor}} = 5 \times 10^3$ is small compared to $C_{\text{hs}} \approx 6.23 \times 10^5$, the natural resonance frequency is practically unaffected. Therefore, B_{moor} does not shift the resonance frequency to a first approximation but instead reduces the resonance peak amplitude.

Hence, there is no frequency tuning gain in this case.

B) Tuning as Robustness/Sensitivity

By increasing the damping:

- The system response becomes less "sharp," meaning it is less sensitive to parameter uncertainties.
- The likelihood of peaks and violation events decreases.

In practical simulations:

- Fail bins in BEST configuration: $34 \rightarrow 32$.
- Fail bins in BASE configuration: $6 \rightarrow 6$.

For the tested case, $B_{\text{moor}} = 5 \times 10^4$ N·s/m.

From the log data:

$$B_{\text{rad}}(\omega_{\text{target}}) \approx 7.8 \times 10^2 \text{ N} \cdot \text{s/m} \tag{4.14}$$

where:

- $B_{rad}(\omega_{target})$ is the radiation damping coefficient evaluated at the target angular frequency [N·s/m]
- ω_{target} is the angular frequency corresponding to the most energetic sea state [rad/s]

Hence, at the target frequency:

$$B_{\text{moor}} \approx 64 \times B_{\text{rad}} \tag{4.15}$$

This represents a strong damping value, making it suitable for sensitivity studies or conservative cases where the effect of external damping needs to be clearly observed.

The results of the CorPower design, for both the base and optimised cases studied at the Portugal location, are presented in Table 4.1.

Table 4.1: Comparison base and optimised case

Parameter	**Base case**	**Optimised case**
Average Power [kW]	29.40	79.20
Maximum Power [kW]	132.30	204
Annual Energy Production [MWh/year]	257.50	693.70
Capacity Factor [%]	26.10	45.7
K_{pto} [N/m]	5×10^4	-3.14×10^5
B_{pto} [N/s*m]	3×10^5	5×10^5
Relative Capture Width [%]	12	29

4.2.2 CETO 6

The design of the CETO 6 wave energy converter, conceptually follows what done for the CorPower for what concern the workflow used.

The difference with CorPower is that CETO 6 is a fully submerged, heave-only device, operating below the free surface where the wave-induced pressure field is attenuated and inherently more frequency-selective. This configuration reduces the influence of shorter and higher-frequency components, while enhancing the response around a limited range of wave periods. As a result, the hydrodynamic excitation and capture width of the device are more concentrated within a relatively narrow frequency band. For this reason, CETO 6 exhibits a more pronounced resonant behaviour: its response is strongly amplified when the incoming wave conditions are close to its natural period, but it decreases more rapidly outside this optimal range. This makes the device particularly sensitive to peak wave periods, as most of its energy capture is associated with sea states near resonance, while its performance in off-design or intermediate conditions is less significant. In this sense, CETO 6 can be described as "peak-oriented", meaning that its energy absorption is maximized around specific spectral peaks rather than distributed over a broad range of sea states. By contrast, CorPower is designed to maintain a wider bandwidth response, allowing for more consistent energy absorption in typical, moderate sea conditions that contribute most to the annual energy production. In Figure 4.5, the heave RAO of the CETO 6 system in its fully submerged configuration highlights this sharply resonant dynamic behaviour.

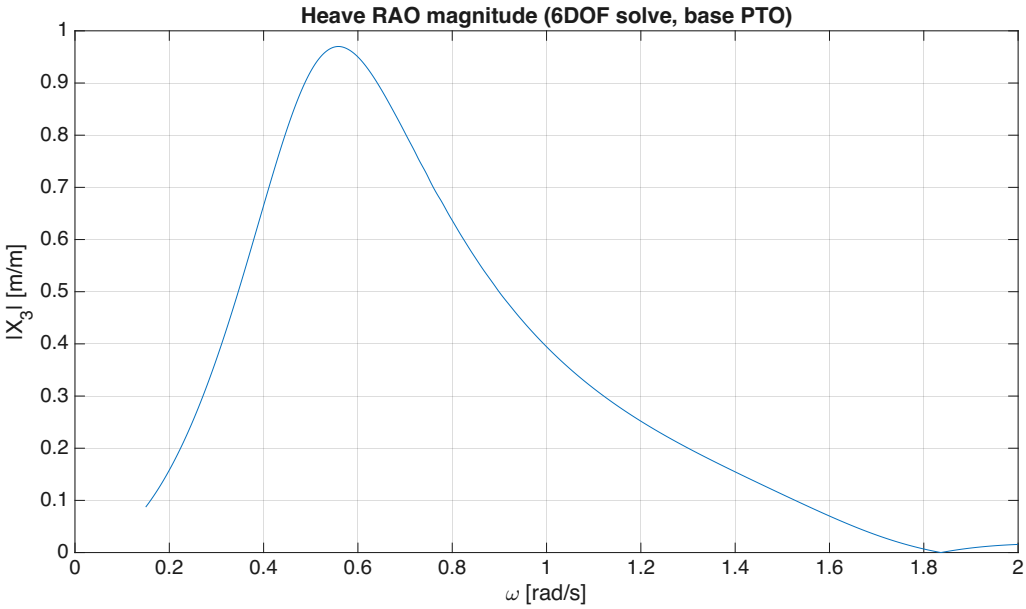

Figure 4.5: Heave motion

Figure 4.5 shows the heave RAO of the CETO 6 system in its fully submerged

configuration, highlighting a sharply resonant dynamic behaviour. The response exhibits a unitary peak around angular frequency $\omega \approx 0.6$ rad/s, corresponding to a wave period of roughly 10 s, where the device motion is strongly amplified relative to the incident wave. This is consistent with the notable high mass of the device and a consequent long resonant period. Away from this narrow frequency band, the RAO magnitude decays rapidly, revealing a limited ability to absorb energy from sea states with either shorter or longer characteristic periods. As a consequence, the bulk of the energy production tends to be concentrated in a small number of favourable sea states, leading to a moderate overall capacity factor even though instantaneous power peaks can be relatively high when conditions align with resonance.

The Power Take-Off system is modelled as a linear combination of damping and stiffness, allowing both dissipative and reactive control. Absorbed power is computed from the viscous damping contribution, while the reactive stiffness modifies the phase relationship between excitation force and velocity, enabling improved energy capture near resonance. Compared to an idealised PTO model, this formulation explicitly accounts for physical limitations of the conversion system.

Base case

Control of motion limits and constrained PTO tuning

The first feature already implemented in the base case is control of the vertical (heave) motion, which is a critical design requirement. In the absence of hard kinematic limits on the PTO stroke, a submergence constraint is introduced based on the position of the body with respect to the mean sea level. Consistently with the CETO 6 information, the center of the body is located at a depth of approximately 7 m, while the overall body height is taken as $H = 4$ m. By prescribing a minimum safety clearance of 3 m between the upper surface of the body and the free surface, to allow the passage of the small boats, the maximum admissible heave amplitude, A_{max} is obtained as

$$A_{\max} = 2.0 \text{ m}. \tag{4.16}$$

The motion constraint is evaluated on the most severe sea state in the wave climate, characterised by $H_s = 3.8$ m, $T_p = 9.6$ s and an occurrence probability of 2.3%. It is known that the heave motion can generally be defined with the formula:

$$X(\omega) = H(\omega) \times A[m] \tag{4.17}$$

where:

$$H(\omega) = RAO = \frac{X_3}{\eta} \tag{4.18}$$

where:

- X_3 is the heave displacement amplitude [m]
- η is the incident wave surface elevation amplitude [m]
- The RAO is evaluated at the peak period T_p of the considered sea state

Assuming a wave amplitude $a = H_s/2$, the submergence requirement can be expressed in terms of the heave RAO as

$$A_{heave} \approx \left|\frac{X_3}{\eta}\right|_{T_p} \times a \leq A_{max}$$

In this way when the heave motion is higher than the threshold, is then considered not physical feasible.

The tuning, based on the sea state, in this case is performed modifying the mooring stiffness. The mooring stiffness is decided based on the the most energetic sea state, allowing in this way the resonance between the device and the most energetic sea state, following also the principle for which the CETO 6 is a peak-oriented device.

The maximum power is set equal to 750kW, following the data found in literature [25].

The resulting power matrix and energy density matrix for the base case are shown in Figures 4.5 and 4.6.

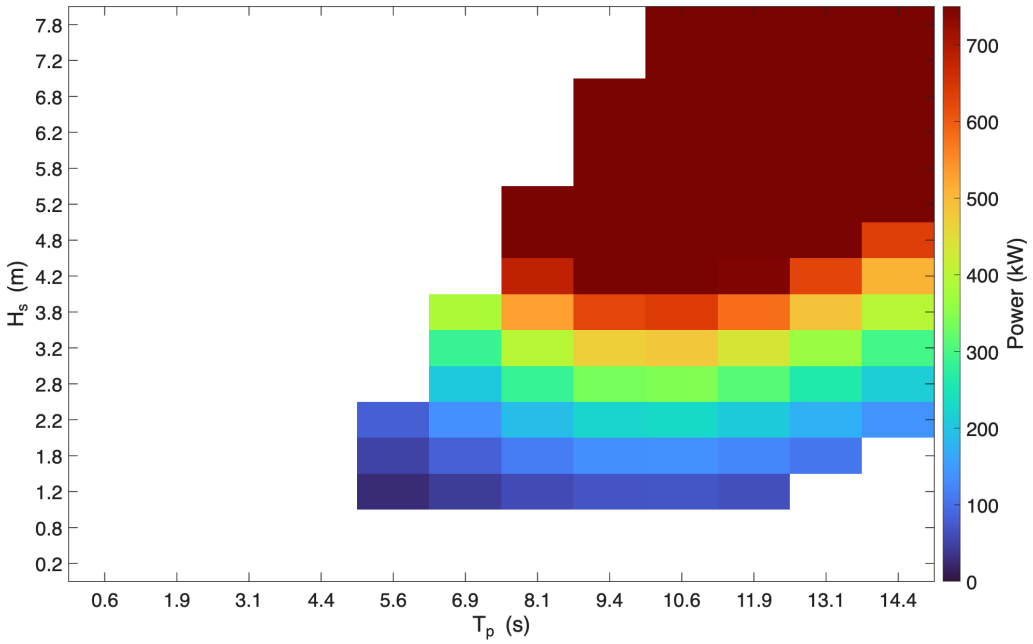

Figure 4.6: Power matrix of CETO 6 for the base case in Australia

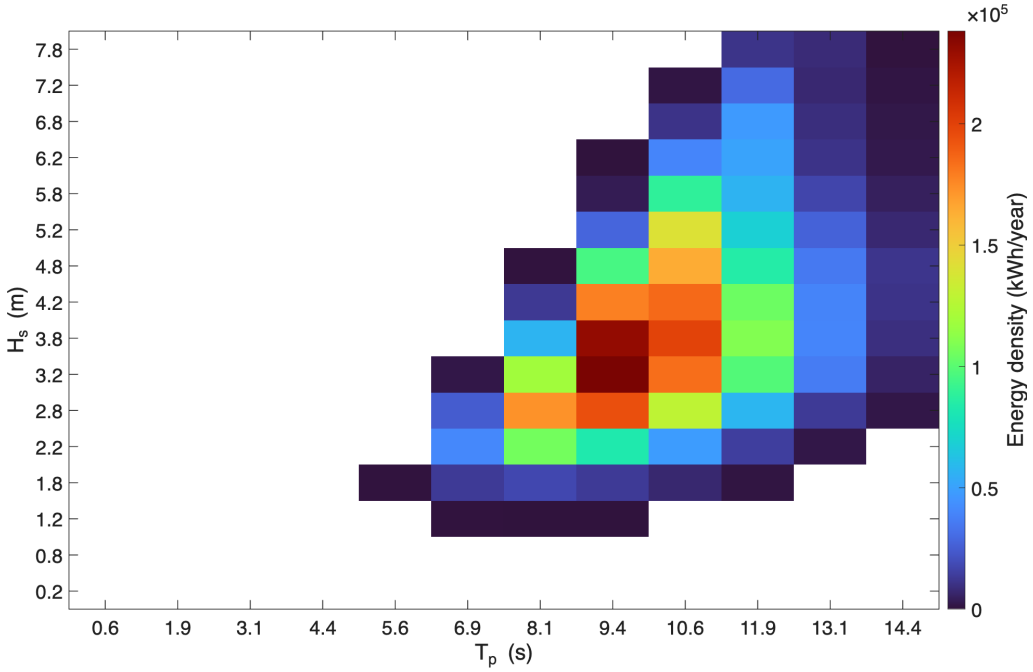

Figure 4.7: AEP analysis of CETO 6 for the base case in Australia

Optimised case

The optimization is carried on with a sweep search to find the optimal value of the stiffness and the damping of the PTO to maximize the Annual Energy Production, as in the CorPower optimization. These combination are then analysed to check whether the heave motion violates or not the translational limitations.

In figure 4.8 and 4.9 the power matrix and the energy density matrix are displayed for the optimised case.

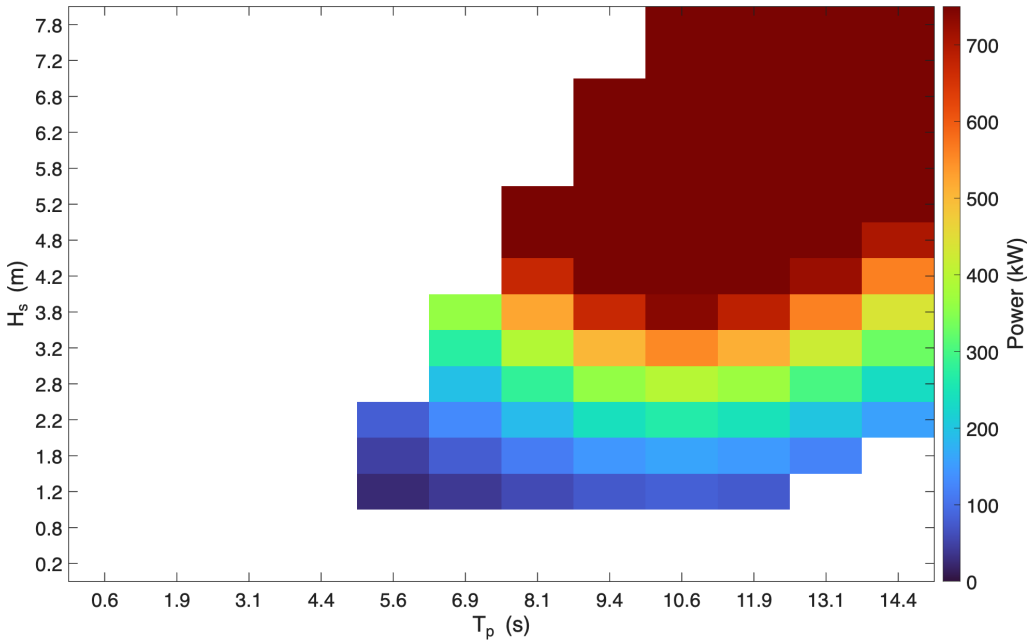

Figure 4.8: Power matrix of CETO 6 for the optimised case in Australia

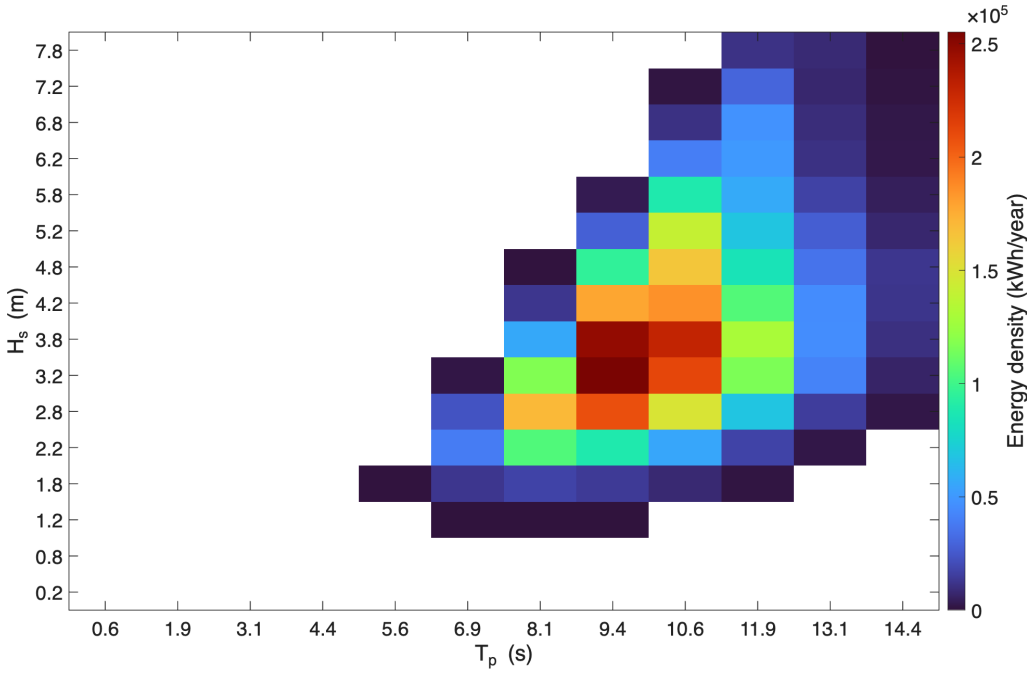

Figure 4.9: AEP analysis of CETO 6 for the optimised case in Australia

The optimization allows a gain in the Annual Energy Production equal to ≈20 MWh/year, the 4.80% of the one generated in the base case.
The results of the CETO 6 design, for both the base and optimised cases studied at the Australia location, are presented in Table 4.2.

Table 4.2: Comparison base and optimised case

Parameter	**Base case**	**Optimised case**
Average Power [kW]	441.49	465.08
Maximum Power [kW]	750	750
Annual Energy Production [GWh/year]	3.90	4.07
Capacity Factor [%]	58.87	62.01
K_{pto} [N/m]	3.0×10^5	-3.1×10^5
B_{pto} [N/s*m]	6.0×10^5	2.4×10^6
Relative Capture Width [%]	40	42

Chapter 5

Scaling Methods and WEC Simulations

5.1 Scaling procedures

The transition from theoretical hydrodynamic models to practical structural design is often constrained by the geometric complexity of Wave Energy Converter (WEC) components. To address this challenge, the scaling methodology adopted in this study is based on the definition of a standardized structural specimen.

The primary objective of the scaling process is to enable an economic assessment of the WEC, allowing the estimation of structural costs and, subsequently, the calculation of the Levelised Cost of Energy (LCOE). The use of a representative specimen, together with simplified geometrical models for the two WECs, is intended to reduce the complexity of the analysis, making it more conceptual and generalizable.

5.1.1 Procedure and scaling workflow

Rather than conducting a full-scale structural analysis for every design iteration, a representative geometry, such as a thin-walled cylinder or a sphere, is selected to emulate the main buoyant or load-bearing element of the WEC. This specimen serves as a reference framework for three main reasons.

1. **Standardization.** The adoption of a canonical geometry enables the application of classical structural theories (e.g., thin-shell formulations), thus yielding analytical solutions that can be consistently compared across different scales and configurations.

2. **Load mapping.** The complex hydrodynamic loads, pressures and moments, derived from numerical WEC simulations are projected onto the specimen surface. This procedure allows the estimation of the minimum wall thickness s required to ensure structural integrity under the target Sea State.

3. **Economic scalability.** The standardized specimen exhibits a predictable

manufacturing cost per unit mass or volume. Once validated for a specific Sea State, this cost functions as a modular economic metric, enabling the estimation of structural investment across diverse WEC designs and environmental conditions within a unified scaling framework.

In summary, the structural specimen operates as a physical proxy that translates the abstract hydrodynamic forcing of the sea into a tangible material volume. When monetized, this volume establishes the link between structural design and the Levelised Cost of Energy (LCOE), thereby quantifying the structural cost implications associated with deploying a given WEC in a specific geographic context.

5.1.2 Specimen choice

For the building of the scaled specimen, different geometry are chosen to model the different WEC typologies and in particular the different component of the WEC.

The geometry is chosen between the main geometric 3D archetypes used in engineering modeling, displayed in Figure 5.1.

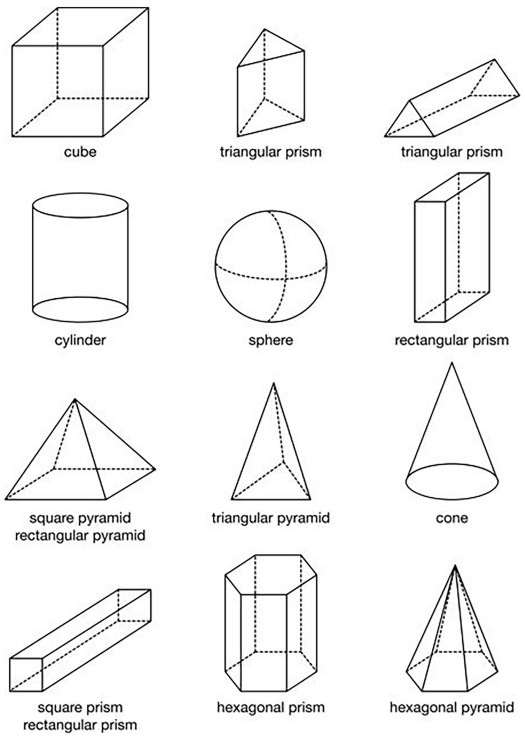

Figure 5.1: Geometric archetypes used for the scaling analysis[27]

For this study, different geometries are selected to analyse the hull and other WEC components. In particular, two distinct hull geometries are considered: a spherical shape for CorPower and a lenticular disc for CETO 6. The lenticular disc is a flattened, lens-shaped geometry that can be approximated as a short circular cylinder with curved outer surfaces. In this model, it represents the CETO 6 buoy as a streamlined oblate shell rather than a perfect sphere or a fully flat disc.

Then, a vertical cylinder is also considered to simulate a control actuator along with a horizontal winch representing an internal component of the hull used to enhance its stability, like a horizontal load-transfer beam. The sizes of both elements vary in proportion to the dimensions of the hull.

5.2 Pressure-based structural analysis

5.2.1 Hydrodynamic load definition

In the current stage of the script, the loading conditions are modeled by combining complex hydrodynamic data (from NEMOH) with classical mechanics principles to capture the "worst-case scenario" experienced by each structural component. The treatment of the three main force components is outlined as follows:

1. **Excitation Force ($F_{\mathbf{exc}}$) from NEMOH**

   This force represents the vertical thrust exerted by the wave on the Wave Energy Converter (WEC), driving its oscillatory motion.

   - *Origin:* The data are extracted from the NEMOH `.h5` files, which provide the excitation force coefficients in heave (vertical motion).
   - *Scaling:* NEMOH outputs excitation coefficients in N/m (Newtons per meter of wave amplitude). The script interpolates the appropriate value corresponding to the wave frequency ($\omega = 2\pi/T_p$) and multiplies it by the actual amplitude $a = H_s/2$ to obtain the total excitation force in Newtons.
   - *Application:* This force is used to compute the *Axial Stress* (tension/compression along the shell) and *Axial Buckling* (the risk of vertical instability under excessive compressive loading).

2. **Total Pressure ($p_{\mathbf{peak}}$)**

   This pressure acts radially on the shell (from the exterior toward the interior) and consists of two main components:

- *Hydrostatic Pressure:* The constant pressure due to the water column above the device ($\rho \cdot g \cdot |z_0|$). It reaches its maximum for the CETO 6 unit (immersed at -5 m) and its minimum for the CorPower unit (near the sea surface).
- *Dynamic Pressure (Airy Wave Theory):* The additional pressure generated by the passing wave, which decays exponentially with depth, very intense for CorPower at the surface and significantly attenuated for CETO 6 at -5 m.

Application: The sum of these two contributions (Δp) defines the *Hoop Stress* (circumferential stress) and the *External Pressure Buckling*, which often governs the collapse behavior of submerged cylindrical shells.

3. **Strength Criteria and Safety Factors**

   Once the total forces are obtained, the script applies two distinct evaluation criteria rather than only checking for material failure:

   - *Yielding:* The material must remain below the elastic limit to avoid permanent deformation. A safety factor SF = 2.0 is applied to the steel yield strength (350 MPa).
   - *Buckling:* This is a failure by geometric instability rather than material rupture—similar to the sudden collapse of an empty can under compressive load. The buckling safety factor is decided based on the fact that the conditions already includes the ultimate sea state (UTS) of the last 30 years of the sea location considered ($\mathrm{SF}_{\mathrm{buck}} = 1.5$).

For each sea state, the final shell thickness (s_{total}) is not computed as the sum of partial contributions, but rather as the maximum required thickness among all assessed criteria (Axial Yielding, Radial Yielding, Axial Buckling, and Radial Buckling). An additional 3 mm corrosion allowance is then included to account for the marine environment.

5.2.2 Stress evaluation and thickness sizing

Definition of Inputs and Environmental Loads (INPUT)

The structural sizing of the specimen is based on determining the critical loads acting at the operating depth z_0, defined according to the type of Wave Energy Converter (WEC) analyzed.

Geometric Parameters: The radius of the component to be sized (R_{spec}) is distinguished from the radius of the host device (R_{dev}), the latter being fundamental for

evaluating the operational draft in the case of floating systems.

Hydrostatic Load: The ambient static pressure depends on the local depth:

$$P_{\text{stat}} = \rho g |z_0| \tag{5.1}$$

where:

- ρ is the seawater density [kg/m^3]
- g is the gravitational acceleration [m/s^2]
- z_0 is the operating depth of the device [m]

Local Hydrodynamic Load: The dynamic pressure induced by the passing wave, computed according to Airy linear theory, decays exponentially with depth:

$$P_{\text{dyn}} = \rho g a \frac{\cosh(k(z_0 + h))}{\cosh(kh)} \tag{5.2}$$

where:

- ρ is the seawater density [kg/m^3]
- g is the gravitational acceleration [m/s^2]
- $a = H_s/2$ is the wave amplitude [m]
- k is the wave number [rad/m]
- z_0 is the depth of the device [m]
- h is the water depth [m]

Hydrodynamic Excitation Force: The vertical macroscopic force F_{target} is derived from heave excitation coefficients obtained through Boundary Element Method (BEM) analysis using the NEMOH software, linearly scaled by the wave amplitude $a = H_s/2$.

Yielding Verification (YIELDING)

Material strength verification ensures that stresses induced by the applied loads do not exceed the allowable stress of the material, defined as $\sigma_{\text{allow}} = \sigma_y/SF$, where σ_y is the steel yield strength and SF is the safety factor.

Cylindrical Shell: The dominant circumferential (hoop) stress due to net pressure Δp is given by:

$$s_{\text{yield},p} = \frac{\Delta p \, R_{\text{spec}}}{\sigma_{\text{allow}}} \tag{5.3}$$

where:

- $\Delta p = P_{stat} + P_{dyn}$ is the net pressure acting on the shell [Pa]
- R_{spec} is the radius of the structural specimen [m]
- $\sigma_{allow} = \sigma_y / SF$ is the allowable stress [Pa], with σ_y the steel yield strength and SF the safety factor

The required thickness for the axial load F_{target} is:

$$s_{\text{yield},f} = \frac{F_{\text{target}}}{2\pi R_{\text{spec}}\, \sigma_{\text{allow}}} \tag{5.4}$$

where:

- F_{target} is the hydrodynamic excitation force in heave [N]
- R_{spec} is the radius of the structural specimen [m]
- $\sigma_{allow} = \sigma_y / SF$ is the allowable stress [Pa]

Spherical Shell: Due to biaxial symmetry, the sphere distributes pressure more efficiently, requiring half the thickness of an equivalent cylinder:

$$s_{\text{yield},p} = \frac{\Delta p\, R_{\text{spec}}}{2\sigma_{\text{allow}}} \tag{5.5}$$

where:

- Δp is the net pressure acting on the shell [Pa]
- R_{spec} is the radius of the spherical specimen [m]
- σ_{allow} is the allowable stress [Pa]; the factor 2 in the denominator reflects the biaxial stress distribution of a spherical shell

Elastic Stability Analysis (BUCKLING)

The buckling analysis prevents structural collapse due to shape instability under compressive or external pressure loads, applying a conservative safety factor $SF_{\text{buck}} = 3.0$.

External Pressure Instability: For the cylinder, the formulation for radial instability under long-shell conditions is adopted:

$$s_{\text{buck},p} = R_{\text{spec}} \left(\frac{E}{4\, \Delta p\, SF_{\text{buck}} (1 - \nu^2)} \right)^{1/3} \tag{5.6}$$

- R_{spec} is the radius of the cylindrical specimen [m]
- E is the Young's modulus of the material [Pa]
- Δp is the net external pressure [Pa]
- SF_{buck} is the buckling safety factor [-]
- ν is the Poisson's ratio of the material [-]

For the sphere, Zoelly's classical equation is used, reflecting the higher stiffness provided by double curvature:

$$s_{\text{buck},p} = R_{\text{spec}} \sqrt{\frac{2E}{3\,\Delta p\, SF_{\text{buck}}(1-\nu^2)}} \tag{5.7}$$

- R_{spec} is the radius of the spherical specimen [m]
- E is the Young's modulus of the material [Pa]
- Δp is the net external pressure [Pa]
- SF_{buck} is the buckling safety factor [-]
- ν is the Poisson's ratio of the material [-]

Axial Instability (Cylinder): The risk of vertical collapse under the applied force F_{target} is evaluated as:

$$s_{\text{buck,ax}} = \sqrt{\frac{2\pi E}{3\,F_{\text{target}}\, SF_{\text{buck}}(1-\nu^2)}} \tag{5.8}$$

- E is the Young's modulus of the material [Pa]
- F_{target} is the compressive axial force [N]
- SF_{buck} is the buckling safety factor [-]
- ν is the Poisson's ratio of the material [-]

Design Synthesis and Margins

The structural optimization process converges toward a final design thickness obtained through an envelope approach of the results:

Worst-Case Selection: For each sea state defined in the site occurrence matrix, the maximum thickness among all yielding and buckling criteria is selected.

Corrosion Allowance: A sacrificial thickness of 3 mm is added to ensure structural

integrity throughout the service life in the marine environment:

$$s_{\text{total}} = \max(s_{\text{yield}}, s_{\text{buck}}) + c_{\text{allowance}} \tag{5.9}$$

where:

- s_{yield} is the minimum thickness required by yielding criteria [m]
- s_{buck} is the minimum thickness required by buckling criteria [m]
- $c_{allowance} = 3\,\text{mm}$ is the corrosion allowance for the marine environment

Final Design Thickness: The final value s_{design} is the maximum computed across the entire wave spectrum analyzed, ensuring structural survival even under the expected Worst Case Scenario (WCS).

5.3 Sensitivity Analysis of Device Radius and Site Location

As discussed in Chapter 3, two different approaches are compared for the scaling procedure of WECs across varying locations and device radii. The first method is based on Froude scaling.

5.3.1 Froude scaling

The Froude scaling is the fundamental physical law which allow testing scaled models for naval application. When addressing the scaling of the mechanical interactions between fluids and solids, the three main types of forces are: inertial, gravitational, and viscous forces. As inertia forces are normally predominant for the scaling of the body-fluid interaction of WECs, the Froude's model law is used to transfer data between different scales. In this analysis is used to scale the power matrix for the estimation of the AEP at different sites and sizes, starting from a reference power matrix defined for a standard device configuration. This method uses a single reference model, from which both the power performance and the hydrodynamic loads are scaled to different radii through Froude similarity laws.

Froude's scaling can be summarized as:

$$Fr = \sqrt{\frac{Inertia forces}{Gravity forces}} = \frac{U}{\sqrt{gL}} \tag{5.10}$$

where:

- U is the characteristic flow velocity [m/s]
- g is the gravitational acceleration [m/s^2]
- L is the characteristic length of the device [m]

$$\frac{U_m}{\sqrt{gL_m}} = \frac{U_f}{gL_f} =\geq Uf = Um\sqrt{S} \tag{5.11}$$

where:

- $S = \frac{L_f}{L_m}$ is the scaling ratio, requiring geometrical similarity
- U is the velocity [m/s]
- g is the gravitational acceleration [m/s^2]
- L is the dimension [m]
- Subscripts m and f stand for Model and Full-scale

These formulas are adapted from [10].

In this project, Froude scaling is applied to two main aspects of the device model:

- *Annual Energy Production (AEP) and rated power.*

  In order to evaluate the influence of device size on energy performance, the reference Power Matrix (defined for a reference radius R_{ref}) is scaled using a non-dimensional approach consistent with the definition of Capture Width Ratio (CWR). Rather than applying a direct empirical scaling law of the form λ^n, the adopted procedure preserves hydrodynamic performance in non-dimensional form and reconstructs the power surface for different geometric scales.

  First, the absorbed power in the reference configuration $P_{\text{ref}}(H_s, T_p)$ is converted into a non-dimensional efficiency parameter:

$$\eta_{\text{ref}} = \frac{P_{\text{ref}}}{P_{\text{wave}} \cdot d_{\text{ref}}} \tag{5.12}$$

  where P_{wave} is the deep-water wave power per unit crest width [kW/m], P_{ref} is the absorbed power of reference device size and $d_{\text{ref}} = 2R_{\text{ref}}$ represents the characteristic active width of the device, assumed equal to the external diameter of the main body. The parameter η therefore corresponds to the Capture Width Ratio and represents an intrinsic measure of conversion efficiency independent of absolute scale.

The performance surface is then expressed in terms of non-dimensional wave parameters:

$$h = \frac{H_s}{d}, \qquad \mu = \frac{d}{L_{p,0}} \tag{5.13}$$

where H_s is the significant wave height, d the device diameter, and $L_{p,0} = \frac{gT_p^2}{2\pi}$ the deep-water wavelength associated with the peak period T_p. This transformation allows the hydrodynamic response to be described as a function of the ratio between wave scale and structural scale.

For a new device radius R_{spec}, the corresponding non-dimensional parameters h_{spec} and μ_{spec} are computed. The scaled efficiency η_{spec} is then obtained by interpolating the reference surface $\eta_{\text{ref}}(h, \mu)$ at the new non-dimensional coordinates. Finally, the scaled Power Matrix is reconstructed as:

$$P_{\text{spec}}(H_s, T_p) = \eta_{\text{spec}}(h_{\text{spec}},\, \mu_{\text{spec}}) \cdot P_{\text{wave}}(H_s, T_p) \cdot d_{\text{spec}} \tag{5.14}$$

with $d_{\text{spec}} = 2R_{\text{spec}}$.

Through this procedure, geometric scaling is introduced exclusively via non-dimensional wave–structure interaction parameters, ensuring physical consistency with Froude similarity principles. The intrinsic efficiency surface is assumed to remain invariant under geometric scaling, while dimensional power levels vary proportionally to the available wave power and the device characteristic width.

This approach relies on several assumptions. First, the active width of the device is approximated by its external diameter, which is appropriate for point-absorber-type geometries but may require modification for terminator or multi-body systems. Second, the peak period T_p is used as the spectral descriptor of sea states, consistent with the available Power Matrix data, although the energy period T_e may provide a more robust representation of wave energy in irregular seas. Third, the method assumes hydrodynamic similitude under Froude scaling and neglects potential scale-dependent viscous or control effects. Finally, interpolation outside the reference non-dimensional domain may introduce additional uncertainty.

This non-dimensional Capture Width Ratio scaling framework is consistent with the methodology described in the *Handbook of Ocean Wave Energy* [10].

- **Hydrodynamic loads.** The hydrodynamic coefficients are available at a reference scale $R_{\text{full scale}}$. When evaluating a device with radius R_{model}, the wave frequency is first mapped to the reference scale according to:

$$\omega_{\text{ref}} = \omega\sqrt{\lambda}, \tag{5.15}$$

in order to query the hydrodynamic database consistently. The excitation force per unit wave amplitude is then scaled as:

$$F_{\text{model}} = F_{\text{ref}}\,\lambda^2. \tag{5.16}$$

The same frequency mapping and force scaling are applied when evaluating the loads under the Ultimate Sea State (ULS) conditions.

In this project, the scaling parameter is defined as $\lambda = R_{\text{model}}/R_{\text{full scale}}$. Although this convention is specular to the standard one adopted in basin model testing, it proves functional to the structure of the developed computational framework. The consistency of the results is preserved through the correct transposition of the physical quantities: in particular, the wave frequency is scaled according to $1/\sqrt{\lambda}$ for querying the hydrodynamic database, while the excitation forces and the produced power follow the scaling laws λ^2 and $\lambda^{3.5}$, respectively, ensuring the full physical validity of the numerical model.

Building on this, it is possible to calculate the thickness for different radii of the device and for different locations by applying the scaling. The way the thickness varies with the radius then allows the computation of the device mass and, consequently, its cost.

5.3.2 Physical model

The second approach uses the script developed in this project to directly evaluate device performance for different radii and locations.

In this case, a dedicated geometry is generated, with Fusion360, for each radius of both devices and relies on radius-dependent inputs, with AEP assigned from precomputed vectors and loads extracted from the corresponding NEMOH model of each device size. The nominal power was not directly extracted from the numerical simulations, as these only provide average and peak power values. Instead, it was defined through scaling laws based on the reference device, ensuring a consistent and physically coherent definition of rated power while avoiding potential biases from indirect estimates.

The methodology is applied as follows:

CAD construction

A .stl file is built in Fusion360 for every radius of the two devices, with all the consequent converted file, as shown in Figure 5.2, in order to obtain the right format for the NEMOH computation.

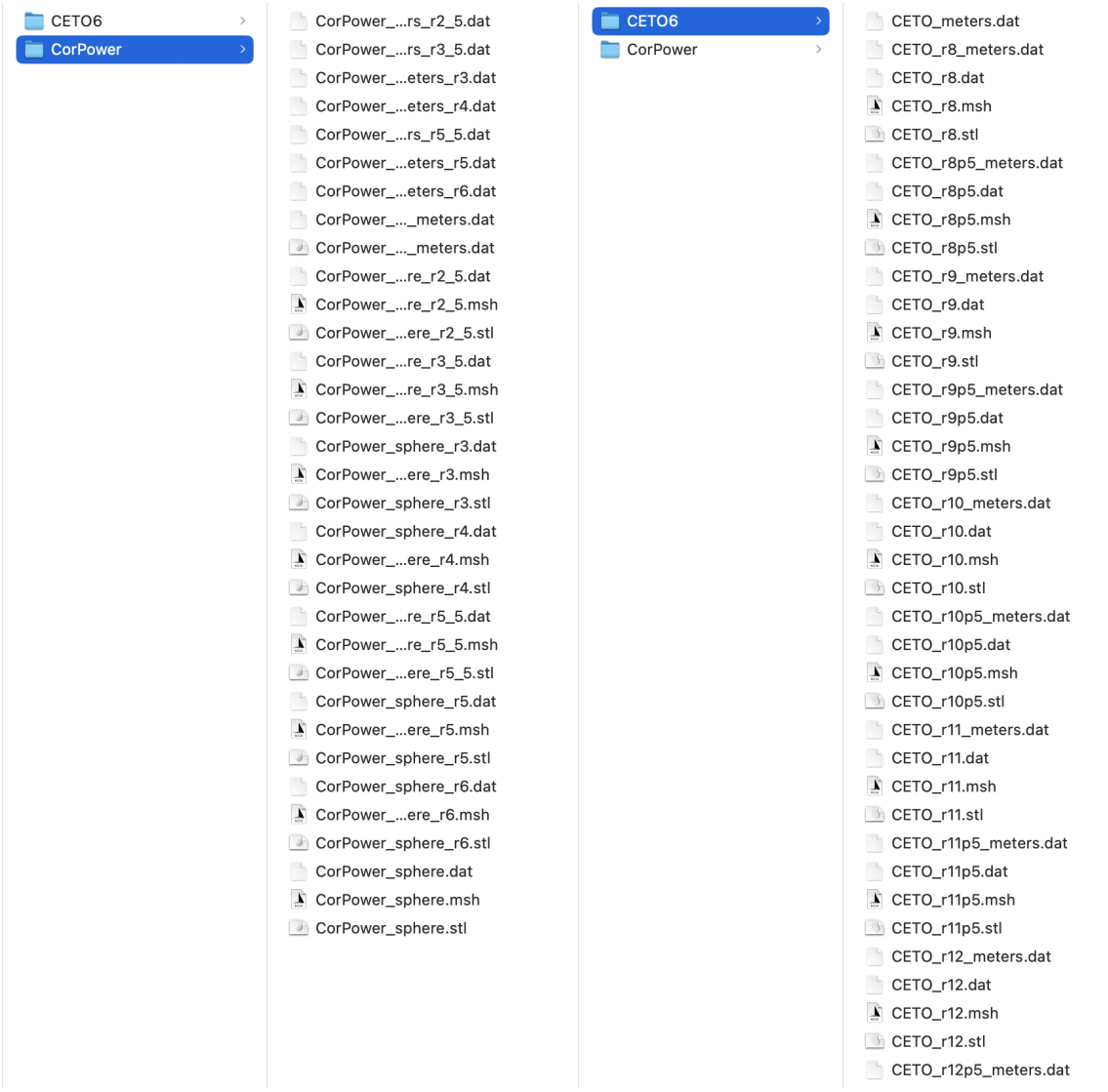

(a) (b)

Figure 5.2: Structure of the Fusion360 design files used for WEC modelling: (a) CorPower , (b) CETO 6

NEMOH computation

Once the input data is correctly formatted, a NEMOH simulation is performed for each radius of the two devices using a Python script to obtain the hydrodynamic results. The hydrodynamic results are saved in different folder, as shown in Figure 5.4, each one corresponding to a combination of device and radius.

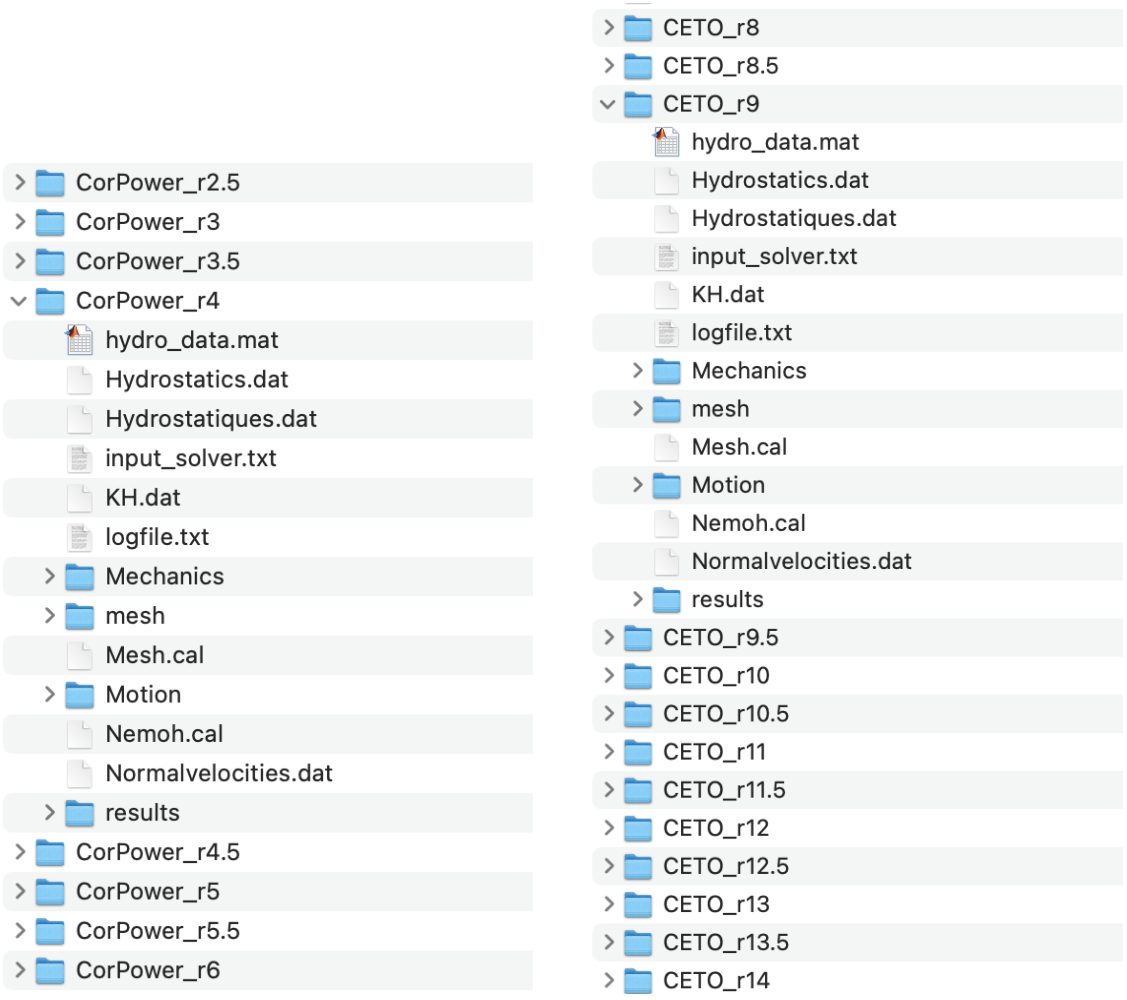

(a) (b)

Figure 5.3: Organization of NEMOH simulation output files: (a) CorPower , (b) CETO 6

WECs simulation

Having all the required data, the simulation is performed for every combination of radius and location for the two WECs. This allows the direct calculation of the AEP value for each configuration, leading to more precise results and, as in the standard case, retaining the optimised value for every scenario. Figure 5.4 illustrates how, by modifying the sea state input, defined as the occurrence file (occFile) in the CorPower case and as the seaFile in the other case, it is possible to account for different sea state locations. Additionally, by changing the hydroFile, the NEMOH input file is updated, enabling the simulation of different radii.

CETO_frequency_domain_DEFINITIVO.m

/Users/lucabolla/Desktop/Tesi/CETO_project_wecSim/CETO_frequency_domain_DEFINITIVO.m

```
1   %% ------------------------------------------------------------------
2   %  CETO - Frequency-domain - 6DOF (single body) - PTO in heave only
3   clear; clc;
4
5   projectDir = '/Users/lucabolla/Desktop/Tesi/CETO_project_wecSim';
6   seaFile    = fullfile(projectDir,'matrixes','sea_state_occurrence_Australia.mat');
7
```

(a)

CorPower_frequency_domain_DEFINITIVO.m

/Users/lucabolla/Desktop/Tesi/CorPower_project_wecSim/CorPower_frequency_domain_DEFINITIVO.m

```
1   %% ------------------------------------------------------------------------
2   %% CORPOWER - FREQUENCY DOMAIN ANALYSIS
3
4   clear; close all; clc;
5
6   %% ------------------------------------------------------------------------
7   %  USER INPUTS
8   %% ------------------------------------------------------------------------
9   projectDir = '/Users/lucabolla/Desktop/Tesi/CorPower_project_wecSim';
10
11  occFile    = fullfile(projectDir,'matrixes','sea_state_occurrence_Portugal.mat');
12
13  hydroFile  = fullfile(projectDir,'CorPower_r4.5.h5');
```

(b)

Figure 5.4: MATLAB scripts used for CorPower and CETO 6 simulations: (a) CorPower , (b) CETO 6

Physical scaling

From these simulations, the AEP values for all combinations are obtained and applied within the physical scaling scenario. As illustrated in Figure 5.5, vectors containing the AEP corresponding to each radius, for every location and for both devices, are considered.

WEC_scaling_DEFINITIVO.m

/Users/lucabolla/Desktop/Tesi/Scaling/WEC_scaling_DEFINITIVO.m

```
elseif devIdx == 2
    % =========================
    % DEVICE = CorPower
    % =========================
    switch siteIdx
        case 1   % Germany
            AEP_GROSS_R = [2.5 3 3.5 4 4.5 5 5.5 6];
            AEP_GROSS_Y = [127.8 165.4 201.7 237.9 272.7 306.5 338.2 364.7 ];

        case 2   % Scotland
            AEP_GROSS_R = [2.5 3 3.5 4 4.5 5 5.5 6];
            AEP_GROSS_Y = [251.6 342.9 440.4 537.3 640.5 744.7 817.7 828.0];

        case 3   % Portugal
            AEP_GROSS_R = [2.5 3 3.5 4 4.5 5 5.5 6];
            AEP_GROSS_Y = [270.1 368.7 475.0 580.6 693.7 799.7 852.2 854.3];

        case 4   % Australia
            AEP_GROSS_R = [2.5 3 3.5 4 4.5 5 5.5 6];
            AEP_GROSS_Y = [447.3 619.8 809.2 1000.9 1193.8 1339.0 1365.2 1346.6];

        otherwise
            error('siteIdx non riconosciuto per CorPower.');
    end

else
    error('devIdx non riconosciuto.');
end
```

(a)

WEC_scaling_DEFINITIVO.m

/Users/lucabolla/Desktop/Tesi/Scaling/WEC_scaling_DEFINITIVO.m

```
% AEP manuale dipendente da DEVICE + SITE
% =========================================================
if devIdx == 1
    % =========================
    % DEVICE = CETO
    % =========================
    switch siteIdx
        case 1   % Germany
            AEP_GROSS_R = [8 8.5 9 9.5 10 10.5 11 11.5 12 12.5 13 13.5 14];
            AEP_GROSS_Y = [659.52 689.64 708.97 722.85 735.59 744.45 749.26 751.27 755.65 754.69 750.64 744.33 736.01];

        case 2   % Scotland
            AEP_GROSS_R = [8 8.5 9 9.5 10 10.5 11 11.5 12 12.5 13 13.5 14];
            AEP_GROSS_Y = [1618.10 1791 1939.6 2043.6 2119.5 2187.6 2252 2307.9 2353.3 2399.3 2431.3 2445.5 2449.8];

        case 3   % Portugal
            AEP_GROSS_R = [8 8.5 9 9.5 10 10.5 11 11.5 12 12.5 13 13.5 14];
            AEP_GROSS_Y = [1742.4 1853.1 2045.2 2188.7 2293 2374.5 2447.1 2507.9 2561 2612.3 2659.4 2684.1 2698.2];

        case 4   % Australia
            AEP_GROSS_R = [8 8.5 9 9.5 10 10.5 11 11.5 12 12.5 13 13.5 14];
            AEP_GROSS_Y = [2735.1 3137.4 3514.6 3812 4064 4210.4 4324.6 4432.1 4523.6 4608.7 4693.8 4739.3 4765.8];

        otherwise
            error('siteIdx non riconosciuto per CETO.');
    end
```

(b)

Figure 5.5: Section of the script for the scaling of the WECs: (a) CorPower , (b) CETO 6

Load calculation

In contrast to the method based on Froude scaling, in this case the loads that the device must withstand under different sea states—and for each radius—are not derived by scaling a standard device. Instead, they are directly obtained from the NEMOH results available for each radius of the two devices, as shown in Figure 5.3. From these values, it is possible to determine how the thickness varies with the radius, and consequently to estimate both the mass of the device and its cost.

The calculation of the thickness, and its variation with the radius, allows the estimation of the device mass and, consequently, provides the basis for analyzing the associated costs.

5.4 Cost formation

5.4.1 CAPEX

CAPEX (capital expenditure) represents the upfront investment required to design, procure, and install an asset so it becomes operational. In techno-economic assessments, CAPEX typically includes equipment supply, manufacturing, transport, installation, and grid/interconnection costs incurred before commissioning. In this project the contributions for the CAPEX are the following, and are calculated as described below.

- Hull: This methodology allows to set an alternative way to asses the cost of the hull, which even if is a simplified technique, allow to avoid the problem regarding the lack information of the actual WECs. In this project the cost of the hull is calculated following this formula:

$$CAPEX_{Hull} = V_{Hull}(t) Cost_{tonofsteel} \tag{5.17}$$

  V_{Hull} is the volume of the Hull. In this way the cost of the Hull, changes following the thickness of the sphere. The cost of the raw steel is around 695 €/ton [28], then to taking into account the cost of the manufacturing, the final cost is assumed to be: 4630 €/ton.

- Power Take-Off system: The PTO cost is considered equal to 925 €/kW [29]. The cost of the PTO is therefore scaled according to the rated power of different configurations, until the PTO power is saturated at that moment also the cost is consequently capped to the maximum.

- Balance of System (BoS): The Balance of System (BoS) costs were disaggregated into foundation and mooring, installation, and grid connection components. These are calculated as a percentage of the total costs, following [11], verifying also the coherence with the percentage of PTO and Hull costs. These costs are considered fixed, not depending on the size of the device.

- Decommissioning costs: The decommissioning costs are set to be around 420 €/kW [11].

5.4.2 OPEX

OPEX (operational expenditure) refers to the recurring costs incurred during the operational lifetime of an asset. In techno-economic analyses, OPEX typically includes

operation, maintenance, repairs, insurance, logistics, and other annual expenses required to ensure continued and reliable performance. In this project, OPEX is calculated as an average of 8% [11].

5.5 Economic calculations

5.5.1 KPI, Key Performance Indicator

The KPI used in this work represents an additional economic indicator, distinct from the LCOE, aimed at evaluating costs associated with specific components of WECs. In particular, it focuses on elements that are not part of the hull and are not included in other cost categories such as moorings, grid connection, or other project-related expenses. The two components analyzed through this KPI, rather than the LCOE, are the vertical cylinder and the horizontal winch. For the CorPower device, the vertical cylinder corresponds to a tubular component of the PTO (power take-off) or pre-tension system, while the horizontal element represents a load-transfer beam integrated within the hull to enhance its structural integrity. In the case of the CETO 6 system, the vertical cylinder refers to the hydraulic cylinder, whereas the horizontal element is a structural component designed to transfer the tether load. Both these element are related and change with the radius of the hull.

The KPI is calculated as the ratio between the cost of the component and the net AEP for the corresponding radius.

$$KPI = \frac{Cost}{AEP} \tag{5.18}$$

5.5.2 LCOE

The parameter calculated to define the economical feasibility of the different devices in the different locations, and used to have an index to verify the best WEC in every location, is the Levelised Cost of Energ, LCOE. As already mention in the third chapter, the LCOE, is the discounted average cost of producing one unit of electricity over the entire lifetime of a project. It is calculated as the ratio between the present value of total costs (CAPEX, OPEX, and decommissioning) and the present value of total energy produced, typically expressed in €/MWh. LCOE is used to compare the economic competitiveness of different energy technologies on a consistent basis, independent of scale and project lifetime. It is particularly useful for investment decisions, policy assessments, and technology benchmarking, as it condenses complex technical and financial variables into a single comparable metric.

It is very useful because it allows to compare different technologies.

The Levelised Cost of Energy (LCOE) is calculated using a discounted cash flow (DCF) approach as the ratio between the present value of total project costs and the present value of total energy produced over the project lifetime:

$$\mathrm{LCOE} = \frac{\mathrm{PV}_{\mathrm{cost}}}{\mathrm{PV}_{\mathrm{energy}}} \tag{5.19}$$

where *PV (Present Value)* represents the value of future cash flows discounted to year zero using a discount rate r, accounting for the time value of money.

The discount rate r is optimistically considered equal to 0.05 (5%) [24].

For a project lifetime of n years:

$$\mathrm{PV}_{\mathrm{cost}} = CAPEX_0 + \sum_{t=1}^{n} \frac{OPEX_t}{(1+r)^t} + \frac{DECOM}{(1+r)^n} \tag{5.20}$$

$$\mathrm{PV}_{\mathrm{energy}} = \sum_{t=1}^{n} \frac{E_t}{(1+r)^t} \tag{5.21}$$

In this model:

- $CAPEX_0$ is the upfront investment at year 0,
- $OPEX_t = f_{\mathrm{opex}} \cdot CAPEX_0$ is the annual operational expenditure,
- $DECOM$ is the decommissioning cost at the end of life,
- $E_t = AEP_{\mathrm{net}}$ is the annual net energy production, including availability effects.

The final LCOE is typically expressed in €/MWh.

5.5.3 Particular cases

Some features are implemented in the calculations of the LCOE, to make them as realistic as possible. In particular the modeling is modified to take into account:

- WEC Farm, applied to consider the fact that often there will not be one single WEC installed, but a farm of WECs. This allow, as for the other RES to achieve more power, and also the reduction of the costs, following the economy of scale. Economies of scale for farm level Balance of System (BoS) expenditures are represented through a power-law scaling

$$C(N) = C(1) \cdot N^{b} \tag{5.22}$$

with $b < 1$, implying a decreasing per-device BoS cost

$$C_{\text{dev}}(N) = C_{\text{dev}}(1) \cdot N^{b-1}. \tag{5.23}$$

A mid-range exponent $b = 0.85$ is adopted, making an analogy with recent techno-economic offshore wind modelling assumptions that account for economies of scale with increasing farm size [30].

- Co - Location with an offshore wind farm, The integration of WEC arrays within existing offshore wind concessions allows for substantial CAPEX and OPEX reductions. Shared infrastructure and logistical resources, specifically maintenance vessels and specialized crews, result in superior system availability over standalone configurations. The availability increases from the 75% of the standalone case, to 85%.[31].

.

Chapter 6

Results and Discussion

This chapter presents the results of the techno-economic analysis carried out on the considered Wave Energy Converters. The performance of CorPower and CETO 6 is evaluated across different locations by analysing key performance indicators (KPI) and the Levelised Cost of Energy (LCOE). Two different scaling approaches are compared, namely the Physical Scaling Method (PSM) and the Froude Scaling Method (FSM), in order to assess their impact on both technical and economic outcomes. The analysis first focuses on KPI trends to understand the relationship between cost and energy production, and then evaluates how these trends translate into final economic performance through the LCOE. The main objective is to identify the optimal device configuration and the most suitable site for deployment.

6.1 KPI

KPI is used to analyse two structural elements of the WEC: the horizontal winch, representing the tubular PTO-related component, and the vertical cylinder, representing the internal load-transfer system. Although these components are not treated as primary cost drivers in the full project LCOE, their cost evolution remains relevant for design optimisation, since it provides insight into how local structural choices scale with device size and energy output. Their behaviour with respect to variations in radius and AEP is evaluated using the KPI, which directly considers the ratio between cost and AEP for each specific radius. Therefore, a lower KPI corresponds to a more cost-effective design.

For this analysis, Portugal is selected as the reference sea-state location. This choice avoids overcomplicating the presentation of results, while providing a representative compromise between low- and high-energy sea states. Moreover, Portugal is commonly adopted as a benchmark location in several studies and real-world project developments.

6.1.1 Physical Scaling Method

The trend of the cost increase with the AEP, according to the Physical Scaling Method (PSM), is illustrated for the two different devices in Figures 6.1, 6.2. Although the plots are reported as cost versus AEP, each point corresponds to a different device radius. Therefore, the observed progression along the curve reflects how both cost and AEP evolve as the radius increases

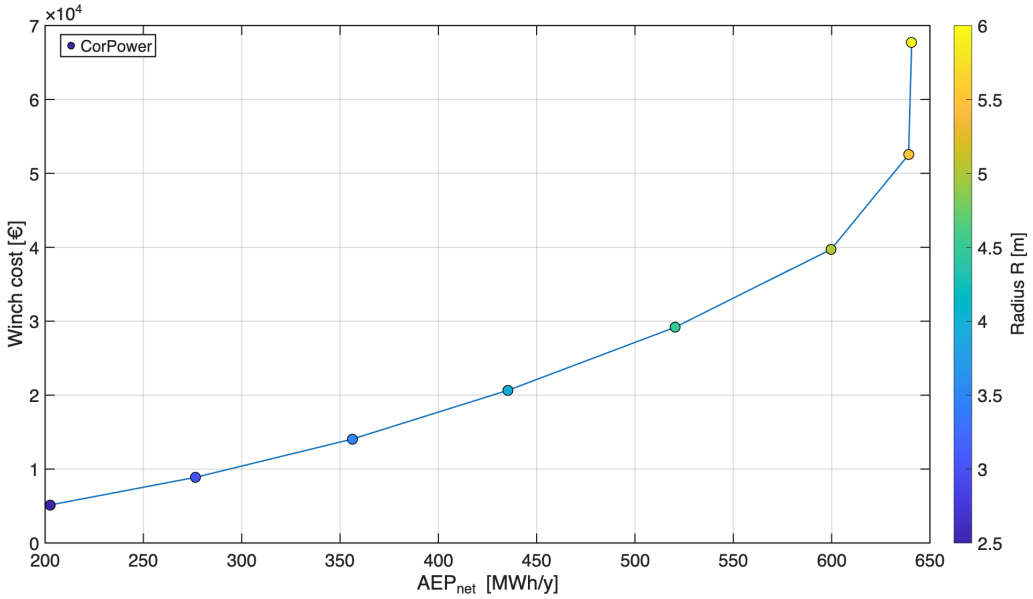

(a)

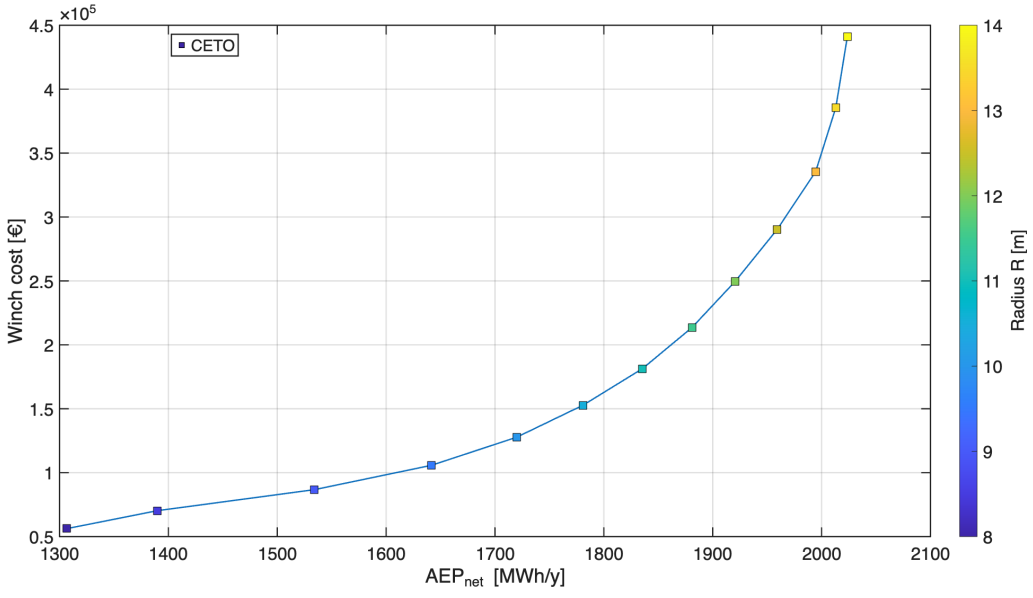

(b)

Figure 6.1: Relationship between cost and AEP for the Winch of CorPower and CETO 6 in Portugal using PSM for: (a) CorPower , (b) CETO 6

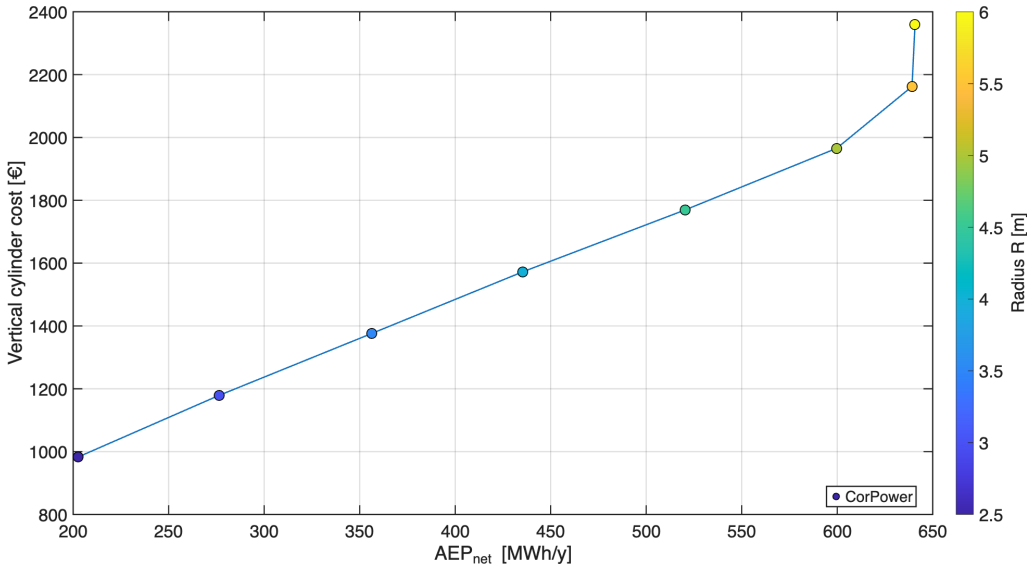

(a)

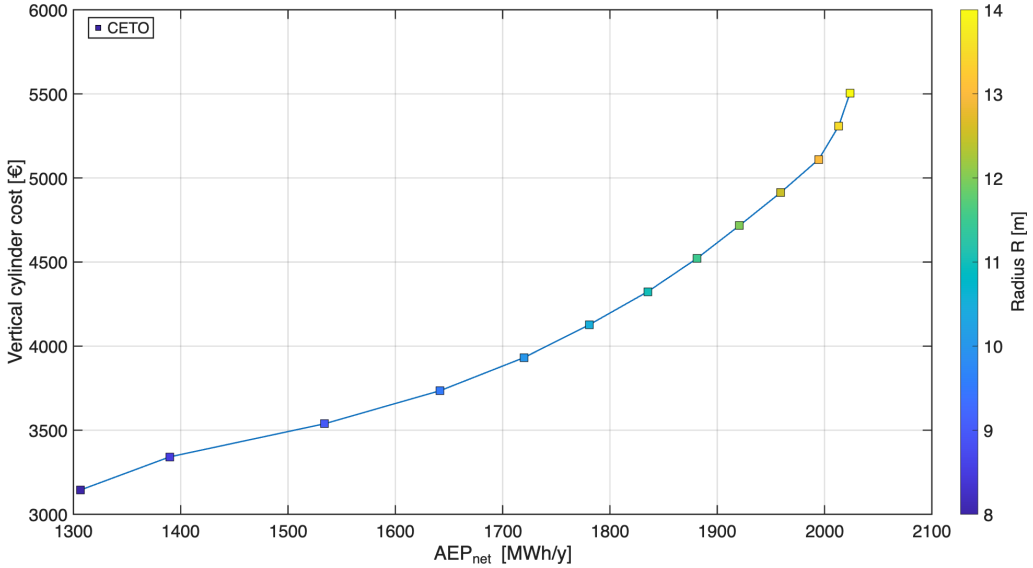

(b)

Figure 6.2: Relationship between cost and AEP for the Vertical Cylinder of CorPower and CETO 6 in Portugal using PSM for: (a) CorPower , (b) CETO 6

Figures 6.1 and 6.2 show that the trend is very similar for both elements and for the two different devices, CorPower and CETO 6. In both cases, the cost increases with radius. The increasing starts at a more gradual rate, followed by a steeper rise. This behaviour is explained by the non-linear relationship between AEP and radius: AEP increases rapidly at smaller radii, then continues to grow at a slower rate as the radius becomes larger.

A notable difference between the two elements is the higher cost associated with their application in the CETO 6 compared to the CorPower device. This is primarily due to the larger dimensions of the CETO 6, which lead to higher structural loads.

The KPI behaviour is then analysed in Figures 6.3 and 6.4, which directly relates cost to energy production. The KPI behaviour of the winch is shown in Figure 6.3, while the corresponding trend for the vertical cylinder is shown in Figure 6.4.

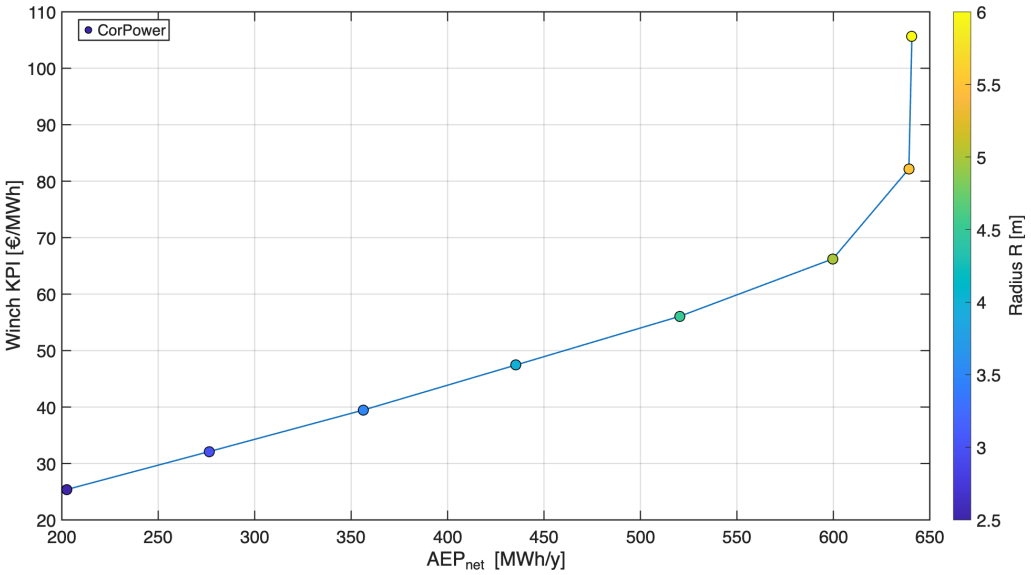

(a)

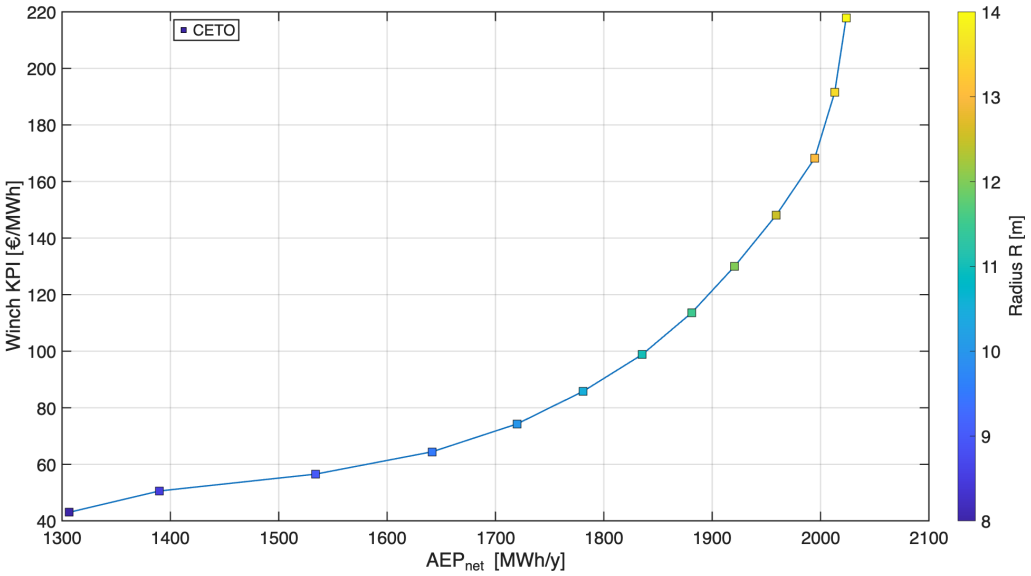

(b)

Figure 6.3: Relationship between KPI and AEP for Winch component in Portugal using PSM for: (a) CorPower , (b) CETO 6

For the winch, the KPI increases monotonically for both CorPower and CETO 6. In the lower-radius range, the increase is relatively moderate because the gain in AEP partially compensates for the increase in cost. At larger radii, however, the cost grows faster than the additional AEP that can be captured, so the KPI rises more sharply.

The KPI trend, for both devices, for what concern the vertical cylinder is presented

in Figure 6.4

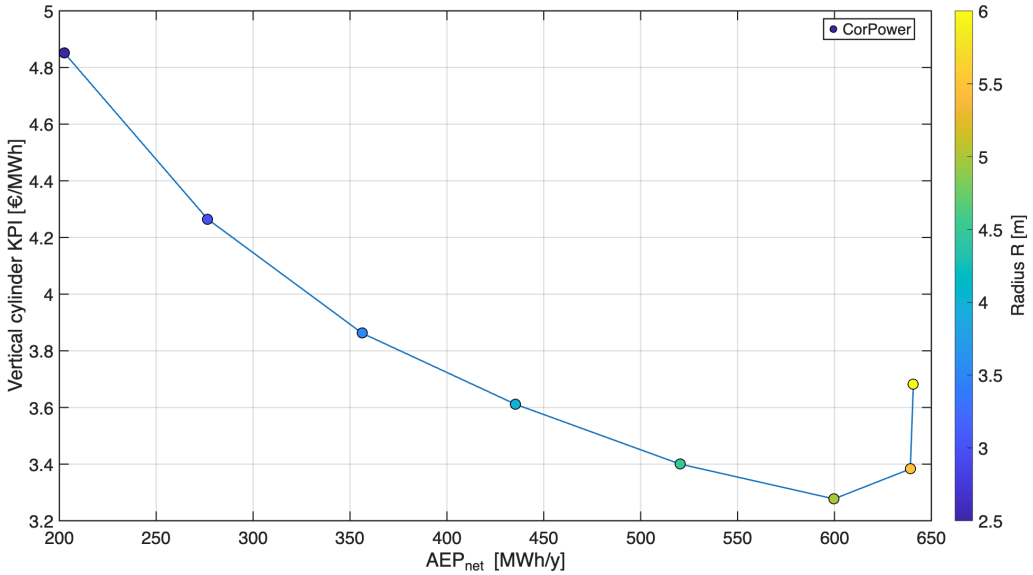

(a)

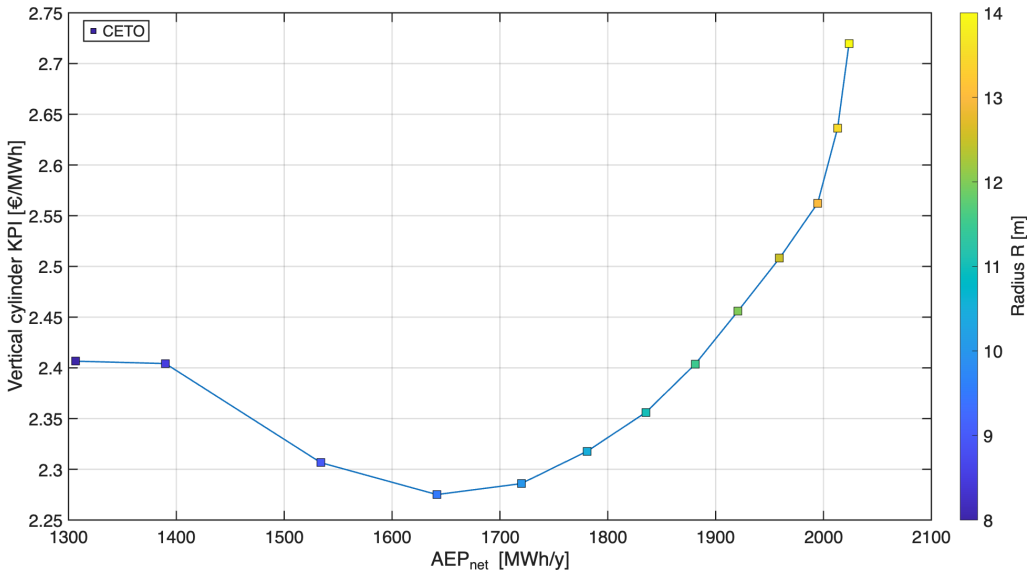

(b)

Figure 6.4: Relationship between KPI and AEP for the Vertical Cylinder component in Portugal using PSM for: (a) CorPower , (b) CETO 6

Figure 6.4 highlights a markedly different behaviour of the vertical cylinder compared with the winch. The vertical cylinder plot one exhibits a non-monotonic KPI trend, with a minimum value at an intermediate radius for both devices. In design terms, this indicates the presence of an optimal size beyond which further increases in radius are no longer economically justified for the vertical cylinder.

Figure 6.5 helps explain the different KPI behaviours by comparing the normalized growth of AEP and component cost with increasing radius. For the winch, the cost curve grows faster than the AEP curve over the entire radius range in both devices.

As a result, the KPI continuously worsens, producing the monotonic increase observed in Figure 6.3.

For the vertical cylinder, the behaviour is different. In the CorPower case, the AEP initially increases faster than the component cost, causing the KPI to decrease. Once the AEP begins to level off while cost continues to rise, the KPI reaches a minimum and then starts increasing again. A similar behaviour is observed for CETO 6: at smaller radii the growth of AEP and cost is comparable, while beyond a threshold radius the cost increases more rapidly than AEP, leading again to a minimum KPI.

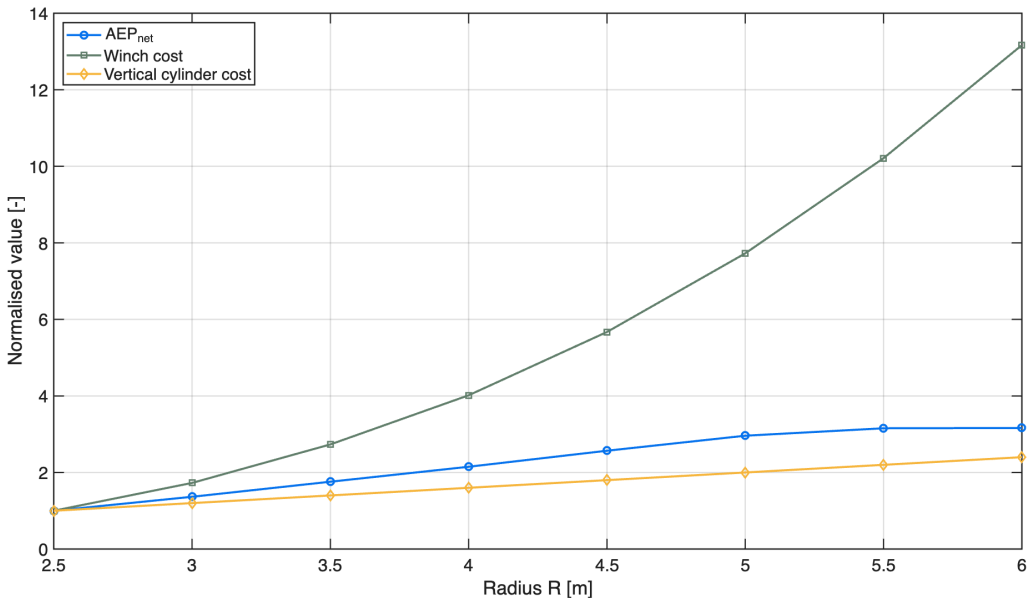

(a)

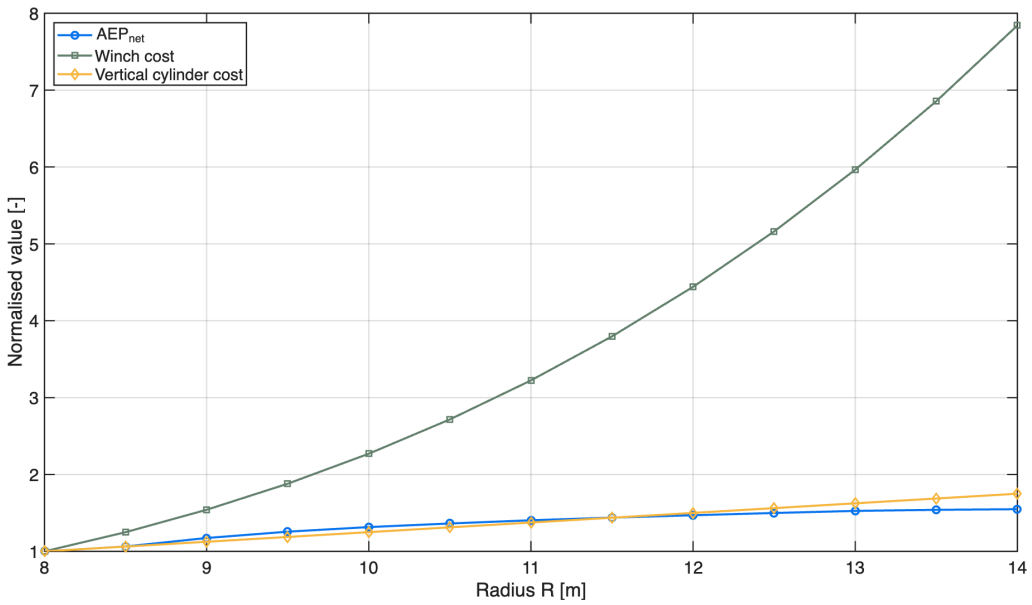

(b)

Figure 6.5: Normalized growth of AEP and component costs as a function of increasing radius in Portugal using PSM for: (a) CorPower , (b) CETO 6

Overall, the KPI analysis shows two distinct behaviours. The winch exhibits a continuously worsening cost-to-energy ratio as radius increases, indicating that larger sizes are progressively less favorable for this component. By contrast, the vertical cylinder shows the existence of an intermediate optimal radius, where the trade-off between structural cost and AEP is most advantageous.

6.1.2 Froude scaling

The Froude Scaling Method is commonly used to estimate the performance of scaled devices based on similarity laws. However, this approach does not fully capture the variation of structural loads and material requirements, which may lead to discrepancies when compared to the Physical Scaling Method. This comparison is essential to assess whether Froude scaling can reliably reproduce the techno-economic behaviour observed with direct simulations.

Starting with the winch and vertical cylinder trend cost, with the AEP and radius increase, for both devices CorPower and CETO 6, shown in Figure 6.6 and 6.7.

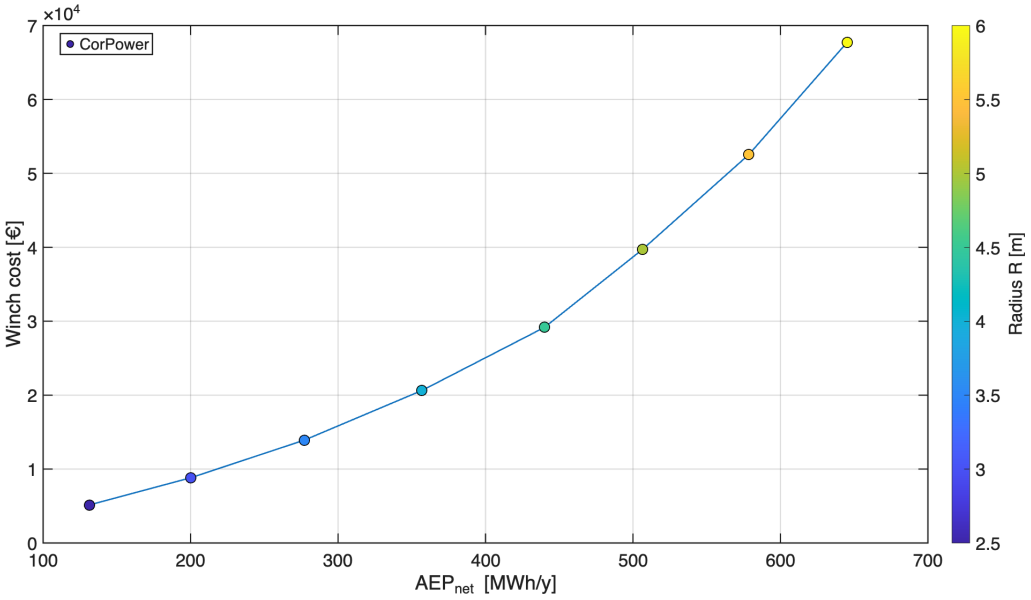

(a)

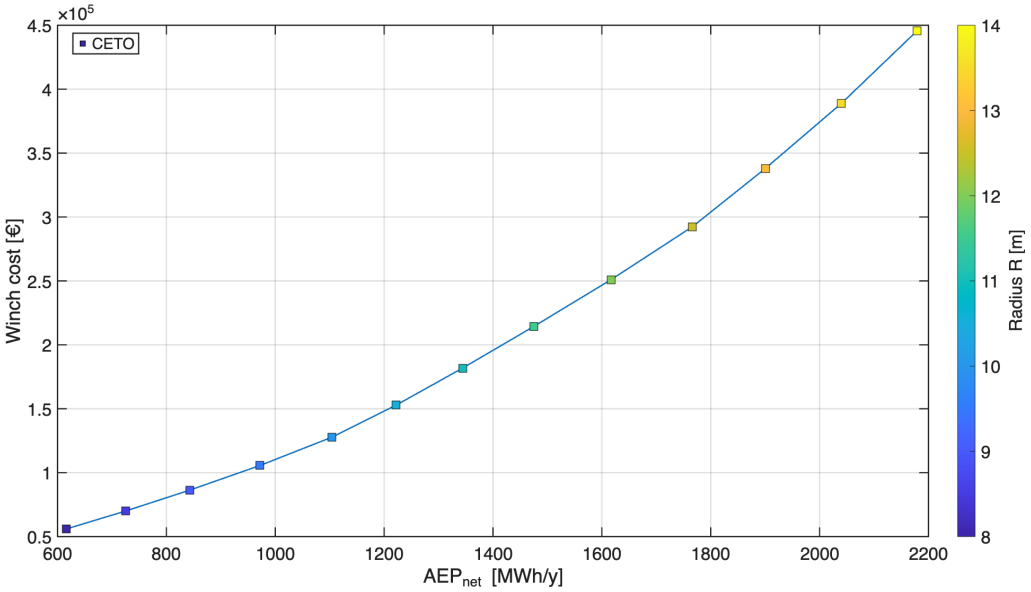

(b)

Figure 6.6: Relationship between cost and AEP for the Winch of CorPower and CETO6 in Portugal using FSM for: (a) CorPower , (b) CETO 6

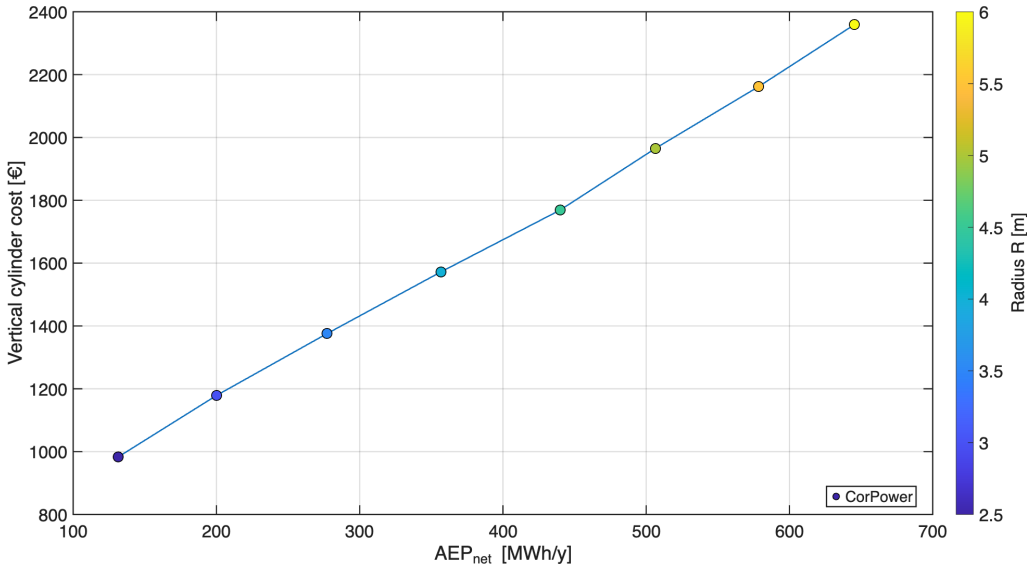

(a)

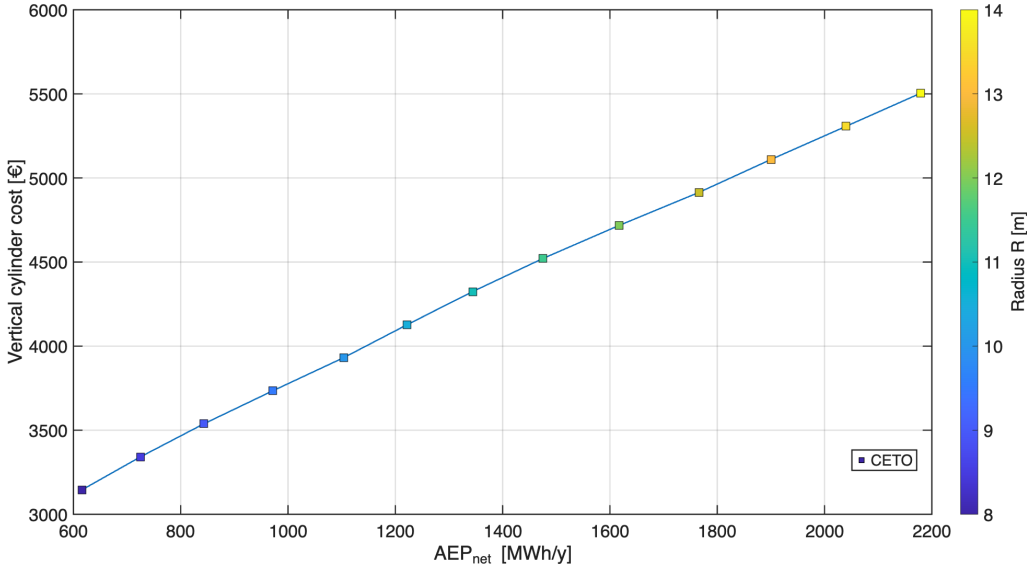

(b)

Figure 6.7: Relationship between cost and AEP for the Vertical Cylinder in Portugal using FSM for: (a) CorPower , (b) CETO 6

Figures 6.6 and 6.7 show that the cost increases with AEP for both components, similarly to the PSM results. The trends are similar to the PSM case, but noticeably smoother, indicating that Froude scaling reduces the non-linear behaviour observed with PSM showing how the Froude scaling tends to dampen the non-linear effects observed in the direct simulations.

The KPI trends obtained with Froude scaling differ significantly from those derived with the PSM. In particular, the non-monotonic behaviour observed for the vertical cylinder is no longer captured. Instead, the KPI shows a monotonic increase for the winch and a monotonic decrease for the vertical cylinder. As a result, no optimal

radius can be identified in the FSM results. This represents a major limitation, since the optimal design point identified using the PSM is completely lost when applying Froude scaling.

For what concern the KPI trend for both the element and the device, the limitation of the Froude scaling are highlighted, in particular regarding an increase of the AEP with radius less realistic resulting in a monotonic trend, increasing for the winch and decreasing for the vertical cylinder, as it is possible to see in Figure 6.8 and 6.9. For this reason the minimum observed in Figure 6.4, regarding the KPI trend for the vertical cylinder for both the device, it is not appreciated in this case as it is possible to appreciate in Figure 6.9.

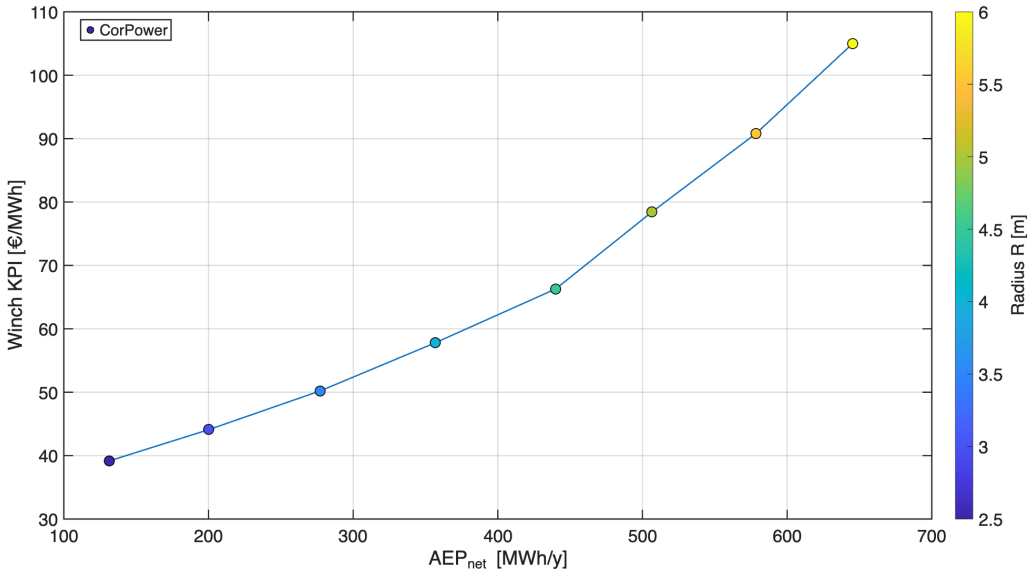

(a)

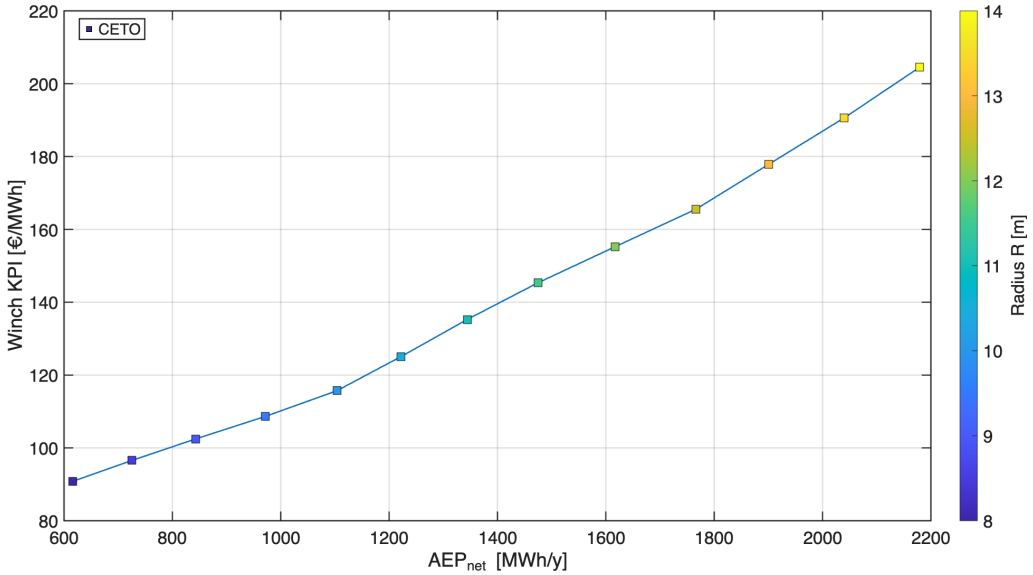

(b)

Figure 6.8: Relationship between KPI and AEP for the Winch component for in Portugal using FSM for: (a) CorPower , (b) CETO 6

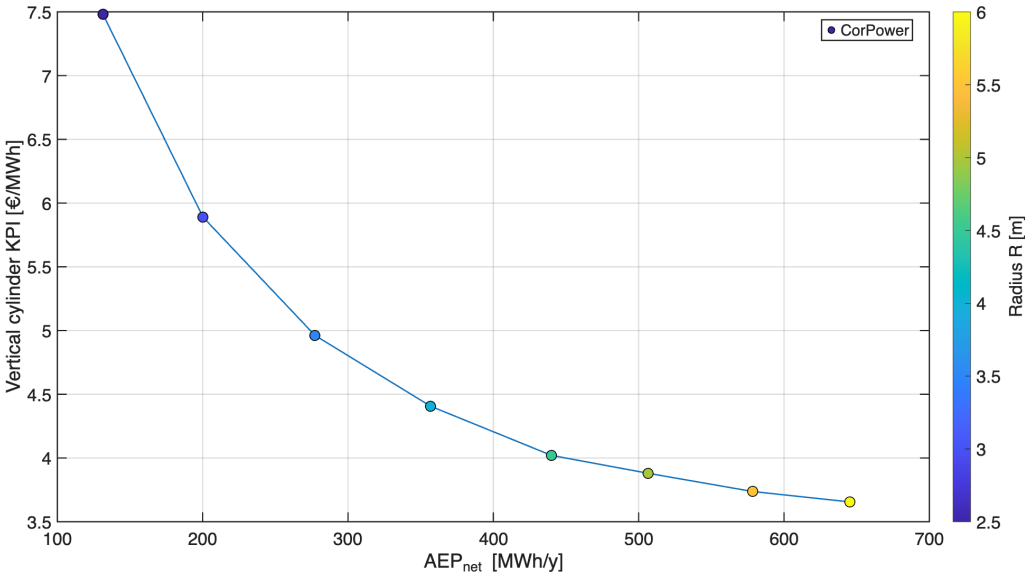

(a)

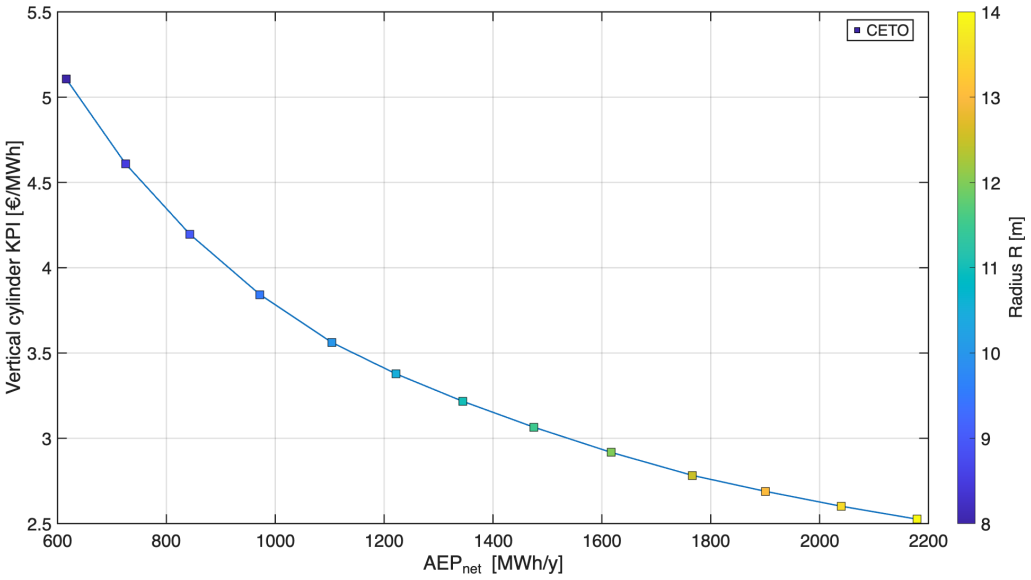

(b)

Figure 6.9: Relationship between KPI and AEP for the Vertical Cylinder component in Portugal using FSM for: (a) CorPower , (b) CETO 6

The reason for this different trend, in particular for the vertical cylinder can be observed in Figure 6.10 and 6.11.

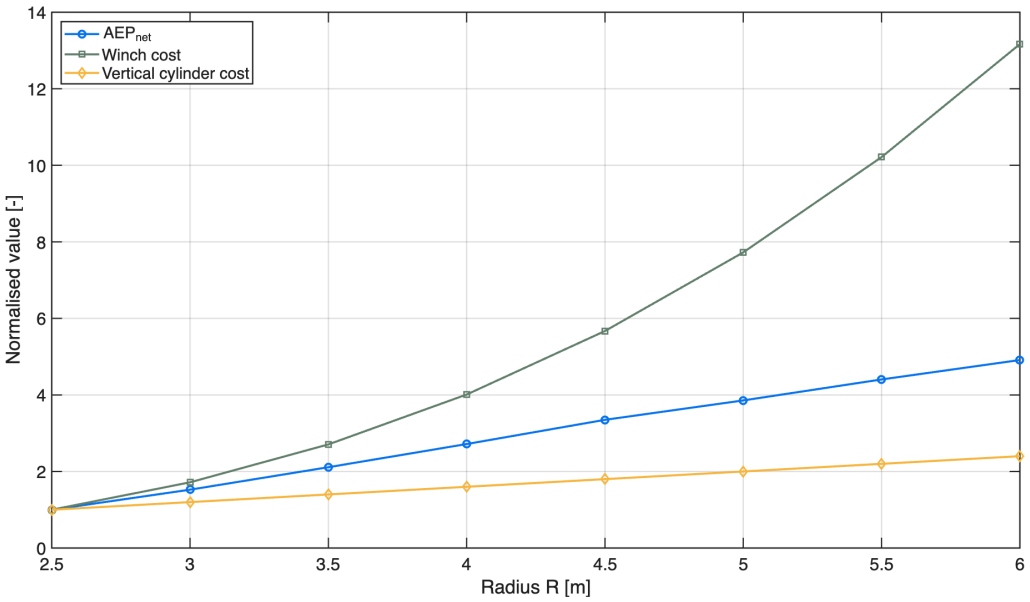

(a)

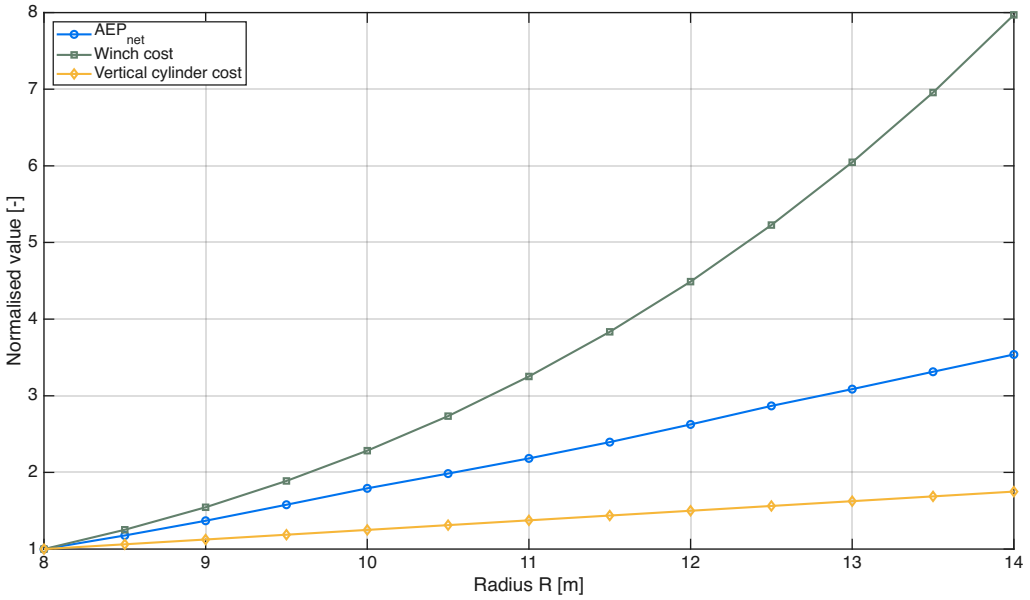

(b)

Figure 6.10: Normalized growth of AEP and component costs as a function of increasing radius in Portugal using FSM for: (a) CorPower , (b) CETO 6

Figure 6.10 illustrates the normalized evolution of AEP and component costs with increasing radius under Froude scaling. In this case, both AEP and cost increase monotonically, without any change in their relative growth rates. Consequently, the cost-to-AEP ratio does not exhibit a minimum, leading to the monotonic KPI trends observed. This limitation arises from the simplified nature of Froude scaling, which preserves geometric similarity but does not fully capture the complex coupling between hydrodynamic response, control strategy and energy production that affects the AEP scaling.

Overall, the comparison between the two approaches shows that the Froude Scaling Method provides a simplified estimation of performance, while the Physical Scaling Method offers a more accurate representation of the interaction between hydrodynamics and structural constraints. Therefore, FSM can be considered suitable for preliminary assessments, whereas PSM is more appropriate for detailed design optimization.

6.2 LCOE

While the KPI analysis provides insight into the balance between cost and energy production, and is used for the economic assesment of the winch and the vertical cylinder, so two secondary components, the Levelised Cost of Energy represents the final metric for evaluating the economic feasibility of each configuration. This section investigates how the previously observed trends influence the overall cost of energy production across different sites and scaling approaches.

6.2.1 Physical Scaling Method

The LCOE results obtained through the Physical Scaling Method (PSM) provide a detailed understanding of the techno-economic behaviour of the analysed WECs across different configurations and locations.

As anticipated in Chapter 5, the device cost—particularly that of the hull, is determined by estimating the required thickness to withstand hydrodynamic loads. The contributions to the equivalent thickness are presented in Figures 6.11a and 6.11b. For these plots, only the Portugal location is considered, as the observed trends are consistent across all analyzed locations, despite differences in absolute values.

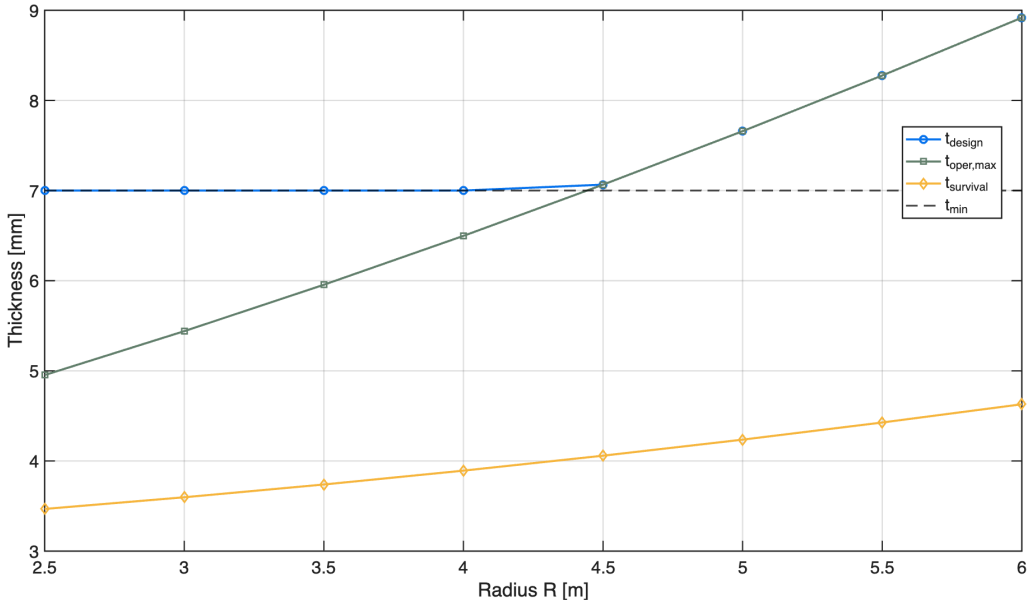

(a)

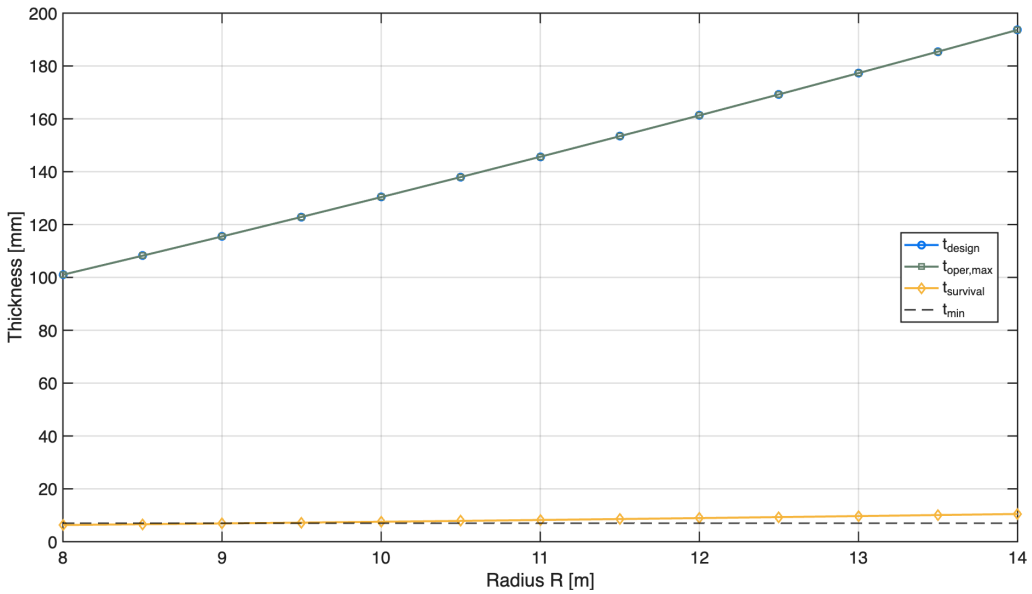

(b)

Figure 6.11: Thickness breakdown for the hull in Portugal using PSM for: (a) CorPower , (b) CETO 6

Figures 6.11 and 6.12 show the evolution of structural thickness components as a function of device radius for both CorPower and CETO 6. For the CorPower device, at smaller radii (approximately 2.5–4.5 m), the design is governed by the minimum commercial thickness, while at larger radii the operational loads become dominant, leading to an increase in structural requirements. In contrast, for the CETO 6 device, the structural thickness is consistently governed by operational loads due to its larger size and higher hydrodynamic forces.

It is also important to analyse how the increase in structural thickness affects the

overall CAPEX of the project, as well as its cost breakdown, and how these evolve with increasing device radius. These data are shown in Figure 6.12a and 6.12b.

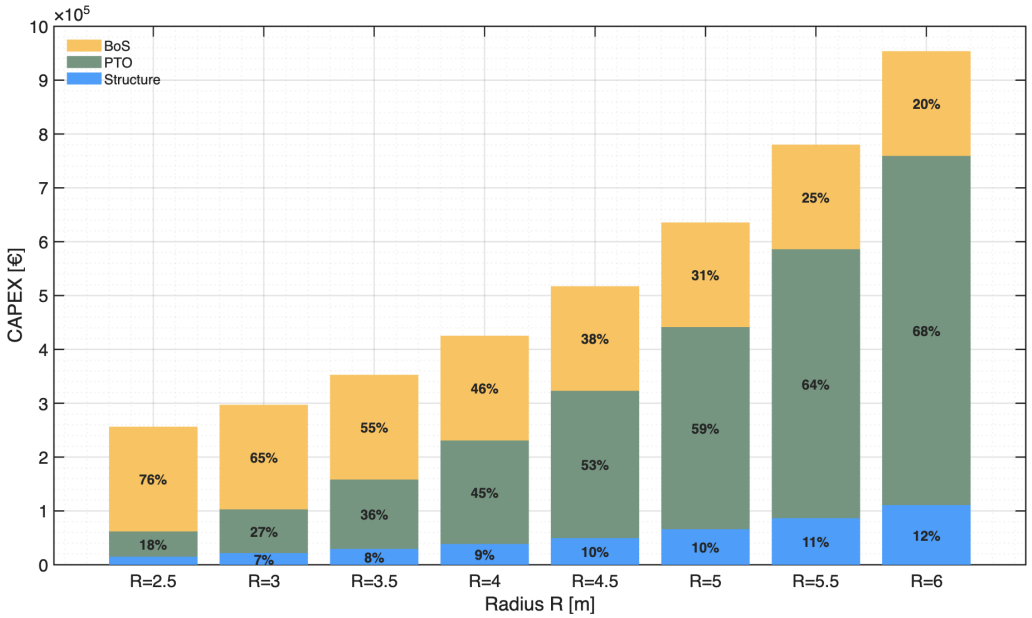

(a)

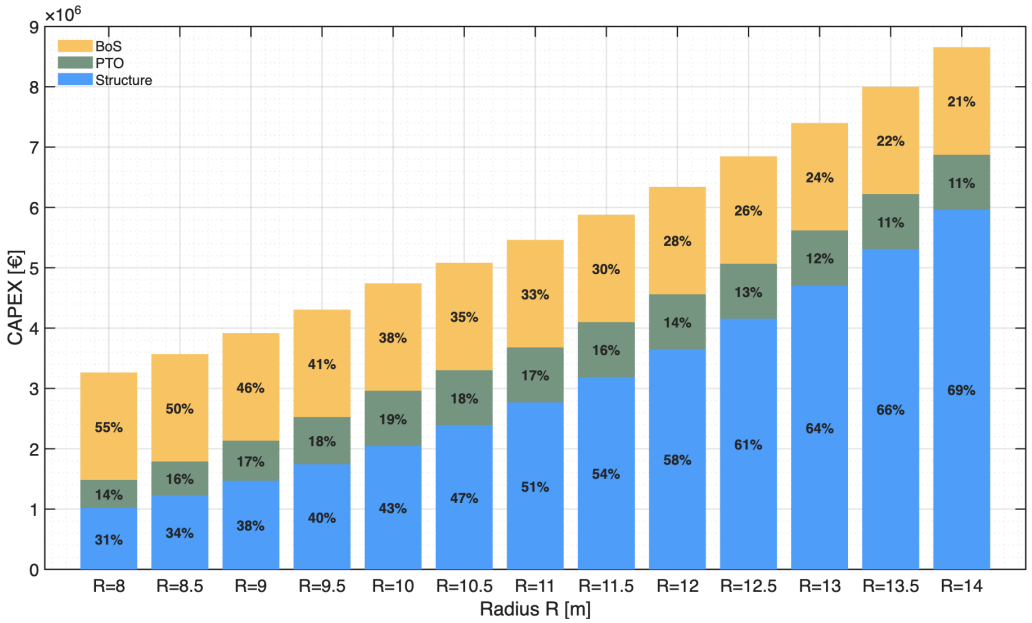

(b)

Figure 6.12: CAPEX breakdown evolution with thickness in Portugal using PSM for: (a) CorPower , (b) CETO 6

Considering 6.12a and 6.12b, the differences between CorPower and CETO 6 become clear.

This difference in structural behaviour has a direct impact on CAPEX distribution. For CorPower PTO system becomes the dominant cost component as the radius increases, mainly due to the increase in energy production, and due to the

lower loads which necessitates lowers thickness. Conversely, for CETO 6, the structural component represents the main cost driver, as the larger dimensions lead to significantly higher loads and material requirements, while the PTO contribution remains relatively constant once the rated power is reached, due to its higher energy production.

The variation in structural thickness directly affects the total mass of the device and, consequently, the CAPEX. This increase in cost must be compensated by a corresponding increase in energy production in order to maintain a competitive LCOE.

The LCOE trends observed in the following figures 6.13 - 16.6 are the result of the combined effect of increasing CAPEX and variations in Annual Energy Production. The optimal configuration is therefore identified as the point where this trade-off is minimized.

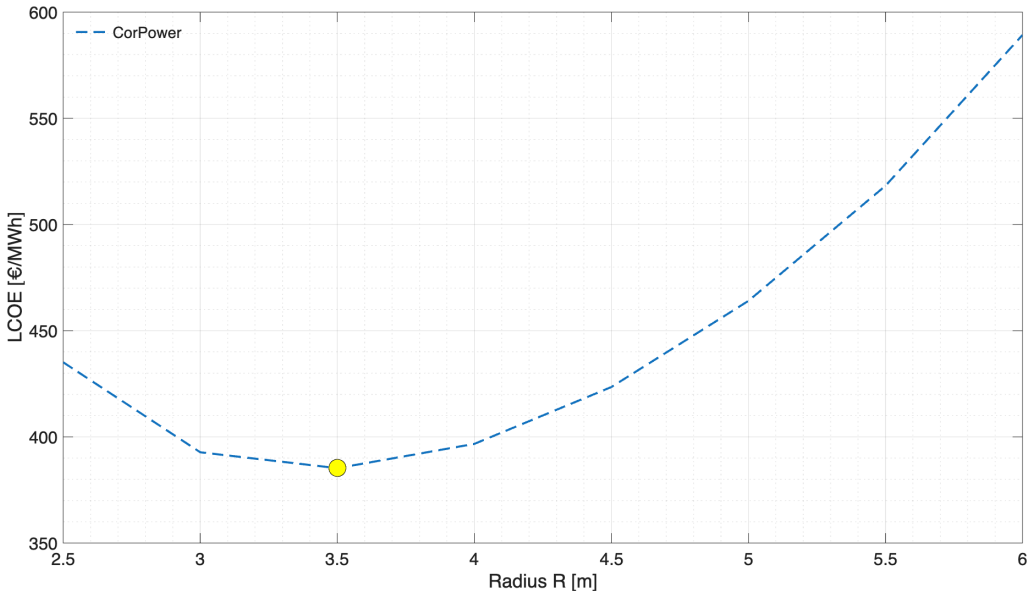

(a)

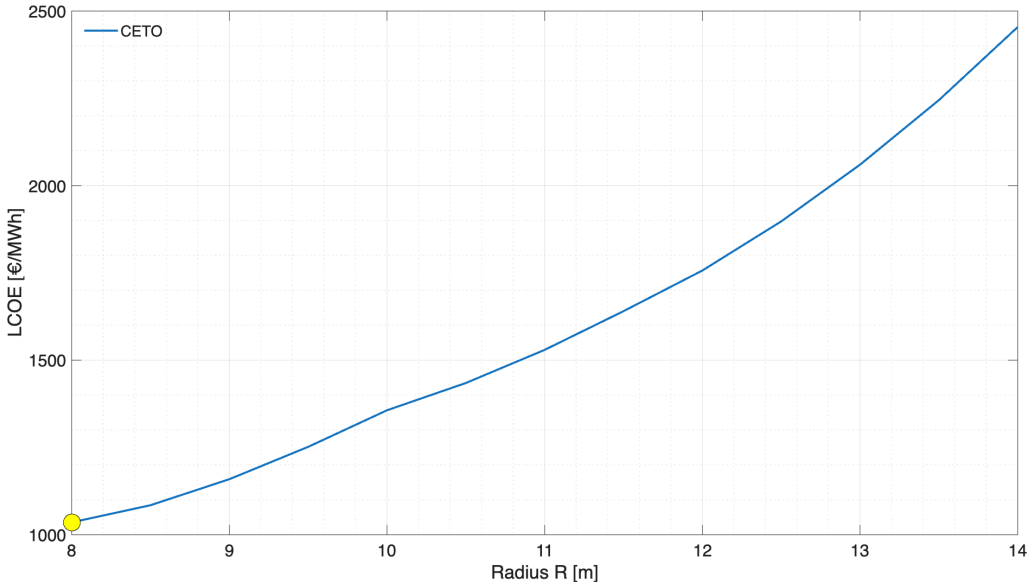

(b)

Figure 6.13: LCOE variation with radius in Germany using PSM for: (a) CorPower , (b) CETO 6

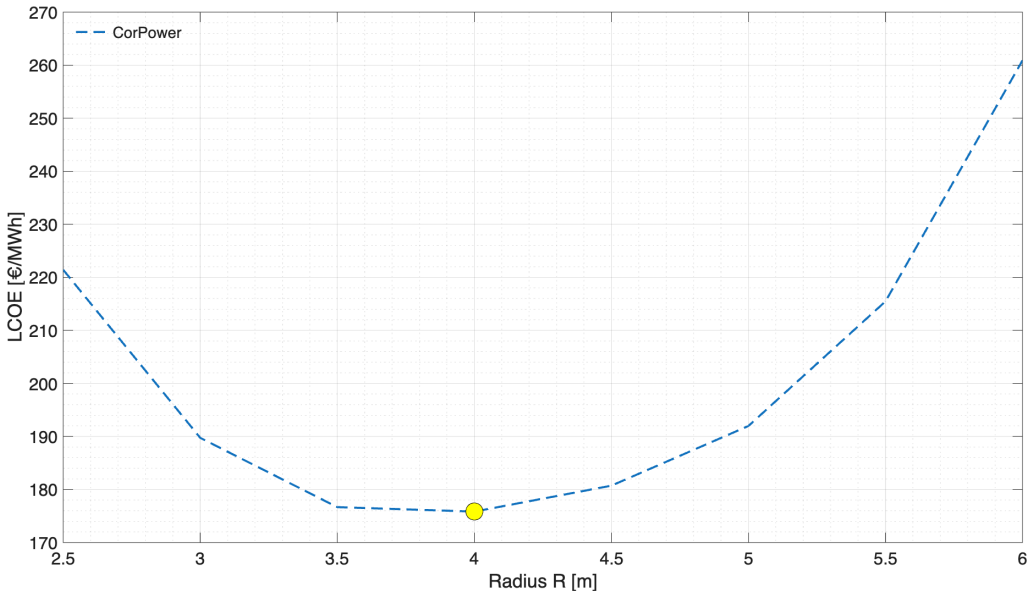

(a)

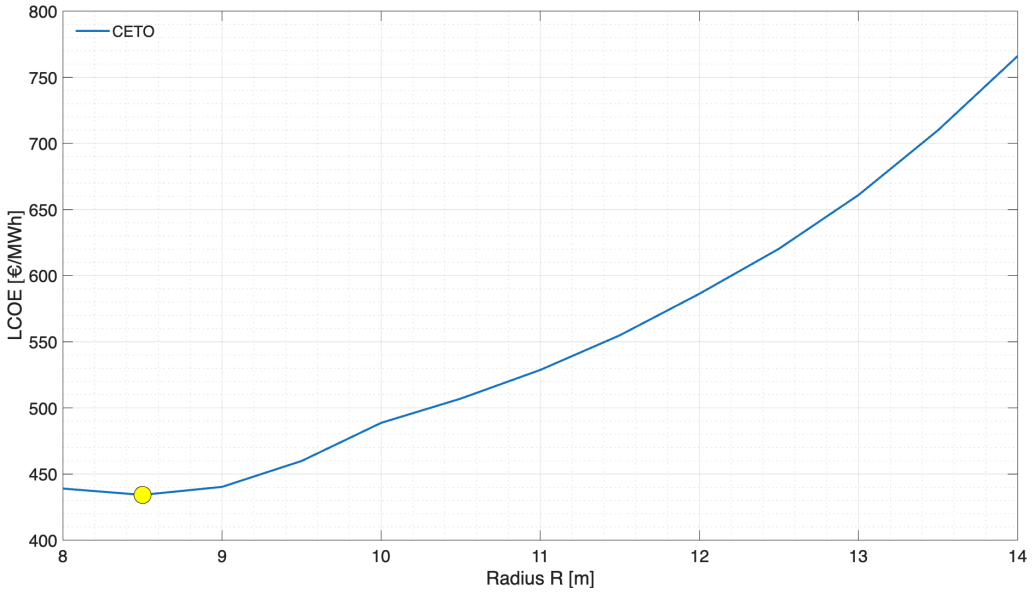

(b)

Figure 6.14: LCOE variation with radius in Scotland using PSM for: (a) CorPower , (b) CETO 6

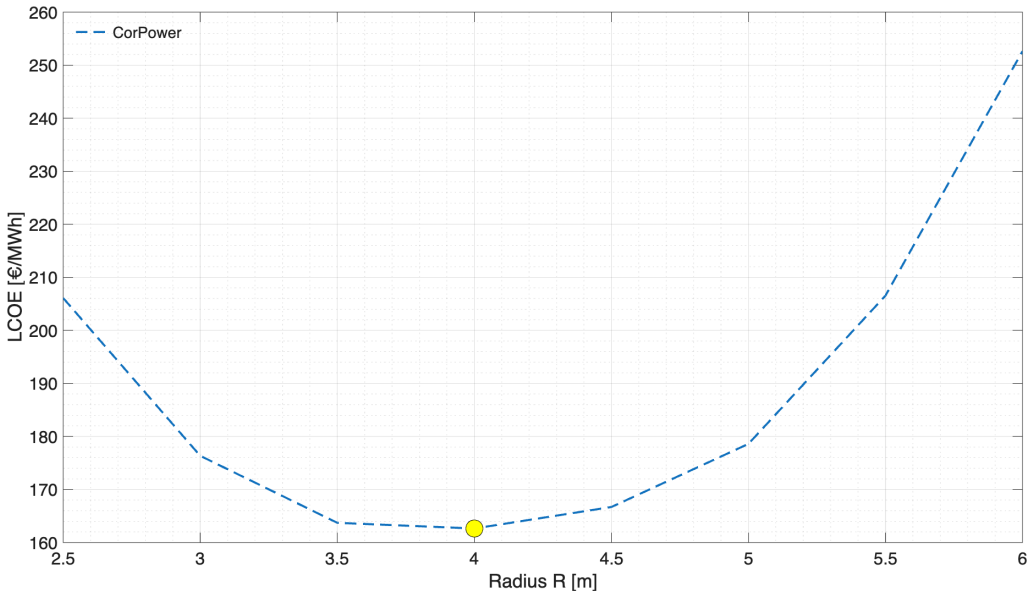

(a)

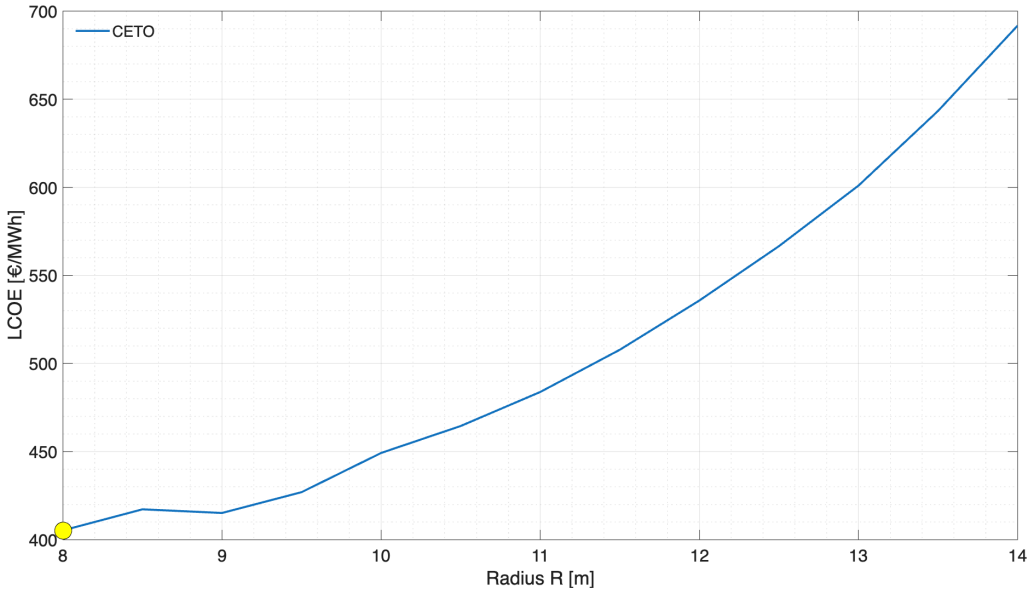

(b)

Figure 6.15: LCOE variation with radius in Portugal using PSM for: (a) CorPower , (b) CETO 6

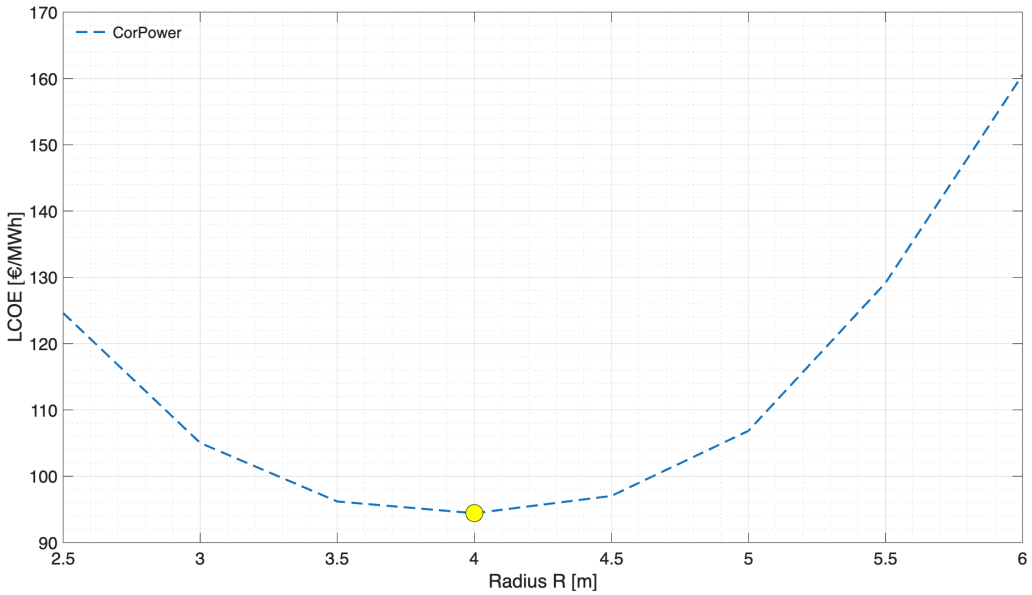

(a)

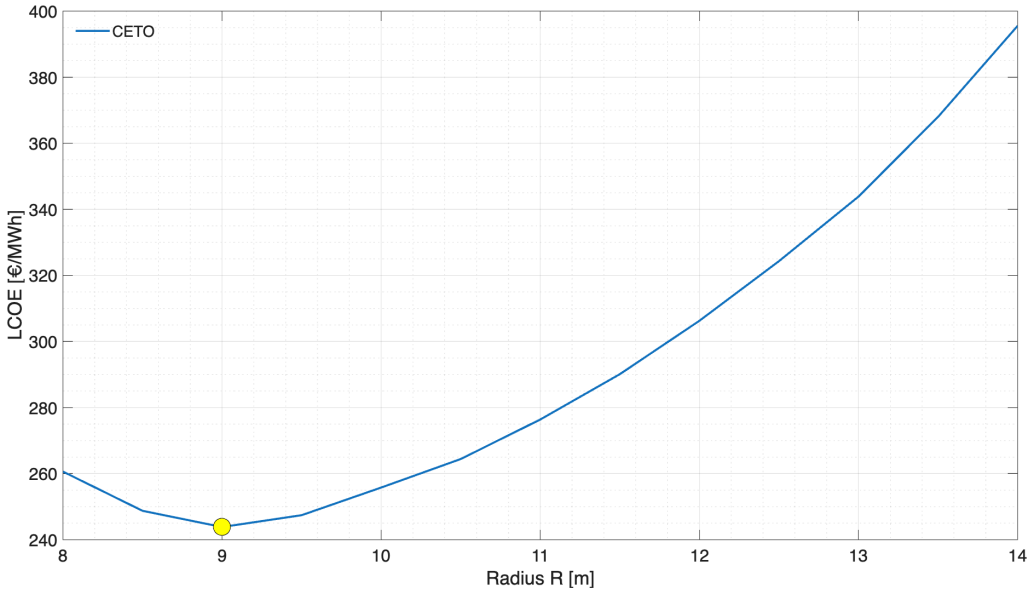

(b)

Figure 6.16: LCOE variation with radius in Australia using PSM for: (a) CorPower , (b) CETO 6

For both devices, the LCOE exhibits a non-monotonic behaviour, as it is possible to appreciate from Figure 6.13–6.16, with respect to the device radius. Initially, increasing the radius leads to a reduction in LCOE, as the gain in energy production outweighs the increase in costs. However, beyond a certain optimal radius, the rapid growth in structural and material costs becomes dominant, resulting in an increase in LCOE.

This behaviour is particularly evident for the CorPower device, which shows a well-defined parabolic trend across all analysed locations. The presence of a clear min-

imum indicates the existence of an optimal design radius that balances energy capture and cost.

For CETO 6, the trend is less pronounced and, in some locations, the minimum LCOE occurs at the smallest radius analyzed. This suggests that the optimal radius has not been fully identified. The decision not to investigate smaller radii was made to avoid configurations that would significantly deviate from the standard dimensions of the commercial device. Moreover, this result may implicitly indicate the infeasibility of the device in the considered locations.

The influence of site conditions is also significant. Locations characterised by higher wave energy potential allow for higher AEP values, which generally translate into lower LCOE. To further assess the effect of site resource availability, the minimum LCOE obtained for a single WEC at each location was compared with the corresponding local wave energy potential, as shown in Figure 6.17.

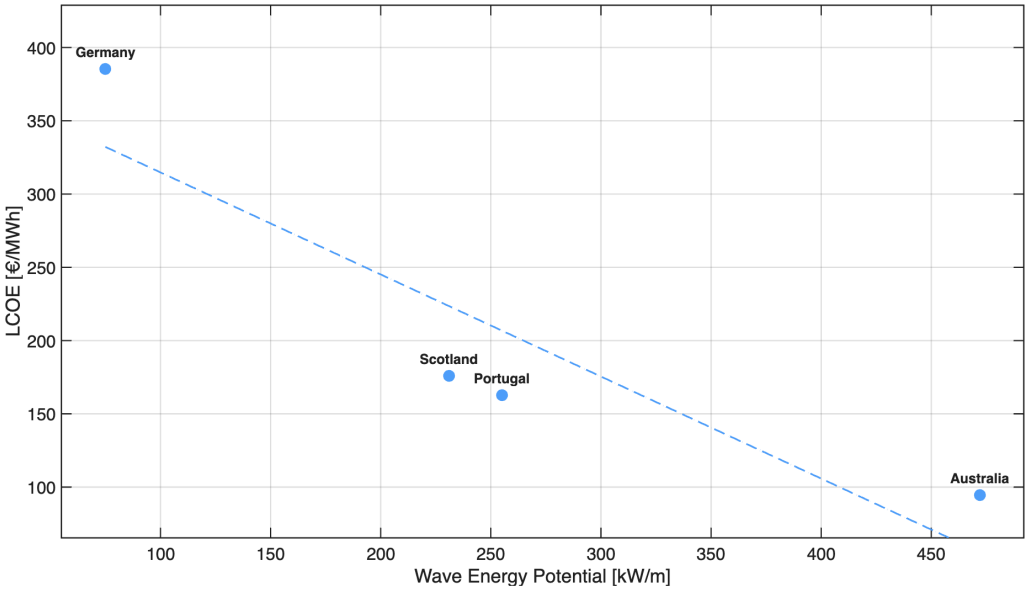

Figure 6.17: LCOE relation with Wave Energy Potential

However, the relative impact of site conditions differs between the two technologies. CorPower demonstrates greater adaptability across a wider range of sea states, while CETO 6 achieves better performance in high-energy environments, where its larger size can be fully exploited.

6.2.2 Froude Scaling Method

The application of the Froude Scaling Method to the LCOE evaluation highlights significant differences compared to the Physical Scaling Method. These differences arise from the simplified treatment of structural and cost-related parameters in the scaling process.

In Figures 6.18a and 6.18b the evolution of the structural thickness as a function of the device radius for both CorPower and CETO 6 are displayed.

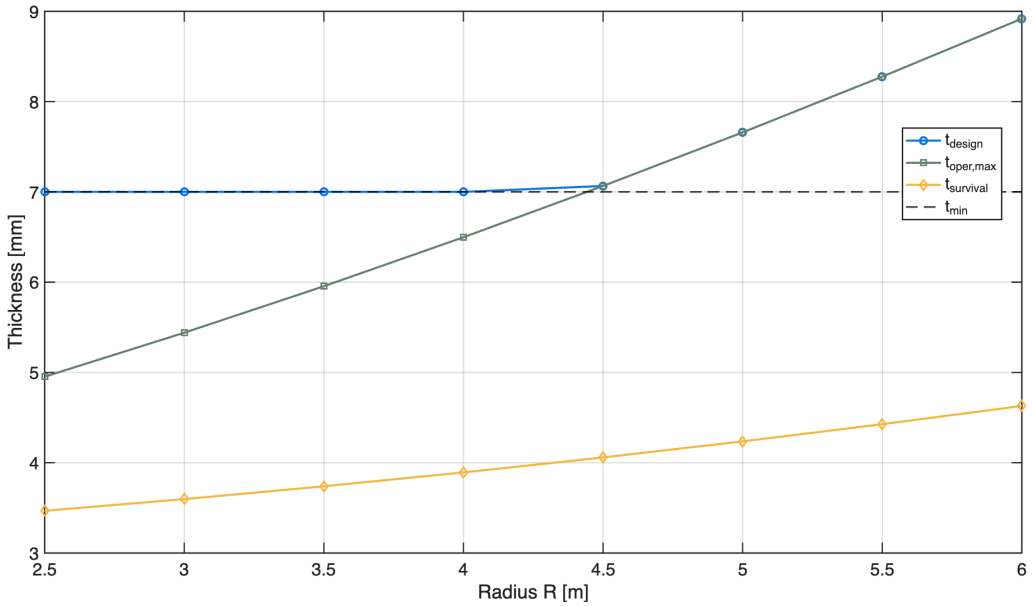

(a)

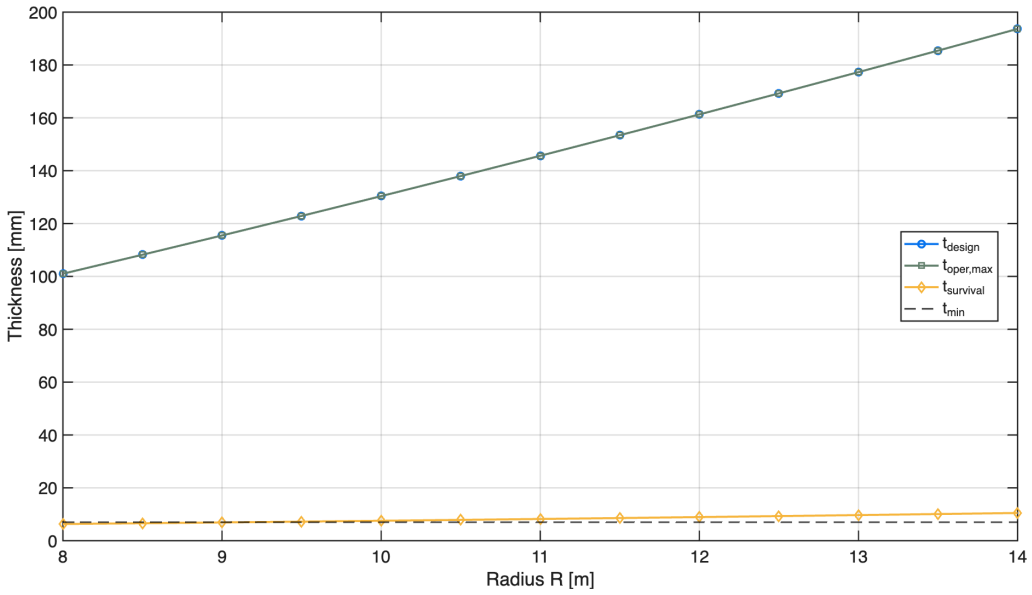

(b)

Figure 6.18: Thickness breakdown for the hull in Portugal using FSM for: (a) CorPower , (b) CETO 6

In Figures 6.18a and 6.18b is possible to appreciate how with the Froude scaling, the analysis of the thickness shows the same result as the one with the PSM, showing how with the two different methods the structural is preserved.

Instead, the analysis of the LCOE shows different results compared with those from the PSM, as can be deduced from Figure 6.19-16.22.

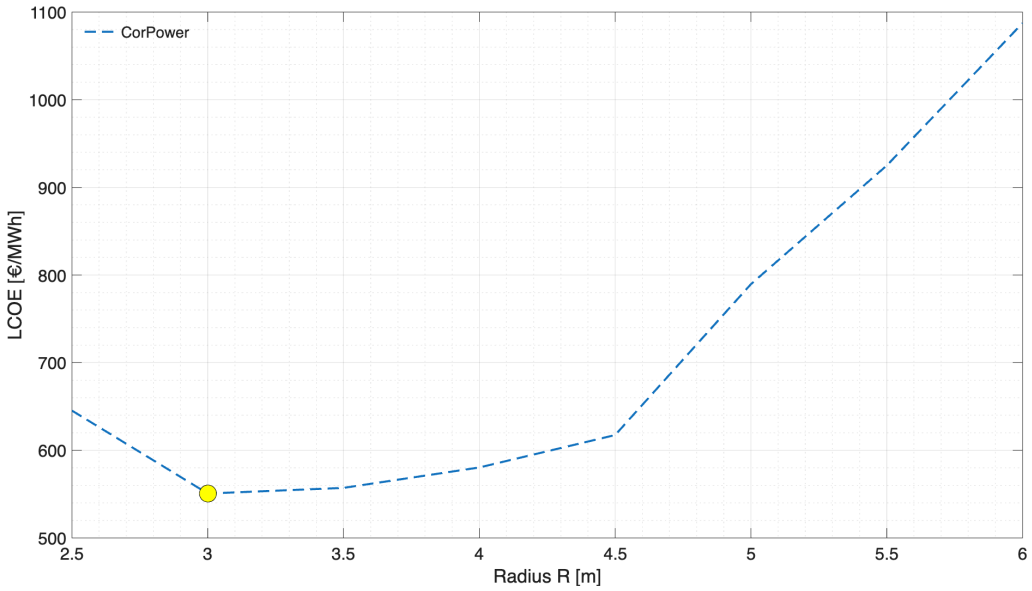

(a)

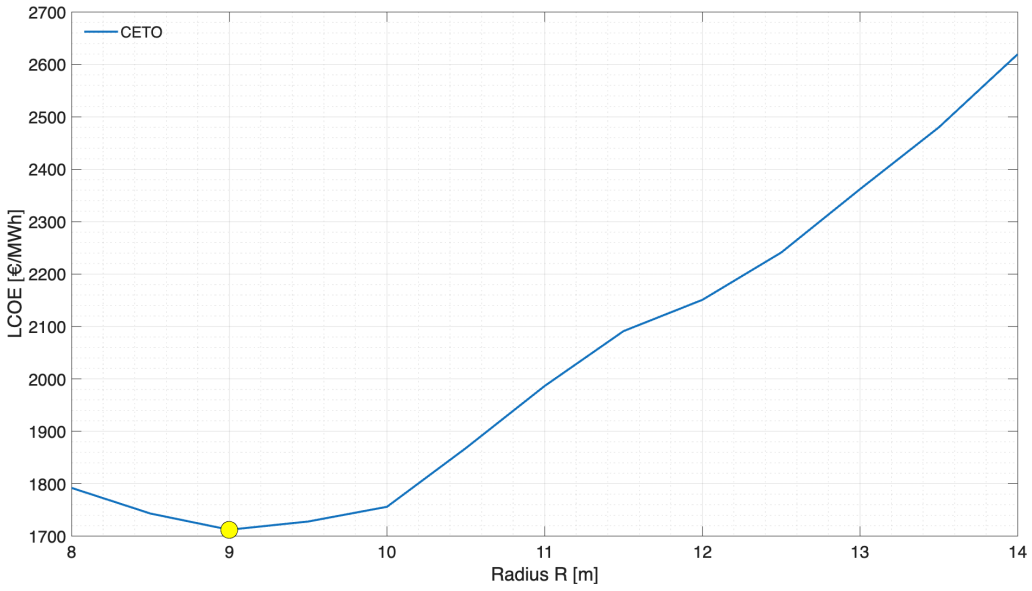

(b)

Figure 6.19: LCOE variation with radius in Germany using FSM for: (a) CorPower , (b) CETO 6

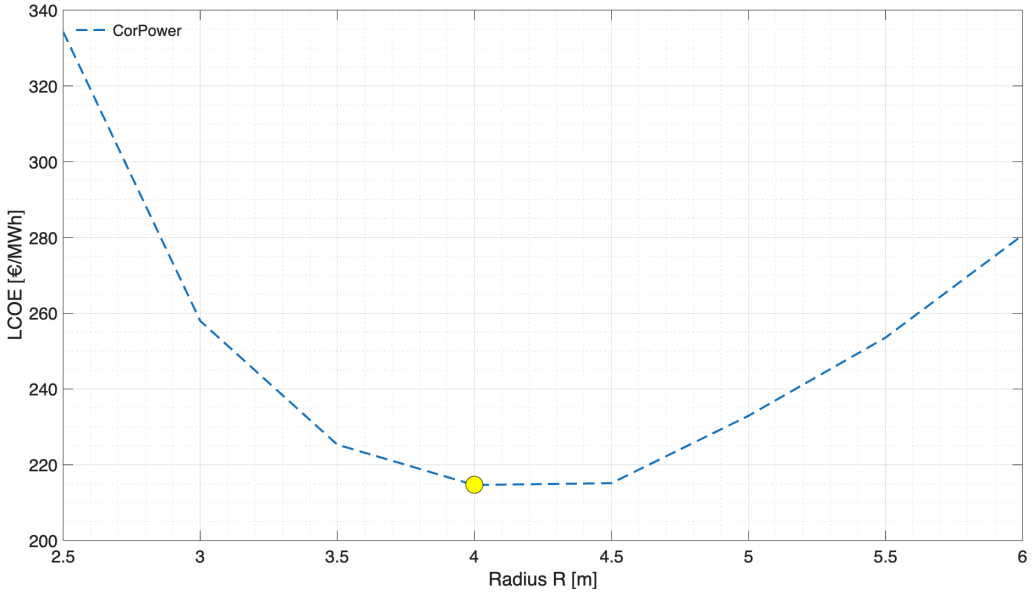

(a)

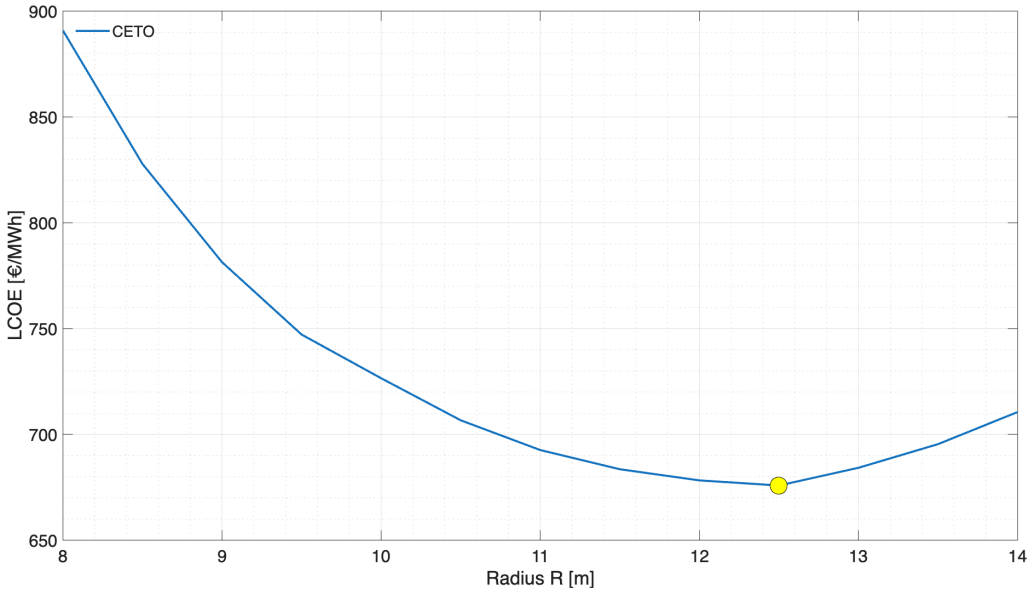

(b)

Figure 6.20: LCOE variation with radius in Scotland using FSM for: (a) CorPower , (b) CETO 6

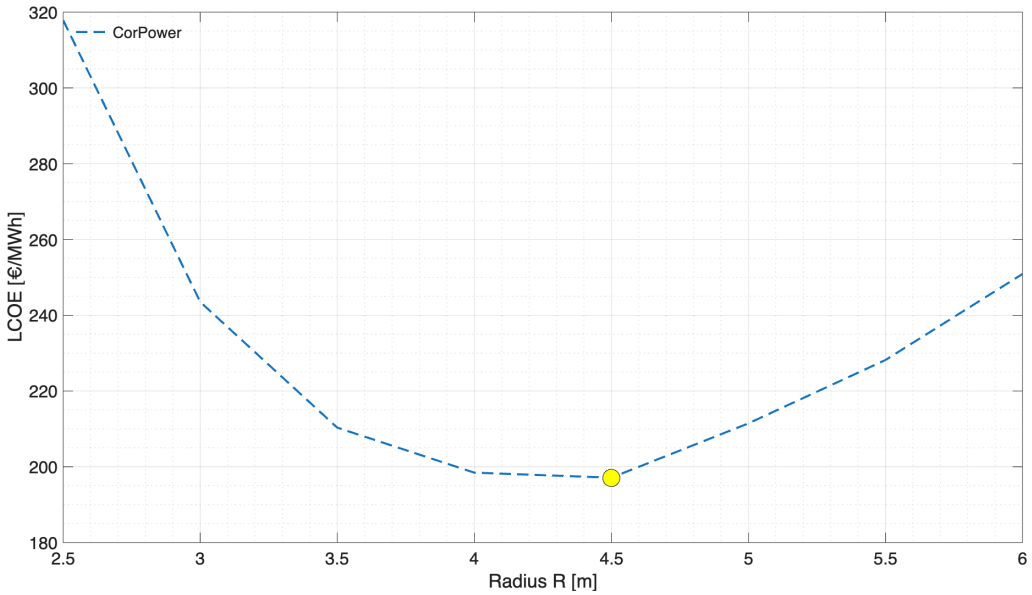

(a)

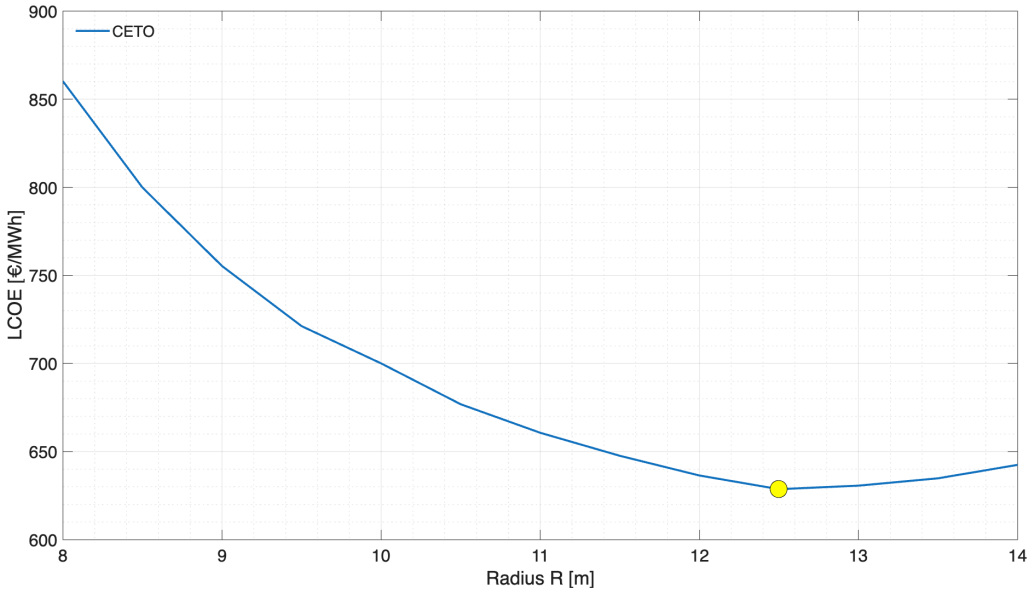

(b)

Figure 6.21: LCOE variation with radius in Portugal using FSM for: (a) CorPower , (b) CETO 6

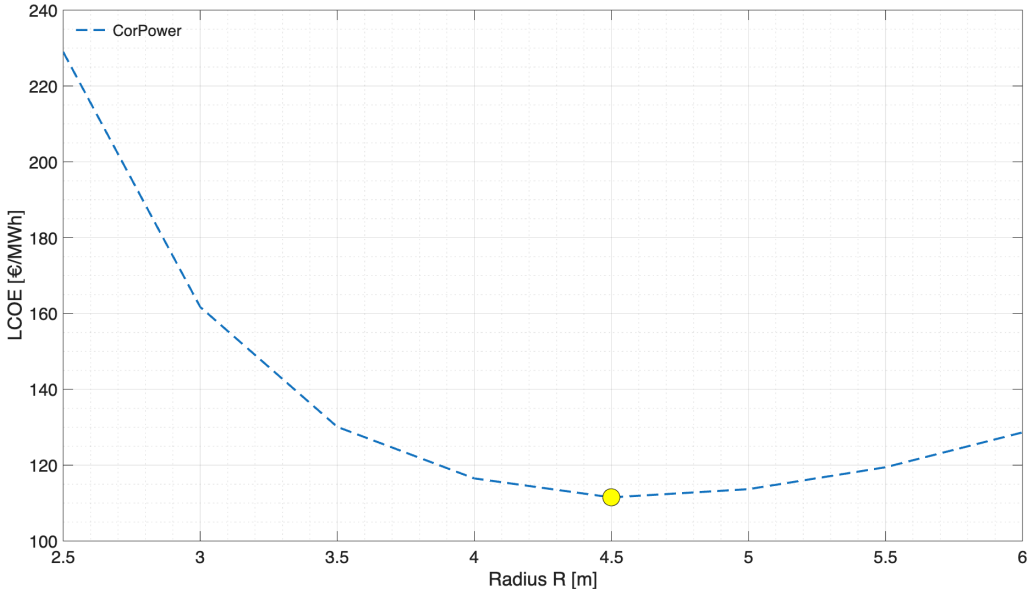

(a)

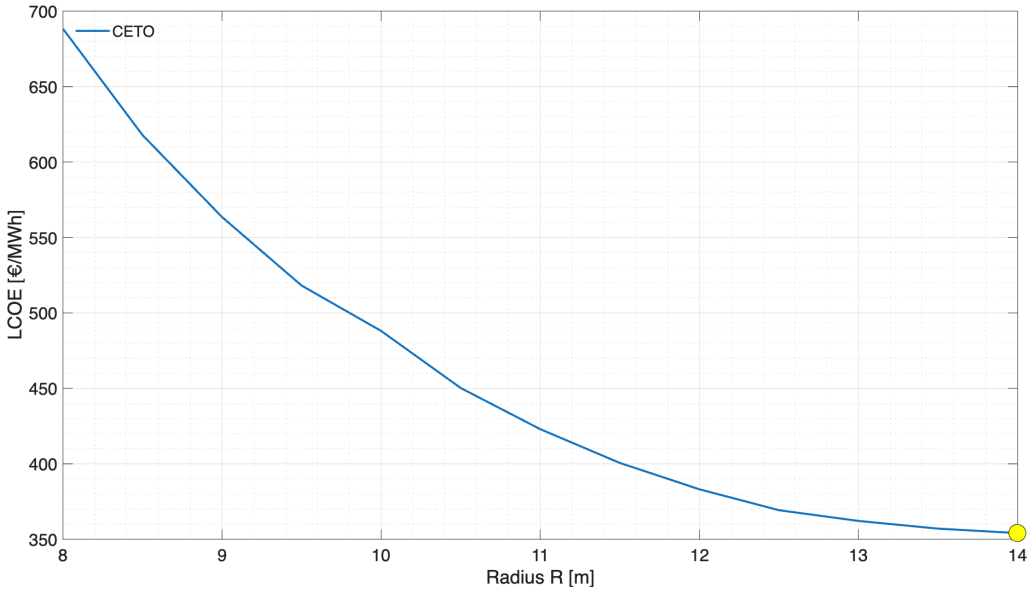

(b)

Figure 6.22: LCOE variation with radius in Australia using FSM for: (a) CorPower , (b) CETO 6

From Figures 6.19–6.22, it can be observed that when applying the FSM, the optimal radius tends to shift towards larger values. In particular, for the CETO 6 device in Australia, a clear optimum is not identified within the analysed range, as the LCOE continues to decrease at the upper bound of the radius considered. As mentioned previously, the analysis is intentionally limited to a restricted range of radii in order to remain consistent with realistic device dimensions. This also reflects an implicit limitation of the approach, particularly concerning the use of Froude scaling under extreme conditions. In high-energy sites, such as Australia, the combination of large device size and strong wave climate may reduce the re-

liability of the scaling assumptions, making the extrapolation to larger radii less representative of physically meaningful designs.

The LCOE results and the corresponding radius, calculated using both the PSM and FSM methods, are presented in Tables 6.1 and 6.2.

Table 6.1: LCOE values for a single WEC installation across different locations [€/MWh]

Location	$CorPower_{FSM}$	$CETO\ 6_{FSM}$	$CorPower_{PSM}$	$CETO\ 6_{PSM}$
Germany	550.69	1712.17	385.26	1035.32
Scotland	214.65	675.85	175.83	434.25
Portugal	197.11	628.67	162.64	405.28
Australia	111.51	354.10	94.42	243.84

Table 6.2: Optimal device radius for different locations [m]

Location	$CorPower_{FSM}$	$CETO\ 6_{FSM}$	$CorPower_{PSM}$	$CETO\ 6_{PSM}$
Germany	3	9	3.5	8
Scotland	4.0	12.5	4.0	8.5
Portugal	4.5	12.5	4.0	8
Australia	4.5	14	4.0	9

From Tables 6.1 and 6.2 it can be observed that the FSM approach, especially for the CETO 6 device, shifts the optimal radius towards values larger than the standard configuration, whereas the PSM predicts optimal radii below the standard size. This difference has a clear physical and engineering explanation. The Physical Scaling Method explicitly accounts for the variation of hydrodynamic loads and structural stresses with the device size. As the radius increases, wave excitation forces grow approximately with the device volume (R^3), while structural resistance depends on thickness and material strength. To withstand these increased loads, the required structural thickness and mass increase significantly, often following a nonlinear trend. As a result, CAPEX grows faster than the corresponding increase in Annual Energy Production, leading to a penalization of larger radii and therefore to lower optimal values. In contrast, the Froude Scaling Method is based on geometric similarity and assumes that all physical quantities scale consistently with a fixed ratio. While this approach correctly preserves hydrodynamic similarity, it does not capture the real scaling of stresses, structural thickness, and material constraints. In particular, it neglects the fact that structural design is governed by stress limits rather than purely geometric scaling. Consequently, FSM tends to underestimate the increase in structural costs and overestimates the economic viability of larger

devices, shifting the optimal radius towards higher values. This behaviour is consistent with findings in the literature, where it is widely recognized that Froude scaling is suitable for hydrodynamic modelling but insufficient for structural and techno-economic assessments, as it does not account for nonlinear stress scaling and material constraints. For this reason, the results obtained with the PSM, which incorporates load-driven structural sizing, are more representative of the actual engineering behaviour of the system and provide more reliable optimal configurations at smaller radii.

The LCOE is then calculated also taking into account, as mention in the previous chapter, the economical advantage that can come commissioning not a single device but a farm of WECs. The analyses is conducted is performed considering different number of devices for the farm. The results, reported in Table 6.3, report the LCOE considering a farm of 100 WECs according to some example found in literature [24].

For CorPower and CETO 6, a different number of devices was considered within the farm due to their differing geometric characteristics. In particular, CETO 6 is larger than CorPower and also exhibits higher energy production.

Since the occupied sea surface scales proportionally to the square of the device characteristic radius, the equivalent number of CETO 6 units was calculated as:

$$N_{\mathrm{CETO}} = N_{\mathrm{CP}} \left(\frac{R_{\mathrm{CP}}}{R_{\mathrm{CETO}}} \right)^2 \tag{6.1}$$

where $N_{\mathrm{CP}} = 100$ represents the reference CorPower deployment scenario.

This approach ensures that both technologies occupy approximately the same marine area, thus enabling a consistent techno-economic comparison under identical spatial constraints, as commonly adopted in wave farm layout studies [10].

In this case, the standard radii, 4.5 m for CorPower and 10 m for CETO 6, are adopted to define the number of CETO6 units within the farm, thereby ensuring consistency in the number of devices across all locations.

Considering the equation 6.1, the number of CETO 6 units in the farm is equal to 20.

Table 6.3: LCOE values for WEC farms across different locations [€/MWh]

Location	$CorPower_{FSM}$	$CETO\ 6_{FSM}$	$CorPower_{PSM}$	$CETO\ 6_{PSM}$
Germany	374.60	1432.9	282.09	832.41
Scotland	167.13	612.55	136.91	356.59
Portugal	161.38	569.79	126.66	325.95
Australia	91.29	327.82	73.50	204.10

The advantages associated with co-locating the wave farm with an offshore wind farm (OWF) are also taken into account. As in the estimation of the number of WECs within the farm, the number of devices that can be accommodated in a real offshore wind farm differs between the two technologies. To determine the actual number of WECs that can be co-located in the offshore wind farms considered in this study—namely the Gode Wind I & II OWF in the German North Sea (for the German site) and the Moray East OWF in the Scottish North Sea (for the Scottish site), an initial number of 50 CorPower devices is assumed to fit within the farm. Based on this, the equivalent number of CETO 6 devices is then calculated as follows:

- 9 CETO 6s, for the GODE I & II wind farm, so for the Germany location
- 10 CETO 6s, for the MORAY East wind farm, so for the Scotland site

The LCOE results, including the benefits of co-location, are presented in Table 6.4.

Table 6.4: LCOE values for co-located WEC and OWF [€/MWh]

Location	$CorPower_{FSM}$	$CETO\ 6_{FSM}$	$CorPower_{PSM}$	$CETO\ 6_{PSM}$
Germany	213.65	1090.06	192.72	550.07
Scotland	128.91	578.99	105.60	253.52

The co-location of wave energy converters with an OWF, as can be appreciated in Table 6.4 represents a key factor that can significantly reduce the overall project costs. The co-location allows to reach value of LCOE equal to 129 [€/MWh] for the Scotland location, becoming closer to the one of the offshore wind energy which by 2030 is estimate to be 90 [€/MWh] [32]. In addition, this configuration can enable a project located in an area with lower wave energy potential to achieve a lower LCOE than a standalone project installed in a site with higher wave energy resources.

Chapter 7

Conclusions

This thesis has investigated the techno-economic performance of different Wave Energy Converter (WEC) technologies across multiple site-specific conditions, with the aim of identifying optimal configurations and assessing their competitiveness within future energy systems. The work combined hydrodynamic modelling, numerical simulations, scaling methodologies and economic evaluation, resulting in an integrated framework for the comparison of WEC technologies under varying environmental conditions. A first key outcome of this study is the development of a structured workflow that links wave climate characterization, device modelling and economic assessment. Starting from sea-state data obtained through the Copernicus database, the analysis progressed through hydrodynamic simulations performed with NEMOH and subsequent processing in MATLAB, allowing the computation of performance indicators such as Annual Energy Production (AEP) and Levelised Cost of Energy (LCOE). This approach enables a consistent comparison between technologies and locations, representing one of the main contributions of the thesis. From a technological perspective, the results highlight how device performance is strongly dependent on site-specific wave conditions. The comparison between the different locations shows that more energetic wave climates generally lead to higher AEP values, but not necessarily to lower LCOE. This confirms that economic performance is governed by a trade-off between energy production and cost increase, particularly related to structural requirements and scaling effects. In this context, the optimization of the device radius plays a crucial role, as it directly influences both hydrodynamic efficiency and capital costs. The comparison between the considered technologies reveals that no single WEC is universally optimal, but rather that each device shows advantages depending on the local conditions. The CorPower device demonstrates strong performance in high-energy environments and benefits significantly from co-location strategies, such as integration with offshore wind farms. This configuration allows shared infrastructure and contributes to a reduction in overall costs, improving economic viability. On the other hand, the CETO 6 technology shows competitive behaviour in specific conditions, particularly where its submerged configuration can offer advantages in terms of survivability and opera-

tional stability. Another important outcome of this work is the comparison between Froude scaling and direct (physical) scaling approaches. The results indicate that while Froude scaling provides a useful approximation and is widely adopted in the literature, it may introduce deviations when applied to complex techno-economic evaluations. The direct simulation approach, although more computationally demanding, allows a more accurate estimation of performance and costs. This highlights the importance of selecting appropriate methodologies depending on the level of detail required in the analysis. From an economic standpoint, the study confirms that LCOE remains a critical barrier for the large-scale deployment of wave energy technologies. However, the results also show that significant improvements can be achieved through design optimization, site selection and integration with existing offshore infrastructure. In particular, co-location with offshore wind farms emerges as a promising strategy to enhance competitiveness, reducing installation and grid connection costs. Despite the comprehensive nature of the analysis, some limitations must be acknowledged. The use of linear potential flow theory and simplified cost models introduces uncertainties in the estimation of both performance and economic indicators. Additionally, the resolution of the wave data and the assumptions adopted for scaling and structural analysis may influence the accuracy of the results. Further developments of this research could include the analysis of array effects in WEC farms, the integration with energy storage systems, and a more detailed assessment of environmental and operational constraints. Moreover, the extension of the methodology to additional technologies and locations would further validate its applicability and robustness. In conclusion, this thesis demonstrates that wave energy has a significant potential to contribute to future renewable energy systems, particularly in regions with favourable wave climates. While economic challenges remain, the combination of technological optimization, site-specific design and hybrid offshore solutions can substantially improve the feasibility of WEC deployments. The methodology developed in this work provides a useful tool to support decision-making processes and to guide future research in the field of ocean energy

Bibliography

[1] European Environmental Agency. Share of energy consumption from renewable sources in europe. https://www.eea.europa.eu/en/analysis/indicators/share-of-energy-consumption-from, 2025.

[2] IEA. Energy security in energy transition. https://www.iea.org/reports/world-energy-outlook-2022/energy-security-in-energy-transitions, 2022.

[3] Our World in Data. Temperature increase. https://ourworldindata.org/grapher/cumulative-co2-emissions-region, 2025.

[4] International Energy Agency. Global co2 emissions from energy combustion and industrial processes and their annual change, 1900-2023. https://www.iea.org/data-and-statistics/charts/global-co2-emissions-from-energy-combustion-and-industrial-processes-and-their- 2025.

[5] Offshore-Energy.biz. Corpower ocean's next-gen wave energy device hits waters offshore portugal. https://www.offshore-energy.biz/corpower-oceans-next-gen-wave-energy-device-hits-waters-offshore-portugal/, 2023.

[6] G. Bracco. Ocean energy introduction.

[7] Ocean Energy Europe. Ocean energy, stats and trends 2024. https://www.oceanenergy-europe.eu/wp-content/uploads/2025/04/Ocean-Energy-Stats-Trends-2024.pdf, 2025.

[8] E. Baca, R. T. Philips, D. Greene, and H. Battey édis. Expert elicitation for wave energy lcoe futures. NREL, 2022.

[9] G. Bracco. Wave energy converters.

[10] A. Pecher and J. P. Kofoed. *Handbook of Ocean Wave Energy*. Springer, 2017.

[11] C. Guo, W. Sheng, D. G. De Silva, and G. Aggiédis. A review of the levelized cost of wave energy based on a techno-economic model. *Energies*, 16(5):2144, 2023.

[12] D. E. M. Classification of wave energy converters. *Recent Adv. Petrochem. Sci.*, 2(4), 2017.

[13] EMEC. Corpower ocean. https://www.emec.org.uk/about-us/wave-clients/corpower-ocean/, 2025. Accessed: 2025-10-14.

[14] CorPower Ocean. Corpower ocean completing c4 inspection and upgrades. https://corpowerocean.com/corpower-ocean-completing-inspection-upgrades/.

[15] CorPower Ocean. Wave energy technology — corpower ocean. https://corpowerocean.com/wave-energy-technology/, 2025. Accessed: 2025-10-14.

[16] Carnegie Clean Energy. Ceto technology. https://carnegiecce.com/ceto-technology/, 2025. Accessed: 2025-10-14.

[17] Tethys. Perth wave energy project. https://tethys.pnnl.gov/project-sites/perth-wave-energy-project, 2025. Accessed: 2025-10-22.

[18] OpenEI. Carnegie clean energy ceto 6. https://openei.org/wiki/PRIMRE/Databases/Projects_Database/Devices/Carnegie_Clean_Energy_CETO_6, 2025. Accessed: 2025-10-22.

[19] Erfan Amini, Danial Golbaz, et al. A parametric study of wave energy converter layouts in real wave models. *Energies*, 2020.

[20] Copernicus Marine Service. Copernicus marine data store. https://data.marine.copernicus.eu/login?redirect=%2Fproduct%2FGLOBAL_MULTIYEAR_WAV_001_032%2Fdownload, 2025. Accessed: 2025-11-04.

[21] Azambuja. Final areas for marine renewable energy in portugal. https://bluegrid.pt/final-areas-for-marine-renewable-energy-in-portugal/, 2025. Accessed: 2025-10-20.

[22] Australian Renewable Energy Agency. Carnegie ceto 6 technology. https://arena.gov.au/projects/carnegie-ceto-6-technology/, 2025. Accessed: 2025-10-14.

[23] LHEEA/Nemoh. Nemoh gitlab repository. https://gitlab.com/lheea/Nemoh. Accessed: 2025-11-17.

[24] M. deCastro, G. Lavidas, B. Arguilé-Perez, et al. Evaluating the economic viability of near-future wave energy development along the galician coast using lcoe analysis. *Journal of Cleaner Production*, 2024.

[25] Ajab Gul Majidi, Victor Ramos, Paulo Rosa Santos, et al. Power production assessment of wave energy converters in mainland portugal. *Renewable Energy*, 2018.

[26] Nathan Tom. Review of wave energy converter, power take-off systems, testing practices, and evaluation metrics. https://docs.nrel.gov/docs/fy23osti/82807.pdf.

[27] BBC. Geometric archetypes used in structural engineering. https://www.bbc.co.uk/bitesize/articles/zcjf46f#zwkbvwx, 2023.

[28] London Metal Exchange. London metal exchange. https://www.lme.com/metals/ferrous/lme-steel-hrc-nw-europe-argus#Trading+day+summary, 2026.

[29] Wave Energy Scotland. Very large scale wave energy converters analysis of the innovation landscape. https://www.waveenergyscotland.co.uk/media/dfjfaipz/wes_ls07_er_very_large_scale.pdf, 2018.

[30] Mostafa Rezaei, Alexandr Akimov, and Evan Gray. Techno-economics of offshore wind-based dynamic hydrogen production. *Applied Energy*, 374:124030, 2024.

[31] Wave Energy Scotland. Wave and floating wind energy: Opportunities for sharing infrastructure, services and supply chain, 2023.

[32] IEA. Offshore wind outlook 2019. https://iea.blob.core.windows.net/assets/495ab264-4ddf-4b68-b9c0-514295ff40a7/Offshore_Wind_Outlook_2019.pdf, 2019.